Lakehead University

Stable isotope (N, O, H) geochemistry, petrology and compositions of biotite of the Musselwhite Mine, Ontario: implications for mineralisation

Carissa Isaac

A thesis submitted to the Department of Geology in partial fulfillment of the requirements for the degree of Master of Science

Fall 2008

Acknowledgements

I would like to thank the following people:

Musselwhite Mine for financial support, site access and access to drill core and database files.

FedNor for financial support in conjunction with Musselwhite Mine.

Andrew Cheatle, John Biczok, and all the staff of the Musselwhite Mine for sharing their knowledge and expertise with me.

John Biczok and Dr. Pete Hollings for collecting samples for me when my father was in hospital.

Anne Hammond, Al Mackenzie, Keith Pringnitz and Ain Raitsakas for their help with the processing of my samples and with the use of lab equipment.

Andrew Conly and the Geology department for their knowledge and support.

Pat Moran, Malcolm Alexander, Larissa Stevens and all my friends, both here and abroad for their insight, information, and keeping me sane throughout the process.

Finally, I would like to thank Dr. Pete Hollings for his guidance and support throughout the past two years, without which I would not have succeeded.

Thank you all.

Abstract

Musselwhite Mine is located on the south shore of Opapimiskan Lake, approximately 480 km north of Thunder Bay. Hosted in the ~2.8Ga North Caribou Lake greenstone belt of the North Caribou Terrane, Superior Province, Musselwhite is currently classified as a shear hosted orogenic gold deposit. The deposit is hosted in an iron formation within a volcanic pile of intermediate to felsic metavolcanic rocks, metabasalts and komatiitic metabasalts and has been metamorphosed to amphibolite grade.

Twenty biotite and 30 quartz samples have been analyzed for $\delta^{15}N$, $\delta^{18}O$ and δD from Musselwhite Mine as well as 12 biotite samples from the granitoid rocks surrounding the North Caribou Lake Greenstone Belt. Nitrogen isotopes in biotite from Musselwhite Mine are characterized by a $\delta^{15}N$ range from -1.3 to 11.1 per mil. Oxygen and hydrogen isotopes of biotite samples from the mine range from +7.1 to +10.1 per mil for $\delta^{18}O$ and -55 to -100 per mil for δD.

Oxygen isotope signatures from quartz samples from Musselwhite range from +12.4 to +17.1 per mil. Values for the silicate facies iron formation and mineralized zones are consistent with previous work by Otto (2002) and indicate fluid compositions that fall within both the magmatic and metamorphic range.

Biotite samples from granites and metasedimentary rocks adjacent to the deposit have a $\delta^{15}N$ range of -6.9 to +6.1 per mil. Oxygen and hydrogen isotopic ranges for the granitoid plutonic rocks are +2.0 to +4.0 per mil and -59 to -80 per mil respectively; values are typical of felsic plutonic rocks.

The $\delta^{15}N$, $\delta^{18}O$ and δD stable isotopic data generated for Musselwhite Mine suggest that magmatic fluids played a role in the formation of the deposit.

Table of Contents

List of Chapters:

List of Appendices:

List of Figures

List of Tables

List of Plates

CHAPTER 1: INTRODUCTION

1.1 Introduction

The Musselwhite mine is located approximately 480 km north of Thunder Bay on the southern shores of Opapimiskan Lake in the North Caribou Lake greenstone belt. The mine is classified as an orogenic gold deposit (Otto, 2002; Blower and Kiernan, 2003), producing an average 2500 tonnes of ore per day and with proven and probable mineral reserves of approximately 1.98 million ounces (Goldcorp, 2008).

Extensive research has been previously undertaken at the Musselwhite Mine in an effort to understand the formation of the gold deposit in relation to its host rocks. Limited accessibility, sparse outcrop, and the short field season have resulted in much of the research taking place underground at the mine scale. Although the stratigraphy of the mine has been extensively characterized (Wells, 1995; Otto, 2002; Moran, 2008), the relationship of the mine geology to the regional geology is not well understood.

1.2 Scope

This project was designed to expand on preliminary isotopic research undertaken at the mine (Otto, 2002) and uses nitrogen, oxygen and hydrogen isotopes in biotite in addition to oxygen isotopes of quartz to better characterize the nature of the fluids in the alteration zones of the deposit and, if possible, to discern if there is a characteristic isotopic signature associated with gold mineralization. Regional isotopic work was undertaken in order to compare and contrast the isotopic signatures at the mine scale with those at the regional scale. Samples were also collected and whole-rock geochemistry

was undertaken and examined at the regional scale to gain a better understanding of the nature of the regional rocks of the North Caribou Lake greenstone belt.

1.3 Exploration History

The Musselwhite property was discovered in 1962 by Allan and Harold Musselwhite who were exploring at the time for Kenpat Mines, Inc.. At the same time, Rio Tinto discovered Au mineralization near Pasemon River, west of Zeemal Lake (Breaks et al., 1989). From 1962-1967 Kenpat Mines Inc. undertook geological mapping, trenching, a ground magnetometer survey and drilled eight holes (Breaks et al., 1989). The property was re-staked in 1973 by the Musselwhite brothers after Kenpat let the claim go (Breaks et al., 1989). A joint venture in 1974-75 comprised of Dome Exploration Ltd., Canadian Nickel Co., and Esso Minerals Canada explored the property further and drilled another 16 holes (Breaks et al., 1989). Then, in 1976, an extensive drilling program was carried out by another joint venture group (consisting of Mineral Deposit Inventory Record, Geoscience Data Centre, and the Ontario Geological Survey ; OGS). The greenstone belt was re-mapped from 1984-1986 by the OGS (Breaks et al., 1984; Breaks et al., 1985; Breaks et al., 1986; Breaks et al., 2001). The mine began official production on April 1,1997 (Otto, 2002; Moran, 2008). In 2002, the property was jointly owned by Placer Dome, Inc. and TVX Gold Ltd. (Pollard et al., 2002). Placer Dome was 68% owner and operator and Kinross Gold Corporation held a 32% interest in the mine in 2003 (Kiernan and Blower, 2003). In 2006, Barrick Gold Corp., after taking over Placer Dome, Inc. sold its stake in Musselwhite to Goldcorp Inc. (http://www.mining-technology.com/projects/musselwhite/). At the end of 2007

Goldcorp Inc. bought Kinross Gold Corporation's share (Goldcorp, 2008). At the time of publication of this thesis Goldcorp has 100% ownership of Musselwhite Mine.

1.4 Regional Geology

The Superior Province is the largest Archean craton in the world, covering much of Northern Ontario, Northern Quebec, and extending into Manitoba and Minnesota (Fig. 1.1). The craton ranges in age from 3.2 to 2.5 Ga (Thurston et al., 1991). It is bounded to the southeast by the 1.1 Ga Grenville Province, to the northwest by the Trans Hudson Orogen, and it is overlain on its northern and western borders by Paleozoic sediments around Hudson and James Bay and in Manitoba (Fig. 1.1). The Superior Province is thought to represent a series of accreted continental fragments that amalgamated to form the craton (Card, 1990). Card and Cisielski (1986) subdivided the Superior Province into nineteen different subprovinces on the basis of age, rock type and known tectonic boundaries. More recent work by Stott et al. (2007) has further refined the tectonic divisions and has divided the Superior Province into a series of domains and terranes based on recent aeromagnetic surveying, Nd-Sm isotopic and other geochronological evidence (Fig. 1.1).

The Sachigo, Uchi and Berens River subprovinces have been reclassified as the North Caribou Terrane, the Uchi Domain, the Island Lake Domain and the Oxford-Stull Domain (Fig. 1.1; Stott et al., 2007). The Musselwhite mine is situated on the northeastern margin of the North Caribou Terrane (Fig 1.1). The age of supracrustal rocks and batholiths that make up the North Caribou Terrane range from 3.0 to 2.8 Ga

(Stott et al., 1997) with accompanying younger plutonism as other terranes accreted (Rayner and Stott, 2005).

The Musselwhite mine is located in the North Caribou Lake greenstone belt (NCLGB), which lies within the North Caribou Terrane, the largest of the terranes found in the Sachigo Superterrane of the Superior Province (Stott et al., 2007). The North Caribou Lake greenstone belt has been divided into eight different units, four of which occur in the vicinity of the Musselwhite mine. They are: the North Rim metavolcanic rocks (NRV), South Rim metavolcanic rocks (SRV), Opapimiskan Lake metavolcanic rocks (OLV), and the Eyapamikama Lake metasedimentary rocks (ELS; Fig. 1.2; Breaks et al., 2001).

The North Caribou Lake greenstone belt has been metamorphosed to greenschist facies in the north, and amphibolite facies in the south (Breaks et al., 2001). The relationships between the North Caribou Lake batholith and the isograds of the NCLGB suggest that the North Caribou Lake batholith was likely emplaced after the metamorphic grades were imposed, implying peak metamorphic temperatures prior to 2875 Ga (Breaks et al., 2001).

1.5 Assemblages in the vicinity of Musselwhite Mine

1.5.1 North Rim Metavolcanic Unit (NRV)

The rocks of the North Rim metavolcanic unit are dominantly tholeiitic pillowed flows that are moderately to highly deformed with selvages characterized by hornblende with occasional garnet in some locations (Breaks et al., 2001). Vesicles in the rock are filled with quartz and/or carbonate. Pillows with >10% amygdules are quite common in

the unit and their presence suggests a shallow subaqueous environment (Breaks et al., 2001). Rare banded iron formation, ultramafic and carbonate rock suites are found

Figure 1.1: Map of the Superior Province, showing the various tectonic terranes and the location of the Musselwhite mine. After Card and Ciesielski (1986) and Stott et al. (2007).

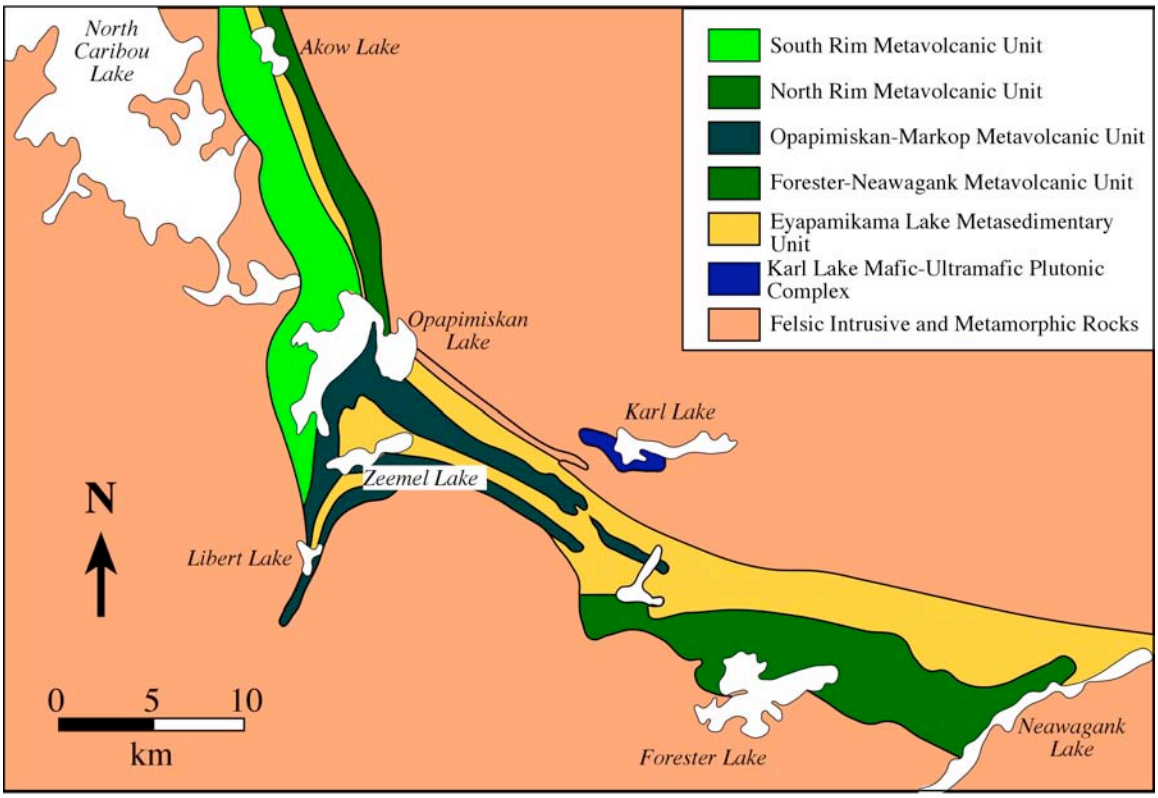

Figure 1.2: Map of the assemblages in the southern portion of the North Caribou Lake greenstone belt in the vicinity of Musselwhite Mine. After Breaks et al. (1986).

within this unit (Breaks et al., 2001). Some felsic-intermediate metavolcanic rocks found in the vicinity of Hatch Lake are locally garnetiferous (Breaks et al., 1985).

Geochemistry of the mafic metavolcanic rocks at Musselwhite indicate that both the OLV and the NRV are part of the "Basement Basalts" that underlie the iron formation (Hollings, 1996; Fig.1.3). An increase in MgO content in the rocks of the NRV near the contact with the OLV suggests that the NRV and OLV may be coeval (Breaks et al., 2001). The rocks of the NRV cannot be traced south of Opapimiskan Lake; either because the unit is truncated by a major shear zone that marks the boundary between the greenstone belt and the adjacent Island Lake Terrane, or because this particular packet of rocks pinches out (Breaks et al., 2001). This suggests that the rocks of the NRV truncate

somewhere within the domain of Opapimiskan Lake but exactly where this occurs is hard to define due to poor exposure and the heavily sheared nature of the rocks. Breaks et al. (2001) documented the NRV unit as contiguous with the ELS to the north and south, and that the unit intercalates at Castor-Pollux lakes (Breaks et al., 2001). However, recent mapping south of Akow Lake indicates that large areas of rock identified as metasedimentary are actually sheared basalts and consequently the ELS may not be continuous through this area (John Biczok, personal communication, 2007).

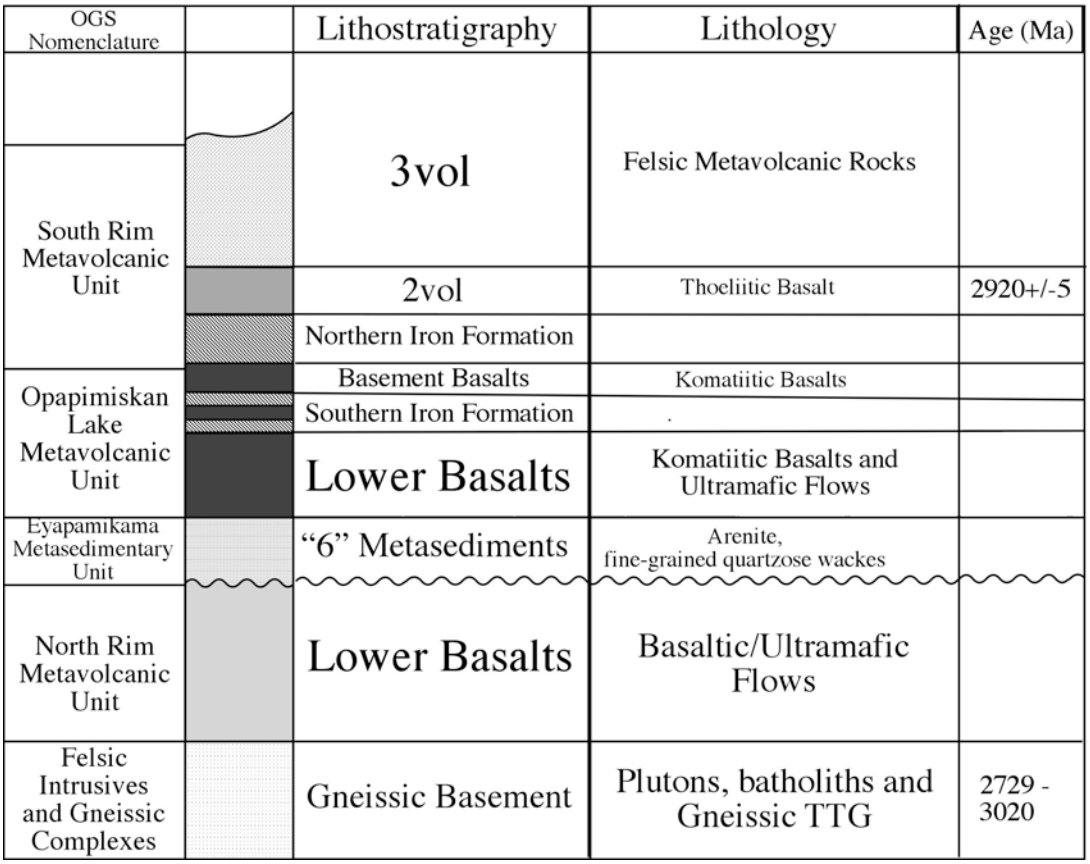

Figure 1.3 Stratigraphic cross section of the Geology of the North Caribou Lake greenstone belt. Courtesy of Musselwhite. Ages are from Klipfel (2002).

1.5.2 South Rim Metavolcanic unit (SRV)

The rocks of the South Rim Metavolcanic unit are characterized by mafic to felsic metavolcanic units. The SRV unit is bounded on the East by the North Caribou Lake

Batholith and stratigraphically overlies the Musselwhite BIF (Fig. 1.2). Mafic units within the SRV are characterized by pillowed flows intercalated with massive flows, and indicate a subaqueous setting. They possess a mineral assemblage of hornblende-actinolite, plagioclase, epidote and chlorite, indicative of greenschist-amphibolite facies metamorphism (Breaks et al., 2001). Relict subophitic textures are visible in low-grade mafic metavolcanic rocks as laths of plagioclase in a chiefly hornblende matrix (Breaks et al., 2001). Subhedral plagioclase phenocrysts comprise up to 5% of some pillows and tend to be concentrated towards pillow centres (Breaks et al., 1985). Some pillows have chloritic selvages up to 1 cm thick and interpillow spaces are filled by a hyaloclastite assemblage of quartz + plagioclase + epidote (Breaks et al., 1985). The SRV hosts numerous quartz + plagioclase + epidote + tourmaline + sulphide veins, concordant with the dominant phase of foliation in the rocks (Breaks et al., 1985). The geochemistry of the mafic rocks are characterised by flat REE curves indicative of MORB –like rocks and lack any Nb–anomaly, suggesting that they have not been crustally contaminated (Hollings, 1996). The tholeiites of the SRV have a geochemical signature comparable to Ontong Java and other oceanic plateau basalts (Hollings and Kerrich, 1998). Felsic rocks comprise only approximately 1% of this unit; they occur as lapilli tuffs, tuff breccia, and some felsic flows (Breaks et al., 2001). Recent drilling at Musselwhite Mine indicates these felsic units are more abundant in the vicinity of Opapimiskan Lake (John Biczok, personal communication, 2008). The felsic rocks show LREE enriched curves indicative of arc settings with pronounced Nb and Ti anomalies (Hollings and Kerrich, 1998). U-Pb dating of zircons from the felsic portions of the unit have yielded an age of 2973± 2.2 Ma (Klipfel, 2002). Xenoliths of this unit are found in the NCLB, demonstrating that the

batholith postdates the volcanic rocks (Breaks et al., 2001). The relationship between the SRV and the OLV is poorly understood, as the contact lies beneath Opapimiskan Lake, and is heavily sheared (Breaks et al., 2001).

1.5.3 Opapimiskan Lake Metavolcanic unit (OLV)

The OLV is comprised of a series of mafic and ultramafic metavolcanic rocks. Primary relict textures include pillows, pillow breccia, flow top breccia and varioles. The rocks consist of massive, pillowed and variolitic flows with narrow (3-5 mm) selvages on the pillows (Breaks et al., 2001). The mineral assemblage is dominated by actinolite with minor plagioclase and chlorite (Breaks et al., 2001). This mineral assemblage correlates with the greenschist facies of metamorphism. The metamorphic assemblage has been overprinted by a strong D_2 fabric and has been extensively sheared (Breaks et al., 2001). Some rare spinifex/polysuture textures are seen in the rocks on the Pipestone River (Breaks et al., 2001). It is likely that the other ultramafic units (such as the Lundmark Lake unit in the southern portion of the greenstone belt; Fig. 1.2) correlate with the OLV, although contacts cannot be observed (Breaks et al., 2001). The majority of known banded iron formation (BIF) in this greenstone belt is contained within this unit and consists primarily of silicate and oxide facies type, with the BIF underlying Opapimiskan Lake being the primary BIF in the unit, though a minor BIF occurs east of Graff Lake (Breaks et al., 2001). If the rocks of the Keeyask Lake Metavolanic (found in the northern portion of the NCLGB; not shown on maps) and OLV are coeval, then the thin metasedimentary cover that overlies the Northern Iron Formation that hosts the Musselwhite deposit is part of the ELS (Breaks et al., 2001).

The trace element geochemistry of the rocks of the OLV reveals that the unit is made up of a suite of Munro-type (Al-depleted) komatiites, high magnesian basalts and a few intermediate rocks (Hollings and Kerrich, 1998). Hollings (1996) notes that some units within the OLV that have been designated as metasedimentary rocks are geochemically identical to the mafic metatholeiites and proposed that these are actually tuffs. Lower and Basement basalts at Musselwhite Mine, have very similar trace element patterns, which suggest they are both part of the OLV (Hollings, 1995; Fig. 1.3). Negative Ti and Nb anomalies within the Basement basalts suggest contamination by more felsic crust; the calc-alkaline samples that contain anomalous Ti have a corresponding V spike that indicates possible spinel accumulation (Hollings, 1995). Ultramafic units have flat HREE on a primitive-mantle normalised diagram characteristic of Al-depleted komatiites, but are too siliceous to be classified as komatiites and also have LREE-enriched patterns (Hollings, 1995). The high LREE and silica contents are interpreted to be the result of contamination of komatiitic melts by an intermediate source (Hollings and Kerrich, 1998) It is thought that the Keeyask Lake metasedimentary rocks or the rocks of Agutua Arm unit are the most likely contaminants (Hollings and Kerrich, 1998). Zr vs. Y plots show two suites in the OLV rocks at Musselwhite: calc-alkaline rocks and tholeiitic metabasalts (Hollings, 1995). The tholeiitic samples display generally flat REE curves (Hollings, 1995). The geochemistry of the high magnesian meta-tholeiites indicates that they are not derived directly from komatiites, but are rather derived from a mixing of komatiitic, plume-derived material with mantle material (Hollings and Kerrich, 1998). The setting of these rocks is interpreted to be that of a mantle plume rising near or under continental crust, allowing for contamination of the

plume with tonalitic material from the underside of the continent (Hollings and Kerrich, 1998). Mixing of mantle material and material from the edges of the plume is thought to be the most likely source of the material from which the magnesian basalts of the OLV were derived (Hollings and Kerrich, 1998).

1.5.4 Eyapamikama Lake Metasedimentary Unit (ELS)

Breaks et al. (2001) grouped all metasedimentary rocks within the North Caribou Lake greenstone belt into a single unit. In the area east of the Musselwhite deposit, the unit is comprised of thinly bedded metawacke, plagioclase arenite, biotite-chlorite metapelite, and amphibole-rich metawacke (Breaks et al., 2001). Further to the southest, the metasedimentary rocks at Heaton Lake are comprised of quartz wacke, quartz arenite and immature, poorly sorted conglomerate, wacke and mudstone (Breaks et al., 2001). All arenite suites are very pure and contain accessory heavy minerals (Breaks et al., 2001).

1.5.5 Felsic Intrusive Rocks

The North Caribou Lake Batholith is a massive, medium-grained, equigranular to hypidiomorphic granite to granodiorite trondhjemite (Breaks et al., 2001). It has a deformed contact with the rocks of the greenstone belt (Breaks et al., 2001). The composition of the batholith varies and has, as a result, a variety of accessory minerals including titanite, apatite, epidote and zircon, as well as iron and titanium oxides (Breaks et al., 2001).

The Schade Lake complex lies on the north side of the NCL greenstone belt between Atikomik Lake and Karl Lake. The complex is comprised of highly deformed hornblende-biotite tonalite, biotite trondhjemite, biotite granite, and biotite-hornblende-quartz diorite with scattered amphibolite enclaves; accessory minerals include muscovite, chlorite, epidote, and titanite (Breaks et al., 2001). A protomylonitic zone up to 30m wide (the Dinnick Lake Fault) bounding the greenstone belt signifies a major shear zone (Breaks et al., 2001).

Small stocks of pegmatitic trondhjemite, granite, granodiorite also cross cut the greenstone belt; accessory minerals include fluorite, green muscovite, and tourmaline (Breaks et al., 2001).

1.6 Age of the North Caribou Lake greenstone belt

Absolute ages for the NCLGB range from ~3.0 to 2.4 Ga (Klipfel, 2002). The oldest rocks of the NCLGB come from the northeastern portion of the belt. The Weagamow Batholith on the northwest edge of the belt has yielded an age of 2990 +/-1.8 Ma (de Kemp, 1987). Ages of the mafic and felsic volcanic rocks of the belt show that they were formed shortly after the Weagamow batholith. Klipfel (2002) reports a zircon age of 2973 +/- 2.2 Ma for felsic units at the mine, which are interpreted to be the felsic units of the SRV. A rhyolite tuff from the west shore of Opapimiskan Lake has yielded an age of 2981.9 +/-0.8 Ma (Davis and Stott, 2001). An age of 2920 +/- 4.7 Ma is reported for the mafic volcanic rocks at Musselwhite, which are identified geochemically with the SRV (Klipfel, 2002).

Material inherited by the metasedimentary units of the North Caribou Lake greenstone belt give a very uniform age of around 2980 Ma (de Kemp, 1987; Davis and Stott, 2001; Kilpfel, 2002). One age from arenites of the Zeemal-Heaton portion of the ELS gives an inherited age of 2853 +/- 1 Ma, indicating that the arenites in the southwest portion of the Eyapamikama Lake metasedimentary unit are likely much younger than and are, at least in part, made of reworked material from the older, more poorly sorted portions of the unit. The overwhelmingly dominant age of ~2980 Ma suggests that the metasedimentary units for the whole belt came from one or a few similarly aged sources. The only units so far identified that could have provided such ages are the felsic metavolcanic rocks of the Agutua Arm and the felsic portion of the South Rim metavolcanic unit. The younger age of the stratigraphically lower mafic units of the SRV create a potential issue with current interpretations, as currently the felsic units of the SRV are interpreted to be a continuation of arc-type magmatism. Zircons from the NCL batholith yield ages of 2869 +/- 3.6 and 2864+/-1 Ma (de Kemp, 1987; Davis and Stott, 2001). Ages of the batholith to the southwest of Opapimiskan Lake range from 2729.4 +/- 7.1 to 2725.8 +/- 3.2Ma (Klipfel, 2002).

The absolute age of mineralisation of the gold of the Musselwhite deposit is of much interest, as understanding timing of emplacement is key to model selection. Several ages have been derived from different materials found at Musselwhite. Pb/Pb modeling of galena samples from the West Anticline Zone at Musselwhite Mine give a crystallization age of 2.894-2.895 Ga (Hall and Rigg, 1986). Sm-Nd dating of whole rock and garnets of biotite-garnet schist interpreted to be associated with Au mineralisation yield a much younger age of around ~2.69 Ga with an age of 2690 +/-9 Ma preferred at

the mine (Maas, unpublished data, 2006). Late-stage, inclusion-free growth is seen on the edges of many garnets in the rocks of the Musselwhite mine (Otto, 2002). The morphology of the garnets strongly suggests that multiple episodes of garnet growth have occurred throughout the deposit and raises questions about Sm-Nd age dating of mineralisation. If the garnets have undergone multiple growth stages, then the Sm-Nd age likely represents a composite age. U-Pb dating of the NRV gave an age of 2932 Ma (Davis in Hollings and Kerrich, 1999). Klipfel (2002) measured Ar-Ar ages of biotite, grunerite and amphibole from both regional batholiths and mine samples in an attempt to determine an age for mineralization, and reported an age range of ~2.66 to 2.44 Ga. Klipfel (2002) interpreted the much younger Ar-Ar ages as a late stage thermal resetting event.

1.7 Metamorphism

Regional metamorphism of the North Caribou Lake greenstone belt is of the Abukuma type and ranges from lower greenschist to low-mid amphibolite facies (Breaks et al., 2001). A general trend of increasing metamorphic grade from the northwest to southeast is seen (Breaks et al., 2001). In addition, a trend of northward-increasing metamorphic grade is seen in the northwestern portion of the greenstone belt (Breaks et al., 2001). A relict contact metamorphic aureole, represented by chlorite overprinted by amphibolite, is seen adjacent to the North Caribou Lake Batholith (Breaks et al., 2001). A maximum metamorphic grade of amphibolite facies has been established by the presence of garnet, staurolite, andalusite, grunerite, and cordierite in various rocks across the belt (Breaks et al., 2001).

Peak metamorphic conditions were estimated by Breaks et al. (2001) using the chlorite-garnet-muscovite-staurolite-biotite-quartz isograd of Froese and Gasparinni (1975) and the staurolite-muscovite-quartz-Al_2SiO_5-biotite isograd of Hoschek (1969). Peak metamorphic conditions using these isograds give a peak temperature-pressure estimation of 400 to 500 °C and 3kbar or less (Breaks et al., 2001). This estimate is comparable to the estimate of 500–550 °C and 3kbar made by Hall and Rigg (1986) using garnet-biotite and arsenopyrite-iron sulphide geothermometry. Geobarometry completed by Otto (2002) using the garnet-hornblende-plagioclase-quartz geobarometer of Kohn and Spear (1990) and the quartz-biotite-plagioclase-garnet geobarometer of Hoisch (1990) gave considerably higher peak pressures of 6.3-9.4 kbar. These values are very high, and are generally not held as accurate due to their inconsistency with other data. Garnet-biotite and garnet-hornblende geothermometry by Otto (2002) yielded peak temperatures of 550-650 °C, which is comparable to the estimates of earlier work. Otto (2002) also determined the peak temperatures for retrograde chlorite at Musselwhite mine to be 210-250 °C.

1.8 Structural geology

There have been four phases of deformation documented in the North Caribou Lake greenstone belt (Hall and Rigg, 1986). The earliest (D_1) phase is characterised by tight to isoclinal asymmetrical folds (Breaks et al., 2001) and is interpreted as part of a regional-scale nappe (Wells, 1995). Later stages of deformation have obscured the original orientation of F_1 folds and S_1 foliations have been either obliterated or rotated parallel to S_2 (Breaks et al., 2001).

The second deformation event (D_2) is the dominant deformation event in the North Caribou Lake greenstone belt and represents the major tectonic event (Breaks et al., 2001). Folds plunge shallowly to the northwest; these folds are very tight in some areas of the Musselwhite property (such as the West Anticline zone and the T-antiform) (Wells, 1995). S_2 foliation is a moderately to strongly developed planar fabric (Breaks et al., 2001) with a strike of 120° and dips steeply southwest to subvertical (Hall and Rigg, 1986). Folds are closed to open asymmetrical, disharmonious and cylindrical with near vertical axial planes (Breaks et al., 2001). Boudinage of iron formation, attenuation of fold limbs and thickening of fold hinges accompanied deformation (Hall and Rigg, 1986; Breaks et al., 2001). Significant flattening and stretching occurred on fold limbs; this extensive flattening may be responsible for the creation of some of the rocks that are interpreted as mylonites (Wells, 1995). Brittle-ductile features such as bookshelf slipping, boudinage and flattening of the competent beds of the NIF are considered to be a late D_2 feature (Wells, 1995). Shear zones are thought to be coeval with folding and are interpreted as forming during the late stages of the D_2 event and possibly extending into D_3 (Wells, 1995). Most importantly, the pyrrhotite mineralization and associated quartz flooding which also hosts the gold occurs within D_2 structures (Wells, 1995). Gold emplacement is interpreted to have occurred during transition between brittle and ductile shearing (Wells, 1995).

The D_3 event marks a period of inhomogeneous strain (Breaks et al., 2001). The D_3 event is a relatively weak event, seen as gentle warping of D_2 fold axes and

crenulation cleavage within metavolcanic rocks (Wells, 1995). Macroscopic F_3 folds are suggested by reversals in lineation trends in some areas (Breaks et al., 2001).

The final stage of deformation (D_4) is characterized by narrow, subvertical, northwest striking chloritized shear zones that crosscut all previous structural fabrics (Hall and Rigg, 1986). These faults and veins cross cut gold mineralization at the Musselwhite mine creating barren quartz-carbonate veins (Otto, 2004).

1.9 Geology of the Musselwhite Property

The Musselwhite gold deposit lies within the metavolcanic rocks of the OLV. Exposure on the surface is very poor, as a result of glacial till deposits (Breaks et al, 2001). Because of the poor exposure, most of the information has been gathered from drill core, with supplementation from surface mapping and mapping within the mine.

The stratigraphy of the Musselwhite mine consists of a pair of iron formations, the upper called the Northern Iron Formation (NIF) and the lower called the Southern Iron Formation (SIF) that are surrounded by a dominantly mafic-ultramafic volcanic pile (Fig. 1.3). The SIF is separated from the NIF by a series of mafic-ultramafic and intermediate metavolcanic rocks (Fig. 1.3). All units have been metamorphosed to amphibolite facies and have been sheared to some degree, making interpretation difficult. The units are of relatively uniform thickness at the mine scale, but vary considerably at smaller scales (Blower and Kiernan, 2003). This localized variation is due to the reaction of the units to folding and shearing during the different episodes of deformation.

The hanging wall rocks are dominantly a felsic to mafic volcaniclastic pile, consisting of felsic ash-tuff to coarse polymictic volcaniclastic rocks overlying a series of basaltic flows (Blower and Kiernan, 2003). These rocks are split into two main units by their composition (felsic or mafic). Felsic metavolcanic rocks comprise the uppermost unit of rocks that host the Musselwhite deposit. They consist of a pile of intrusive and extrusive rocks of dacitic to rhyolitic composition (Blower and Kiernan, 2003). The rocks are comprised of highly siliceous units with massive to finely schistose bands to quartz rich bands (Wells, 1995). The typical mineral assemblage is quartz + muscovite + plagioclase + minor biotite with quartz flooding; the geochemistry of these units is comparable to those of felsic tuff with about 73% SiO_2 (Wells, 1995). The unit is frequently separated from the underlying thoeliitic metabasalt by either a thin garnet-grunerite horizon or garnet-biotite schist that grades upwards into the felsic volcanics (John Biczok, personal communication, 2008).

The rocks of the tholeiitic metabasalt unit consist of fine-to-medium-grained, massive to foliated rocks with a composition of hornblende-plagioclase-quartz (Wells, 1995). Schist seen in the mine ramp area has a mineral assemblage of ~75% actinolite, ~15% plagioclase and ~10% quartz (Wells, 1995). The tholeiitic metabasalts have a trace element geochemical signature of plateaux basalts (Hollings and Kerrich, 1999).

A significant apparent sedimentary or felsic tuff component occurs in small lenses within this unit that locally generates mineral assemblages that look like the silicate-dominant iron formation (Wells, 1995). Hollings et al. (1996) reported that the felsic metavolcanic unit correlates with the South Rim Metavolcanic unit, whereas the tholeiitic

metabasalt unit is comprised of the rocks of the North Rim Metavolcanic and Opapimiskan Lake Metavolcanic units.

The NIF is typically found below these two hanging wall rock units (Fig. 1.3; Blower and Kiernan, 2003). The "footwall mafics" lie between the NIF and the SIF, and are mafic/ultramafic in composition; they consist primarily of pillowed komatiitic basalts (Hollings, 1996; Kiernan and Blower, 2003). Trace element geochemistry on this unit shows that the lower basalts are comprised of Munro-type komatiites, high magnesian basalts and a few intermediate rocks (Hollings and Kerrich, 1998). The geochemistry of the high magnesian basalts indicate that they are derived from a mixing of komatiitic, plume-derived material with mantle material (Hollings and Kerrich, 1998). The NIF is further divided into a series of units (Fig. 1.4). The four major continuous units are: 4F – biotite-garnet schist, 4EA – the garnet-amphibole-grunerite-chert iron formation, 4B – grunerite-chert-magnetite iron formation, and 4H – pyrrhotite meta-argillite (Fig. 1.4; Blower and Kiernan, 2003). Contacts appear to be gradational between units suggesting contemporaneous deposition (Blower and Kiernan, 2003).

The SIF underlies the basement basalts and is dominated by chert-magnetite iron formation with minor carbonate visible in some portions of the formation (Fig. 1.3; Wells, 1995; Blower and Kiernan, 2003). The rocks that underlie the SIF are tholeiitic in composition (Blower and Kiernan, 2003). Some pegmatite dykes are found in the vicinity of the mine, but a link between these and mineralization has not been observed (Blower and Kiernan, 2003).

1.10 Mineralisation

Gold is found as microscopic flakes of native gold, and is associated with pyrrhotite and has been found trapped within garnets and in garnet fractures within the 4EA unit (Otto, 2002). The gold is somewhat stratiform with the 4EA unit, but is not stratabound, and seems to be chiefly associated with shearing. Quartz flooding, biotite-garnet, chlorite-grunerite-carbonate, and chlorite-pyrrhotite flooded areas, veins, and veinlets are commonly associated with gold mineralization (Otto, 2002; Blower and Kiernan, 2003). A possible remobilization or later stage introduction of gold as electrum and gold tellurides associated with tellurides has been found in a unique Po-dolomite-calcite vein within a narrow shear zone cutting basalts of the PQ fold limb a short distance west of the NIF. The mineralogy and textures of this vein are very different in character from the majority of the Musselwhite ore bodies (Liferovich, 2007). Blower and Kiernan (2003) classified Musselwhite Mine as an iron-formation-hosted gold deposit, placing it in the same category with Homestake, Minas Gerais, and Lupin. Otto (2002) classified the deposit as a hypozonal Archean orogenic lode gold deposit.

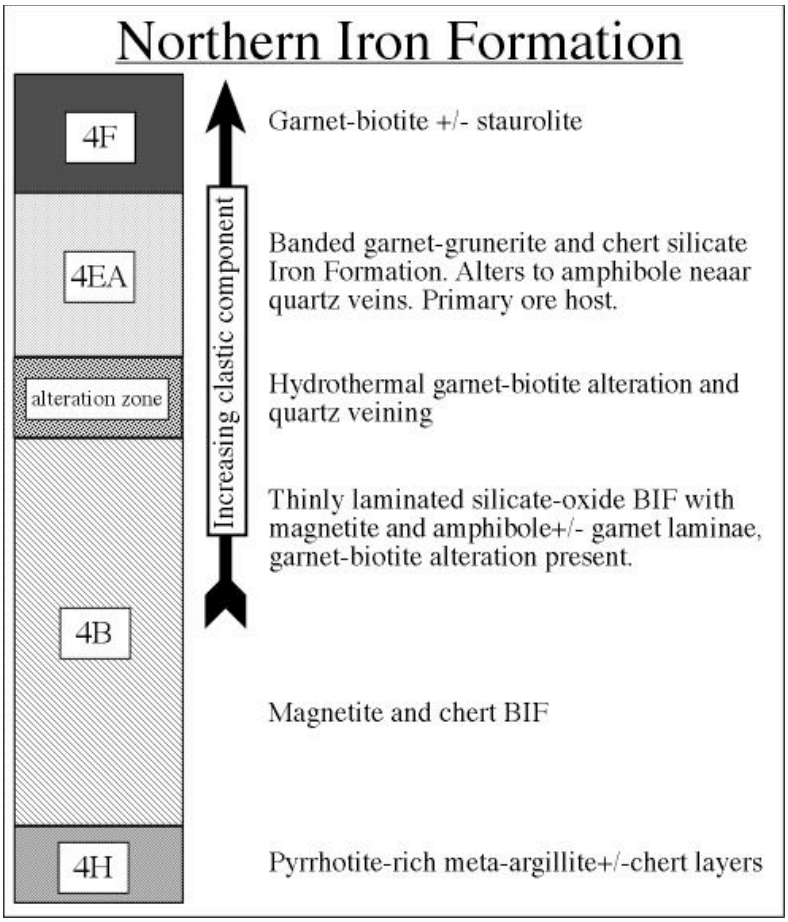

Figure 1.4: Simplified schematic section of the units of the Northern Iron Formation. Courtesy of Musselwhite.

1.11 Previous research on gold

The currently accepted model for Musselwhite Mine is that of an orogenic gold deposit (Otto, 2002). This term is used currently as a catch-all for most Archean greenstone deposits, regardless of gold occurrence, size, host rock and accompanying alteration suite. In an effort to remedy this, the Archean gold deposits have been divided using various different criteria. A common division is the host rock for the gold mineralization; in this division, Musselwhite falls under the sub-type of iron-formation-hosted (Blower and Kiernan, 2003). The economic significance of iron-formation hosted gold deposits is sufficient to have some researchers place them into separate class from

the quartz-carbonate-vein-hosted gold deposits (Poulsen, 1995). However, this is simply a distinction based on host rock type as opposed to a truly unique type of mineralization. Groves et al. (1998) proposed the terms epizonal, mesozonal, and hypozonal in an attempt to classify orogenic deposits in terms of genetic location as opposed to host rock. Examples of gold mineralization associated with orogenic processes are found throughout the geological record, but are especially prevalent in the Archean. Gold mineralization in the Archean is believed to be associated with major scale transtensions across cratons (Colvine, 1989). In general, all orogenic gold deposits are found associated with the stresses of accretion/mountain building (Kerrich, 1989). Gold mineralization tends to occur late in the tectonic events, when ductile deformation gives way to brittle deformation (Kerrich, 1989). Anastamosing shear zones are created during this time. Fluids find conduits along the fractures formed and precipitate minerals including native gold (Sibson, 1988; Groves et al, 1998). Pressure and temperature data has a range from 180 - 700°C and ~1-5 kbar (Groves et al., 1998). Gold is deposited in veins or in sulphide altered wall rock (Colvine, 1989). Quartz flooding/veining and calcite/carbonate veining/flooding is commonly associated with gold mineralization. An unusual suite of minerals is associated with orogenic gold mineralization: arsenopyrite, rutile, scheelite, tourmaline, molybdenite, stibnite and native bismuth are found as accessory minerals to gold mineralization (Kerrich and Cassidy, 1994; Wood et al., 1986). More unusual are the low concentrations of copper, zinc, and lead in orogenic gold deposits, as the concentrations of these elements in the presumed source rocks is considerably greater than that of gold. Another common feature of Archean orogenic gold deposits is the presence of felsic, frequently alkalic, intrusions (Kerrich, 1989). These intrusions are

presumably emplaced during orogenesis, and take advantage of the same paths created by both brittle and ductile faulting as did the gold-bearing fluids. These intrusions tend to be syn- to post kinematic with regards to gold mineralization (Kerrich, 1989).

The source of the gold is of great interest to both the scientific community and industry, and has been debated for decades. Currently, two views are popularly held: either it is fluid exhaled from a magmatic body (magmatic theory; i.e., Wood et al., 1986; Burrows and Spooner, 1987) or it comes from the surrounding rocks that host the deposit (metamorphic theory; i.e., Fyfe and Kerrich, 1982; Kerrich and Cassidy, 1994; Jia, 2001). Those supporting a magmatic-derived fluid model contend that the gold mineralization is derived from the various intrusive rocks frequently associated with these deposits. Those in favour of metamorphic origins argue that concentrations of gold in granitic rocks are very low (somewhere on the order of 1 ppb), so to manage to concentrate gold in the amounts seen in the average producing gold deposit requires considerable enrichment (Fyfe and Kerrich, 1982). At those concentrations one would need to leach roughly $100km^3$ of rock in order to produce a 10 million gram gold deposit at a grade of 5-10 g/t (Fyfe and Kerrich, 1982). Thus, it is argued that the alkalic stocks associated with gold deposits are too small to be the source of the gold and unless the stocks in question are anomalously rich in gold, and that gold is for some reason very efficiently removed from such a stock, it is far more likely that the source fluids are derived from metamorphic processes (Kerrich, 1989). However, there is some evidence that the production of adakitic melts under certain conditions can produce very high gold concentrations in these melts (Mungall, 2002). It must also be noted that depletion of several hundred cubic

kilometers of rock and transport to the site of gold and accessory elements (B, Bi, Hg, W, etc.), while avoiding removal of other more common commodities such as lead or zinc and loss of complexing agents to fluid-rock interaction using only metamorphic fluids is a very complex problem in and of itself.

In an attempt to resolve the issue of origins of auriferous fluids, researchers have conducted a variety of geochemical studies. Among these are isotopic studies, hoping to discern the source of fluids that transported the gold. $\delta^{18}O$ isotopic data calculated for waters in shear zones in these gold deposits tend to be well-constrained, and most have values that sit within the area of overlap between magmatic and metamorphic waters (Wood et al., 1986; Burrows and Spooner, 1987; Kerrich and Cassidy, 1994). Because of the overlap in oxygen isotopic range for magmatic and metamorphic fluids (see Fig 3.1 in Chapter 3), the geochemistry of these deposits is used by both sides in an effort to support their arguments and to cast doubt on the other. Magmatic-fluid theory supporters base their arguments on the fact that the $\delta^{13}C$ values preclude metamorphic degassing (Burrows et al., 1986). In contrast, those in favour of metamorphic origins argue that the $\delta^{13}C$ values are not unique to magmatic fluids and that some of the values reported for lode gold deposits sit outside the accepted range for hydrothermal fluids of magmatic origin (King and Kerrich, 1989). Because of the abundance of oxygen in the crust, and the large area of overlap between the isotopic fields of primary magmatic and metamorphic waters, other isotopes have been used to try to resolve this ambiguity. Of the traditionally studied stable isotopes, nitrogen shows the most promise of giving some resolve to the issue.

Approximately 98% of nitrogen contained on Earth is found in crystalline rocks (Sharp, 2007). The two major speciations of nitrogen within the earth are as N_2 in fluid phases and also as ammonia (NH_4^+). The ammonia species substitutes for K^+ in small concentrations in potassic minerals. Studies undertaken on diamonds have revealed that the mantle has a $\delta^{15}N$ signature of approximately -5‰ (Sharp, 2007). Fluid inclusions found in basalts give a signature of -5 to +5 ‰(Sharp, 2007). Gases retrieved from volcanic activity in island arc systems have a negative $\delta^{15}N$ signature (Sano et al., 2001; Fischer et al., 2002 in: Sharp, 2007). Felsic plutonic signatures vary, but are essentially identical to those of basalts.

The $\delta^{15}N$ signature in sedimentary rocks can be lowered somewhat during diagenesis as a result of the incorporation of organic detritus, depending on the trophic level of the organisms (Sharp, 2007); organic material also contains high concentrations of nitrogen relative to the sediments, so the presence of organic detritus also raises the total N concentration of these rocks (Orberger et al., 2005; Kroos et al., 2006). As rocks are buried, nitrogen is lost from the rocks to the fluid phase, with the lighter isotope ^{14}N escaping preferentially (Haendel et al., 1986). The result is a progressive decrease in overall N concentration and an increase in $\delta^{15}N$ signature during prograde metamorphism.

Because of the difference in isotopic signature between magmatic, meta-igneous and metasedimentary rocks, it becomes possible to use nitrogen to determine the source of fluids creating alteration within a particular deposit.

1.12 Methods

1.12.1 Sample Preparation

From the sixty samples taken from mine core and thirty-eight regional hand samples a total of thirty-five samples were selected for processing and analysis. Samples were photographed, crushed using a tungsten carbide steel mortar and pestle to a size of approximately 0.5 cm, and further crushed using an agate rotary mill for ~20 second intervals. In order to eliminate contamination between samples, the mill, mortar and pestle were cleaned first with water, then with acetone to remove residue before each sample was crushed. The samples were then sieved and the #100 - #200 size fraction of each sample was taken for further processing. Biotite was separated from other minerals using a Frantz mineral separator and, when required, by use of heavy liquid separation using methylene iodide and tetrabromoethane. Samples were then checked using XRD to ensure that the samples were ~98% pure or better. The samples were cleaned with 30% hydrogen peroxide to dissolve any organic material left from processing and then sent for analysis.

Thirty quartz samples were also separated from the crushed samples via Frantz magnetic separation. These samples were bleached in 0.5 M HCl solution for two days to destroy any iron-bearing constituent minerals. The cleaned samples were then analyzed via XRD to ensure purity and cleaned with 30% H_2O_2 to remove any organic compounds accumulated due to processing.

Four sets of quartz-magnetite pairs were also selected from the Musselwhite mine site in an effort to constrain peak metamorphic temperature. Suitable samples of visually "pristine" oxide iron formation (i.e. few to no additional silicates) were selected from

core. These were then processed using the method of Valaas (2004): samples were cut into a thick section to help constrain the mineral pairs spatially. The thick section was then crushed and sieved, and quartz and magnetite were hand picked from the resulting size fractions. Magnetite was removed using a hand magnet. Quartz was hand picked, and any quartz grains with magnetite inclusions were removed using a Frantz magnetic separator. Both were analysed by XRD to ensure purity before being sent for analysis.

1.12.2 Isotopic Analysis

Nitrogen isotopic signatures were analysed using a Costech Elemental Analyzer coupled to a Thermo Finnigan Delta XP Mass Spectrometer. Around 80 mg of sample was loaded in a tin bucket, then pyrolized at 800°C. Oxygen samples were collected as carbon dioxide via a bromine pentafluoride extraction line using the process of Clayton and Mayeda (1963) and then analyzed using a Finnigan Mat 252 Mass spectrometer. The hydrogen isotopic data was collected using a Thermo Finnigan TCEA coupled to a Thermo Finnigan Delta XP CF-MS using. Analyses were carried out by staff at Queen's Facility for Isotope Research. Standards used were N_{air} for nitrogen, whtxtl for oxygen (an in-house standard with a known composition relative to VSMOW) and VSMOW for hydrogen. Errors are 1‰ for nitrogen, 0.2‰ for oxygen and 5‰ for hydrogen.

1.12.3 SEM analysis

After petrographic analysis, nine thin sections were selected, carbon coated and then examined using the JEOL JSM 5900 LV scanning electron microscope (SEM) detector resolution of 133 eV in the Lakehead University Instrumentation Lab (LUIL). Fe, Mg, Ti, K, Na, Ca, Al, and Si were used for silicate identification and estimation of biotite

compositions. Spectra were analysed using LINK ISIS software. Spectra were acquired using a 50 second analysis period (live time) and an accelerating voltage of 20 keV and a beam current of 0.465 nA. Elements were reported as oxides, with total iron being reported as FeO. Standardization was carried out on silicate and oxide standards. FeO was standardized on hornblende (Mn-Hor), periclase for MgO, orthoclase for K_2O, ilmenite was used for TiO_2, jadeite for Na_2O, wollastonite for CaO, corundum for Al_2O_3, pyroxene for SiO_2 .

1.12.4 Whole Rock analysis

Whole rock analyses were provided courtesy of Musselwhite Mine. Analyses were performed by Activation Laboratories Inc. using lithium metaborate/tetraborate fusion of samples coupled with ICP-MS. Detection limits for elements analysed are found in Table 1.1. Eu determinations are semiquantitative in samples having extremely high Ba concentrations (greater than 1%) and data may be semiquantitative for chalcophile elements (Ag, As, Bi, Co, Cu, Mo, Ni, Pb, Sb, Sn, W and Zn) (Actlabs, 2008 http://www.actlabs.com/gg_rock_litho_can.htm).

Table 1.1: Detection limit of elements analysed by Activation Laboratories Inc.

oxide	limit	element	Limit (ppm)	element	Limit (ppm)
SiO2	0.01%	As	5	Sb	2
Al2O3	0.01%	Ba	3	Se	1
Fe2O3	0.01%	Bi	4	Sn	5
CaO	0.01%	Ce	10	Sr	2
MgO	0.01%	Cr	20	Ta	10
Na2O	0.01%	Cu	10	Th	2
K2O	0.01%	Ga	1	U	4
Cr2O3	0.01%	La	1	W	10
TiO2	0.01%	Mo	2	Y	2
MnO	0.01%	Nb	2	Zr	5
P2O5	0.01%	Ni	5	Zn	10
SrO	0.01%	Pb	2	V	5
BaO	0.01%	Rb	2		
LOI	0.01%				

CHAPTER 2 – PETROGRAPHY

2.1 Introduction

Biotite can be found throughout all units at the Musselwhite mine, both metasedimentary and metavolcanic. However, in certain units, such as the oxide facies iron formation, these bands are very small and only occur as a very minor phase so it is generally ignored or overlooked in generalized descriptions of these units. This chapter will describe the biotiferous units found at the Musselwhite Mine, and compare and contrast their occurrence and associated mineral assemblages.

2.2 Previous work

A number of petrological studies have been undertaken on the rocks at the mine. A previous study of the rocks by Wells (1995) helped define the units and alteration assemblages. Otto (2002) completed a brief characterization of the rocks, their mineral assemblages and relationships to aid geothermometry calculations. Additional petrographic work was carried out by Moran (2008) in order to characterize the various sedimentary units in an effort to develop a better depositional model of the rocks that host the Musselwhite deposit.

2.2.1 Garnet-biotite schist (4F)

The study by Otto (2002) characterized the 4F unit by the presence of garnet, biotite and quartz with occasional showings of staurolite and grunerite. Garnets in this unit have inclusion rich cores and inclusion free rims, indicative of two distinct generations of growth (Otto, 2002). Both biotite and garnet have grown along the S_2

foliation (Otto, 2002). The 4F layer is intermittent and frequently forms “pods” within the tholeiitic metabasalt unit, with or without the accompanying unit and is interpreted to be a ferruginous pelitic metasedimentary rock. Breaks et al. (2001) postulated that the 4F unit might possibly correlate with the ELS.

2.2.2 Silicate Facies Iron Formation (4EA)

The 4EA unit is characterized by the mineral assemblage quartz-grunerite-garnet (Wells, 1995; Otto, 2002). It has been classified as a silicate-dominant iron formation (Moran, 2008). Five types of bands have been observed: 1) iron-rich mineral bands that are dominated by grunerite-cummingtonite, garnet, and magnetite, 2) hornblende-rich bands containing hornblende, garnet, plagioclase and quartz as well as minor grunerite, magnetite, ilmenite, and pyrrhotite, 3) biotite-rich bands with associated garnet and quartz, 4) calc-silicate bands containing calcite, clinopyroxene, plagioclase and hornblende and 5) quartz bands with some minor grunerite-cummingtonite intergrowths (Otto, 2002). Hornblende in this unit has dark green-blue pleochroism and is mostly ferro-tschermakitic in composition (Otto, 2002). The grunerite-cummingtonite is coarser in this unit than the underlying 4B, and garnets are rich in grunerite inclusions, and have irregular edges that are intergrown with surrounding grunerite (Otto, 2002). Ga. nets in the iron–rich bands are frequently rotated and contain inclusions of grunerite and ilmenite (Otto, 2002). Some minor retrograde chlorite is seen in this unit (Otto, 2002). Most of the gold is hosted within this unit, although it has been noted that gold mineralization is merely stratiform, not stratabound (Hall and Rigg, 1986). Garnet-biotite, albite and

carbonate alteration as well as quartz flooding is commonly associated with Au mineralization within this unit (Kiernan and Blower, 2003).

2.2.3 Oxide-facies Iron Formation (4B)

The 4B unit is characterized by finely laminated layers composed of quartz, magnetite and grunerite. Some garnet and local biotite-amphibole alteration is present. Otto (2002) identified three compositional layers within the 4B unit: 1) bands comprised of Fe-rich magnetite, prismatic grunerite-cummingtonite with associated minor biotite and hornblende; magnetite and grunerite are often internally layered 2) quartz bands and 3) garnet-rich layers with prismatic grunerite-cummingtonite, biotite, hornblende and quartz. Garnets in the latter layers have resorbed rims and frequently contain inclusions of fibrous grunerite (Otto, 2002). Minor plagioclase, hornblende and calcite are also present in this unit (Otto, 2002).

2.3 Mine Petrography

Biotite-rich units are found within the metavolcanic rocks. Biotite in these units is generally medium to fine-grained, with dark brown to green pleochroism. A significant amount of quartz is associated with the biotite. Some samples display large porphyroblasts of hornblende with biotite inclusions (Plate 2.1a). The contact between biotite-rich units and the adjacent units is typically sharp.

Petrographic examination of samples taken from the 4F unit reveals that the unit contains a significant proportion of quartz and/or plagioclase. The content

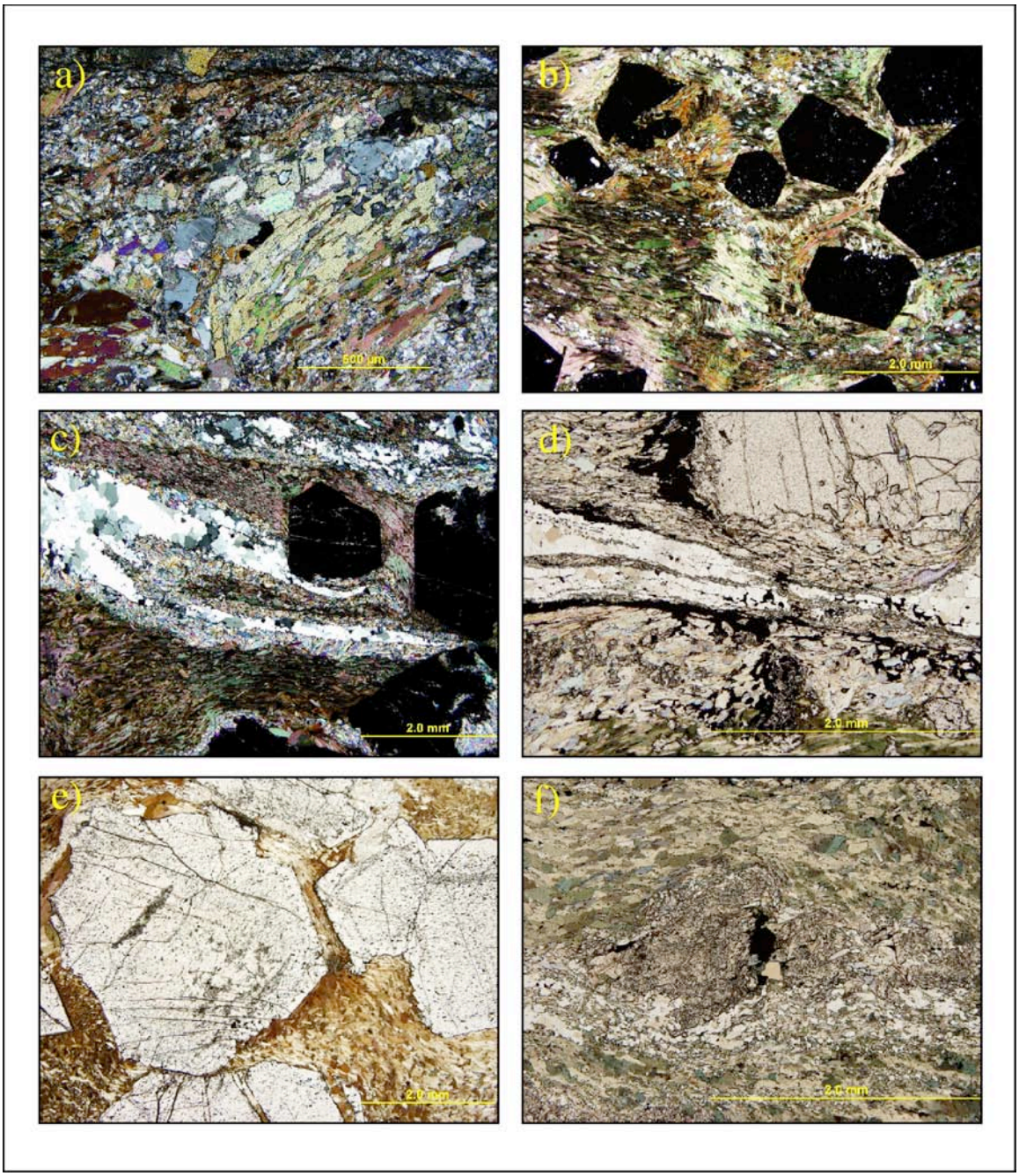

Plate 2.1: Textures of biotiferous units at Musselwhite. a) hornblende crystals with biotite inclusions from biotiferous units in metavolcanic rocks (E358108, XPL) b) typical "4F" biotite-garnet schist (E354043, XPL) c) grunerite mantling of quartz flooding in biotiferous portion of silicate-dominant iron formation(E354026, XPL) d) pyrrhotite mineralization on margins of quartz flooding (E354013, PPL) e) large, equant garnets in the silicate-dominant iron formation (E354016, PPL) f) elongated garnet in silicate-facies iron formation (E354024, PPL).

ranges from sample to sample –quartz and feldspar grains comprise anywhere from less than 5% to up to 60% of the rock. The grains of plagioclase are quite small, irregularly shaped and are randomly oriented. Quartz grains are approximately the same size as plagioclase grains, and occur as equant to anhedral grains. Biotite defines foliation except in the presence of garnet, where it grows around the perimeters of garnets. Garnet grains in the unit are typically small (approximately 0.5-1 mm) and euhedral to subhedral (Plate 2.1b). Larger garnet grains have inclusion-rich cores and clear, inclusion-free rims, whereas the smaller garnet grains are generally inclusion-free, suggesting they are also late stage. The biotite itself is medium to coarse grained and frequently a dark red-brown, possibly indicating high titanium contents.

The biotite-rich portions of the silicate-dominant iron formation unit have a wide variety of textures. Biotite is typically reddish brown to green pleochroic, medium-grained to coarse grained, and generally lies along foliation, although there are typically some laths that deviate from foliation especially in the presence of garnet. When found in the vicinity of garnet, the biotite is often truncated by garnet indicating consumption of biotite during garnet growth, and some inclusions of biotite are seen within garnet. Biotite becomes finer grained approaching quartz flooding, and is typically replaced by grunerite adjacent to the quartz veins (Plate 2.1c). Pyrrhotite is found on the margins of quartz-grunerite bands associated with grunerite, hornblende, biotite, magnetite and garnet (Plate 2.1d).

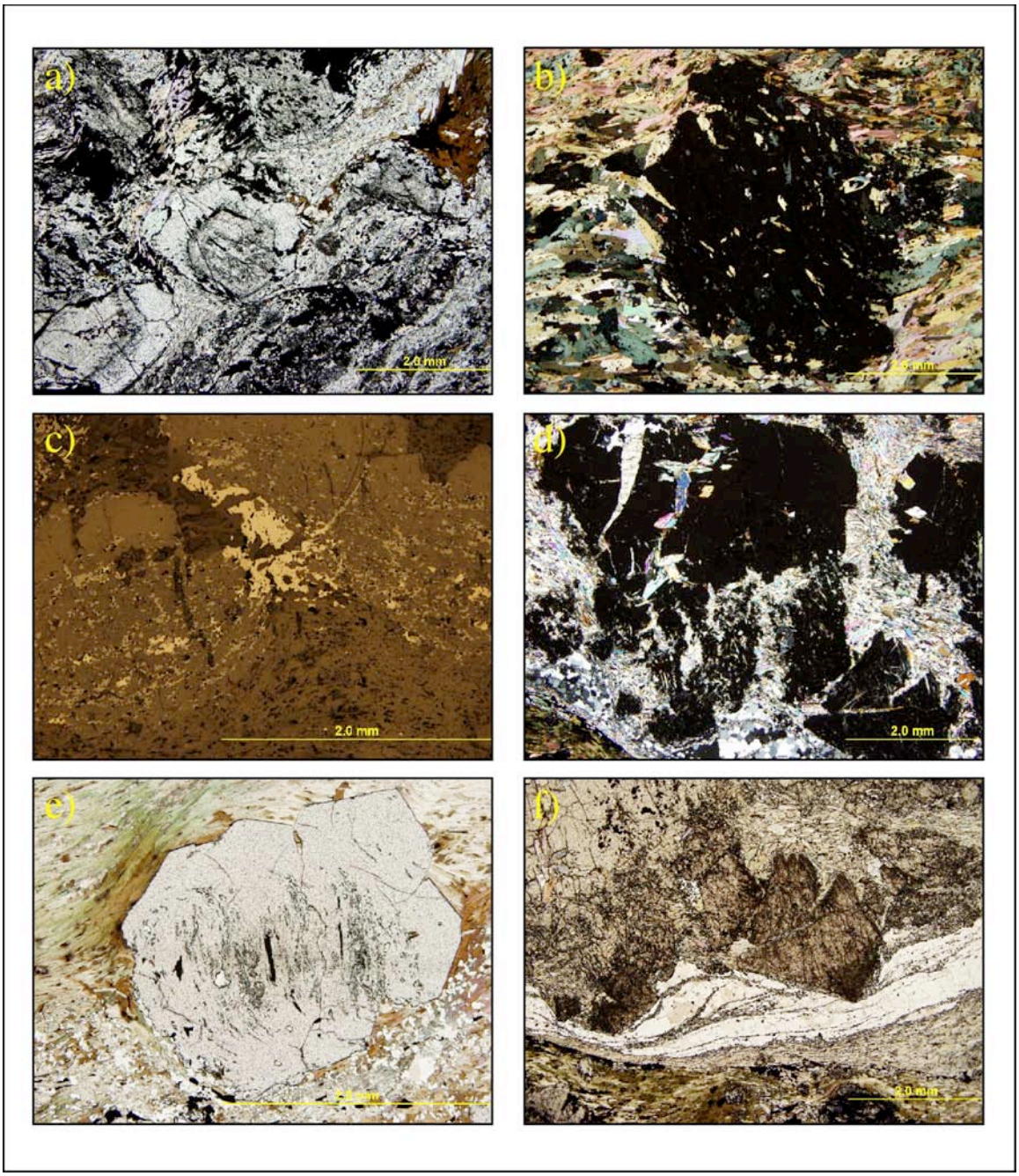

Plate 2.2: Textures of biotiferous units of the silicate-dominant iron formation (4EA unit). a) irregular aggregates of garnet with accompanying grunerite and biotite mineralization (E354013, PPL) b) hornblende inclusions in garnet (E354039, XPL) c) ilmeno-magnetite and pyrrhotite inclusions in garnet (E358103, REFL) d) prismatic grunerite inclusions in garnet (E354013, XPL) e) snowball texture in garnet with inclusion free rim (E358103, PPL) f) pinching of quartz vein by garnet (E354013, PPL).

Garnet is frequently associated with the biotite and range in morphology from large, equant specimens (Plate 2.1e) to elongated specimens (Plate 2.1f) to highly irregular aggregates (these are typically associated with grunerite or biotite; Plate 2.2a). Garnets may or may not have recrystallized edges. Mineral inclusions within garnet include quartz, biotite, hornblende, prismatic grunerite, ilmenite, magnetite, and pyrrhotite (Plate 2.2b-d). Snowball textures of these inclusions in some garnet grains show that these garnet grains have frequently been rotated; however, these inclusions are generally not found in the garnets' outer rims (Plate 2.2e). Quartz flooding and massive quartz veinlets frequently have pinched textures in the presence of garnet (Plate 2.2f).

Biotiferous bands of the oxide-dominant BIF are comprised of many minerals including coarse-grained quartz, calcite, prismatic and fibrous grunerite, hornblende, biotite, and pyrrhotite. Mineral inclusions in garnet are varied but include quartz, calcite, hornblende, grunerite (both of the fibrous and prismatic variety), ilmenite-magnetite, pyrrhotite and biotite (Plate 2.3a-c). Prismatic grunerite and hornblende are included within garnet and also form a rim around some garnet grains along with accessory calcite and chlorite. Magnetite and pyrrhotite are common inclusions in garnet, but only rarely found occurring together. Biotite and calcite inclusions are found filling fractures in garnet. Sample E354040 has massive pyrrhotite veinlets with accessory chlorite, quartz, biotite and grunerite inclusions. Some garnet in the biotite-rich units appear to pseudomorph a tabular mineral, possibly plagioclase (Plate 2.3d). Garnet growth is highly irregular, forming anywhere from subhedral to irregular anhedral "shards" within these

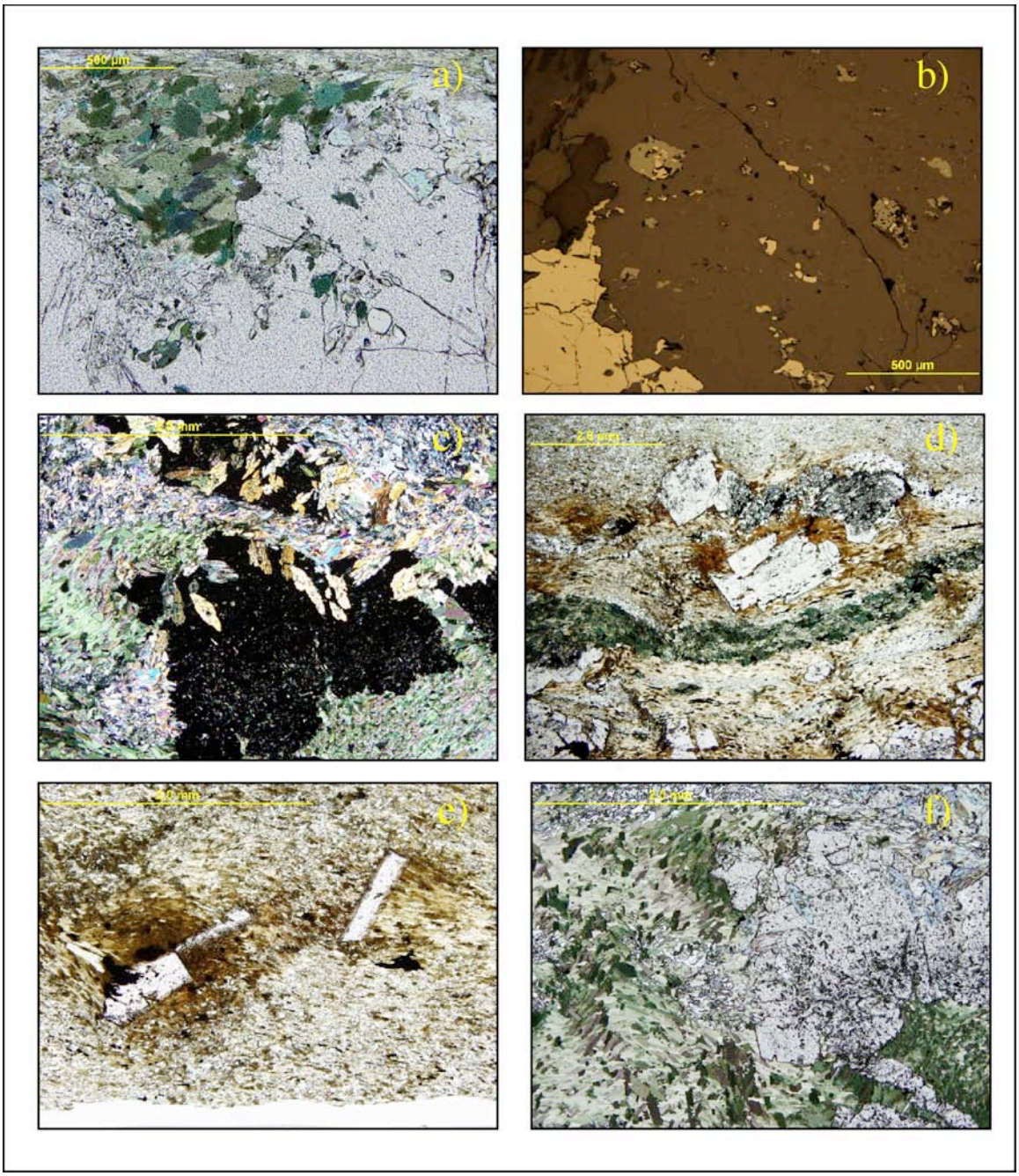

Plate 2.3: Textures found in biotiferous units of the oxide-dominant iron formation (4B unit). a) hornblende (green) and grunerite (colourless) inclsions in garnet (E354020, PPL) b) pyrrhotite and ilmeno-magnetite inclusions in garnet (E35040, REFL) c) coarse-grained grunerite inclusions and fine-grained biotite inclusions in garnet (E354018, XPL) d) garnet pseudomorph of tabular mineral (E354010, PPL) e) shards of garnet (E354010, PPL) f) habit of biotite (green) growth around garnet – note lack of foliation (E354018, PPL).

units (Plate 2.3e), and may sometimes possess euhedral, flat, late-stage growth faces, which generally do not contain inclusions. Garnet grains frequently have an elongated morphology in finer grained, foliated units. Random orientation of biotite growth is common around garnets (Plate 2.3f).

2.4 Regional Petrography

2.4.1 Mafic metavolcanic rocks

Samples from the north of the Musselwhite mine, from the North Shore of Opapimiskan Lake, are deep green in hand sample and contain approximately 25-50% fine grained quartz. This is mixed with 50-70% hornblende, and other minerals such as calcite, plagioclase, biotite and grunerite. Grains of pyrrhotite are also present (Plate 2.4a). Hornblende varies texturally, from very coarse grained, poikiloblastic crystals (Plate 2.4b) to very fine-grained, irregular masses (Plate 2.4c).

Sample E438516 was collected from a mafic metavolcanic unit on the NE margin of the NCLGB (Fig. 2.1). The hand sample is very green, yet contains approximately 30% quartz and another 20% plagioclase feldspar. The remainder of this rock is comprised of hornblende and pyroxene in varying amounts. Mineral grains in this rock are equant and approximately of equal size (Plate 2.4d). The high quartz content suggests an additional input of quartz into the rock.

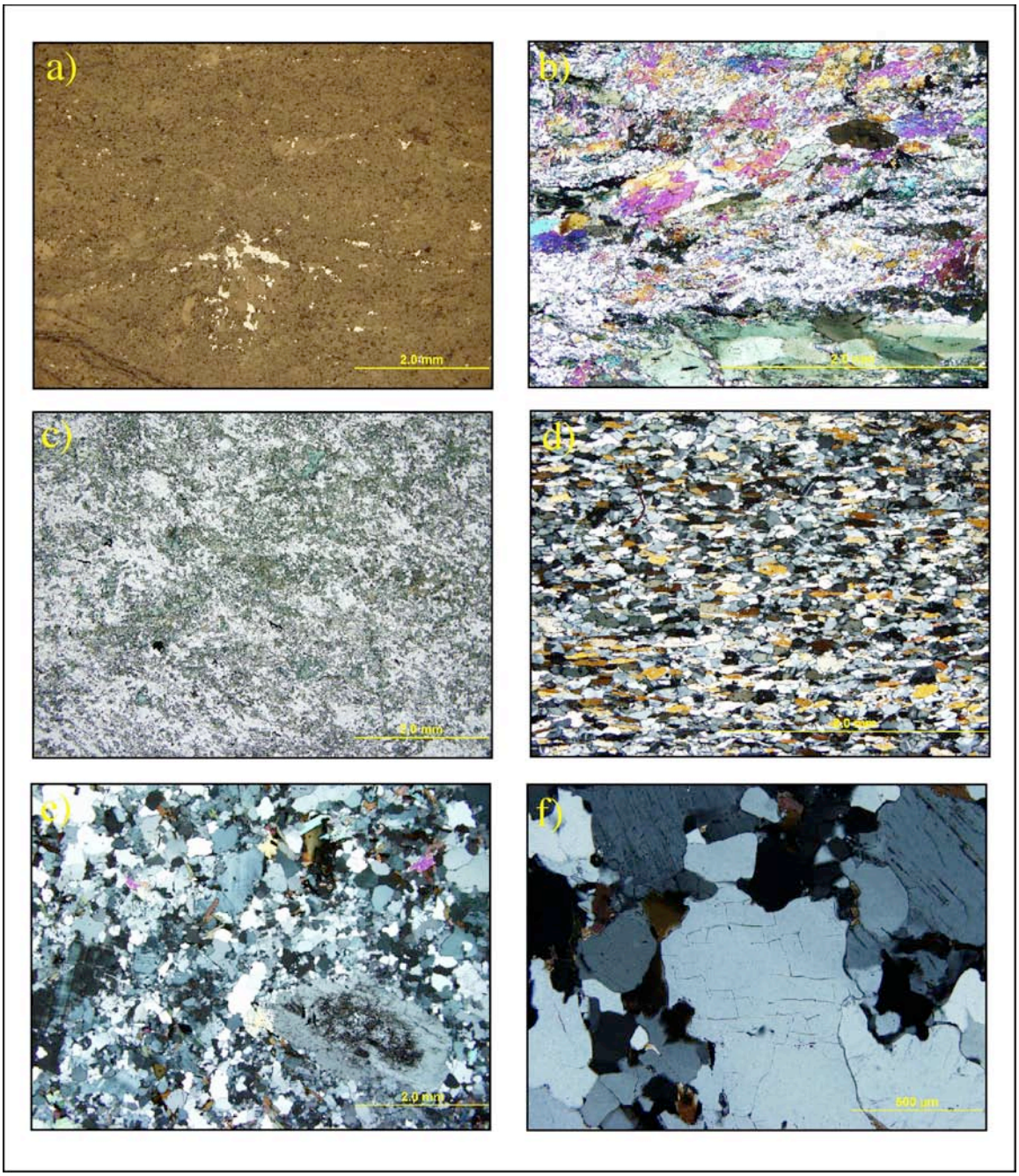

Plate 2.4: Regional rocks of the North Caribou Lake greenstone belt. a) pyrrhotite mineralization in mafic metavolcanic rocks from the north shore of Opapimiskan Lake (E438501, REFL) b) showing coarse-grained aggregates and poikiloblastic hornblende and pyroxene with interstitial quartz (E438506, XPL) c) fine-grained aggregates of hornblende in mafic metavolcanic rock (E438506, PPL) d) mix of hornblende, plagioclase and quartz (E438516 , XPL) e) showing porphyritic texture with feldspar phenocrysts (E438531, XPL) f) brittle fracturing of quartz in granitoids (E438508, XN).

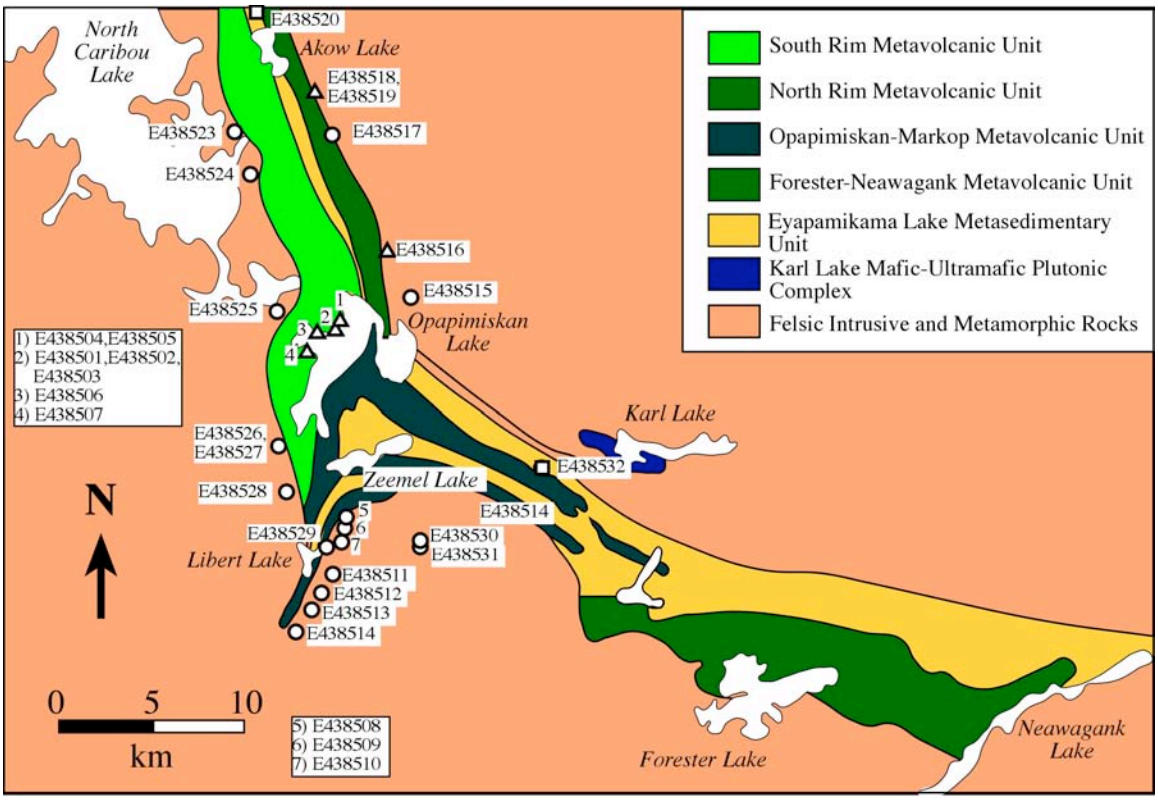

Figure 2.1: map of the North Caribou Lake greenstone belt showing the locations of samples. Triangles = mafic samples, circles = felsic samples, squares = metasedimentary samples.

2.4.2 Granitoid rocks

The felsic plutonic rocks of the North Caribou Lake greenstone belt are typical Archean granitoids. The granitoids vary in texture and grain size, with quartz and finer grained feldspars forming the bulk of the matrix. Accessory minerals vary from sample to sample over very short distances. Minor mineral phases include biotite, muscovite, zircon, hornblende, titanite and baddelyite as well as some minor opaque phases. A few of the plutons are porphyritic, with large feldspar phenocrysts up to 1-2 cm long (Plate 2.4e). Samples from plutonic material adjacent to the greenstone belts display strain textures such as brittle fracturing of quartz and feldspar (Plate 2.4f), deformed growth of

micas in “wavy” morphologies (Plate 2.5a), and recrystallization textures in quartz. Biotite in some samples has been partially replaced by chlorite (Plate 2.5b).

2.4.3 Metasedimentary Rocks

Sample E438532 comes from the southern portion of the Eyapamikama Lake Metasedimentary unit (Fig. 2.1). The rock is composed chiefly of quartz, feldspar and biotite, most of which is fine-grained to very fine-grained with a few larger crystals. Some larger grains are apparent at low power magnification. These larger crystals have very blurry edges, yet are distinct from the fine-grained matrix (Plate 2.5c). Biotite in the rock occurs in small, oriented aggregates and throughout the rock in very fine-grained, randomly oriented laths (Plate 2.5d). A few grains of sulphide, possibly pyrite, are located within the rocks. The grains are approximately 0.5 – 1mm long and are euhedral to anhedral in morphology. Rinds of oxide (likely magnetite) are found on the sulphide, and the sole euhedral grain has inclusions of rutile (Plate 2.5e). Coarse-grained quartz-hornblende-calcite alteration of the rock occurs as medium grained, equant crystals of biotite-free quartz, feather-textured actinolite, hornblende crystals and calcite infilling. Rutile-magnetite and biotite are found on the periphery of a veinlet of this alteration.

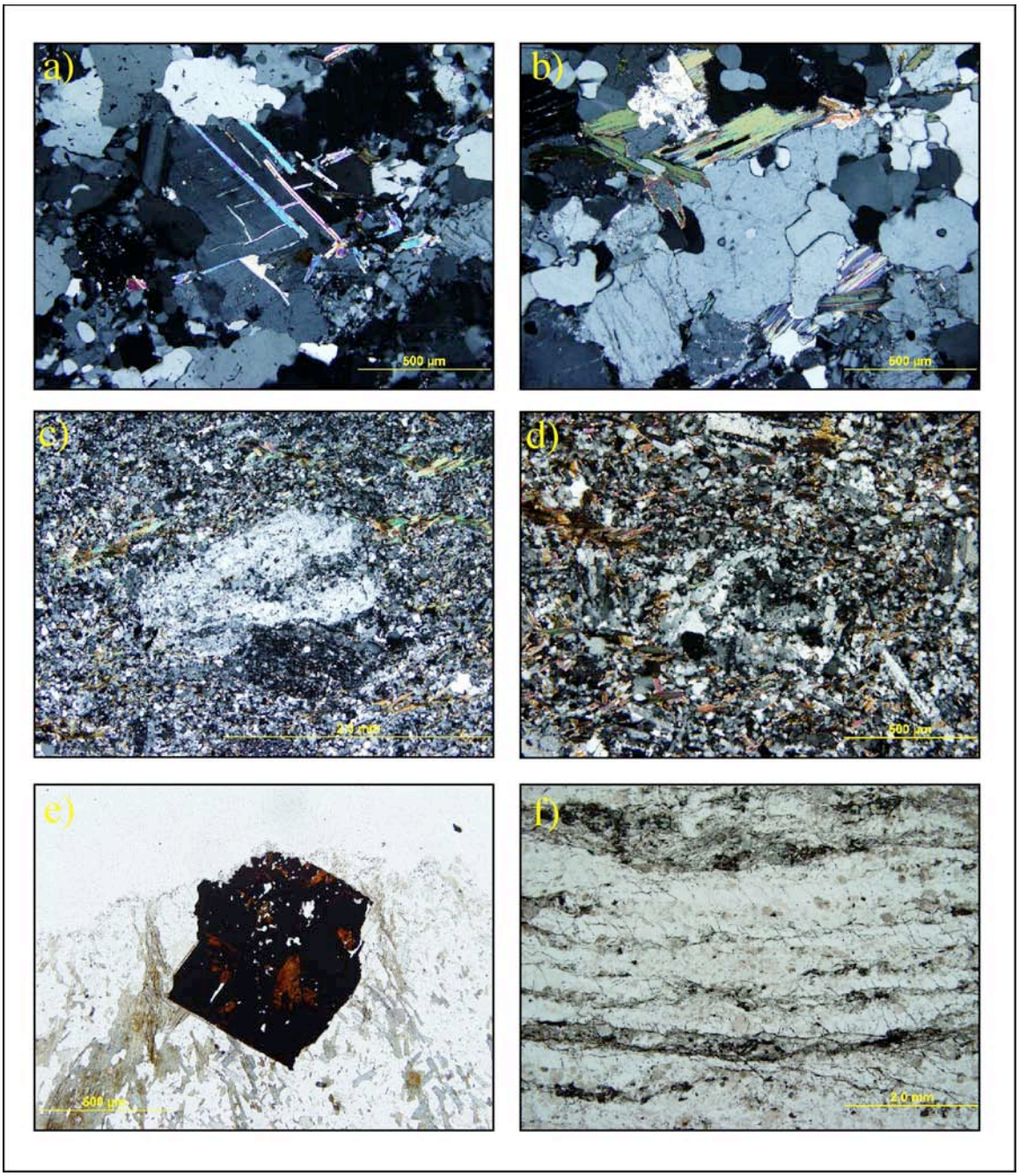

Plate 2.5: Regional rocks in and surrounding the North Caribou Lake greenstone belt. a) wavy growth of mica in fractured feldspar (E438513, XPL) b) biotite (green) being progressively replaced by chlorite (blue; E438515, XPL) c) clast with blurred edges (E438532, XPL) d) fine-grained interstitial biotite in metasedimentary rock (E438532, XPL) e) rutile (brown) inclusions in pyrite grain (E438532, PPL) f) shear planes and grain size reduction in quartz-rich metasedimentary rock (E438520, PPL).

The sample taken from the ELS to the north of Akow Lake (Fig 2.1) is quartz rich, with a few bands that are primarily amphibole. Grain size reduction and slip planes are evident within the rock (Plate 2.5f).

2.5 Discussion

The granitoid rocks surrounding the North Caribou Lake greenstone belt appear to be typical Archean felsic plutonic rocks (Plate 2.4e,f; Plate 2.5a,b). The alteration of biotite to chlorite indicates that fluids have permeated the felsic plutonic rocks, likely aided by brittle deformation of the rocks. The presence of ductile and brittle deformation features in the plutonic rocks to the south of Musselwhite reveals that the pluton had already been emplaced before the onset of ductile and brittle deformation in the North Caribou Lake greenstone belt, and thus likely predate mineralization of the Musselwhite Mine. The age of this complex at around 2730 Ma could possibly set an upper limit for the onset of brittle deformation in the North Caribou Lake greenstone belt.

The mafic metavolcanic samples of the North Caribou Lake greenstone belt show a range of alteration styles. Sample E438516, taken from an area that is defined as the edge of the North Caribou Terrane (the Dinnick Lake shear zone; Fig 2.1; Breaks et al., 2001) is most likely a composite of what was originally mafic metavolcanic material with more felsic material – though whether the felsic material came from a sedimentary or an igneous source is impossible to tell. It is possible that the additional quartz is the result of quartz flooding in the rocks within and immediately adjacent to the shear zone. The lack

of brittle features in this sample could indicate the center of the shear zone, where strain was more uniform.

One sample taken from the north shore of Opapimiskan Lake contains 20% biotite. This could be another pocket of pelitic metasedimentary rock in the mafic metavolcanic sequence, but the sheared texture of the rocks and the presence of massive, fine-grained quartz flooding, quartz and calcite veining and pyrrhotite indicates that biotite is more likely the product of alteration in sheared material.

The mineral association of biotite-grunerite-garnet-quartz-pyrrhotite mineralization is present in all units of the NIF. This assemblage is not restricted to the iron formation itself, but both underlies and caps the deposit and is present in the mafic metavolcanic rocks. The small, discrete bands of aluminous silicate minerals within the iron formation have been previously attributed to the presence of an increasing clastic component in the iron formation (Moran, 2008) and have been interpreted as pelitic lamellae that have undergone straightforward dehydration metamorphism. Moran (2008) also noted that the geochemistry of the biotite garnet schist (which is considered to be the most clastic-rich unit apart from the garnet quartzite unit) indicated only 20-40% of the unit was detrital. If this is true, then the overwhelming majority of the biotite seen at the Musselwhite mine is hydrothermal rather than detrital in origin (or, at the least, has been altered sufficiently that very little of it reflects the original detrital signature).

The habit of garnet and grunerite samples associated with mineralized areas is markedly different than that found in non-mineralized areas, with mineralized samples containing coarse-grained grunerite and irregular very coarse-grained garnet frequently intergrown with one another on the edges of the main quartz veins and accompanying

pyrrhotite mineralization (Plate 2.3c). The change in character of mineralization suggests fluid transport closely associated with gold mineralization. This could explain why mineralization was once thought to be stratabound within the 4ea unit, as subtle differences in the character of the mineral assemblages would be indistinguishable at hand sample scale.

The extreme difficulty in visually distinguishing between biotiferous units occurring in the various portions of the NIF and the adjacent metavolcanic rocks and the difficulty in determining origin based on petrology alone makes it very difficult to visibly establish an associated alteration assemblage for gold mineralization at the Musselwhite mine. While characterisation via petrographic microscope may be a viable way of determining a mineralisation assemblage, it would be a very time consuming method. Mineral geochemistry is a possible solution to what cannot be readily determined visibly.

CHAPTER 3: STABLE ISOTOPE GEOCHEMISTRY

3.1 Introduction

Stable isotopes are regularly used to investigate the origin of fluids that form mineral deposits, especially Archean orogenic gold deposits (e.g., Burrows et al., 1986; Golding and Wilson, 1987; Bierlein et al., 2005; Stemler et al., 2006). Often several isotopic species are used in order to gain a better understanding of the nature of fluids that have interacted with the minerals of the deposit. Oxygen and hydrogen isotopes have been frequently analysed in the past in order to estimate the original composition (and by extension, origin) of the fluids involved in the formation of the mineralisation (Golding and Wilson, 1987). Nitrogen has more recently come to the forefront in the investigation of gold-bearing fluids (Jia and Kerrich, 2001).

There has been, and still exists today, a debate regarding the source of fluids that transported gold in Archean orogenic gold deposits (Hodgson, 1993). Of the two major theories held in favour today, one maintains that the fluids were the product of devolatilisation of nearby felsic intrusions, the other argues for metamorphic fluids being the transport mechanism (Hodgson, 1993). Both use isotopes to support their respective cases.

Historically, oxygen has been considered the most useful isotope to examine in rocks. Its abundance in rocks makes it easy to acquire a measurable signature in small quantities. It is sensitive to changes in temperature, and can be used to estimate the temperature of formation of many different minerals, thus making it possible to estimate the temperature of formation of accessory minerals associated with gold mineralisation. Oxygen was among the first isotopes used to attempt to characterize fluids in gold deposits, especially considering the association of gold with quartz veins (Kerrich and

Cassidy, 1994; Poulsen, 1995; Vallance et al., 2003). The major issue with using oxygen to determine the source of auriferous fluids in orogenic gold deposits is the large window of overlap between metamorphic and magmatic fluid sources (Fig. 3.1). Many gold deposits fall in and around this window of overlap (Kerrich and Cassidy, 1994; Jia and Kerrich, 2000; Pitcairn et al., 2005).

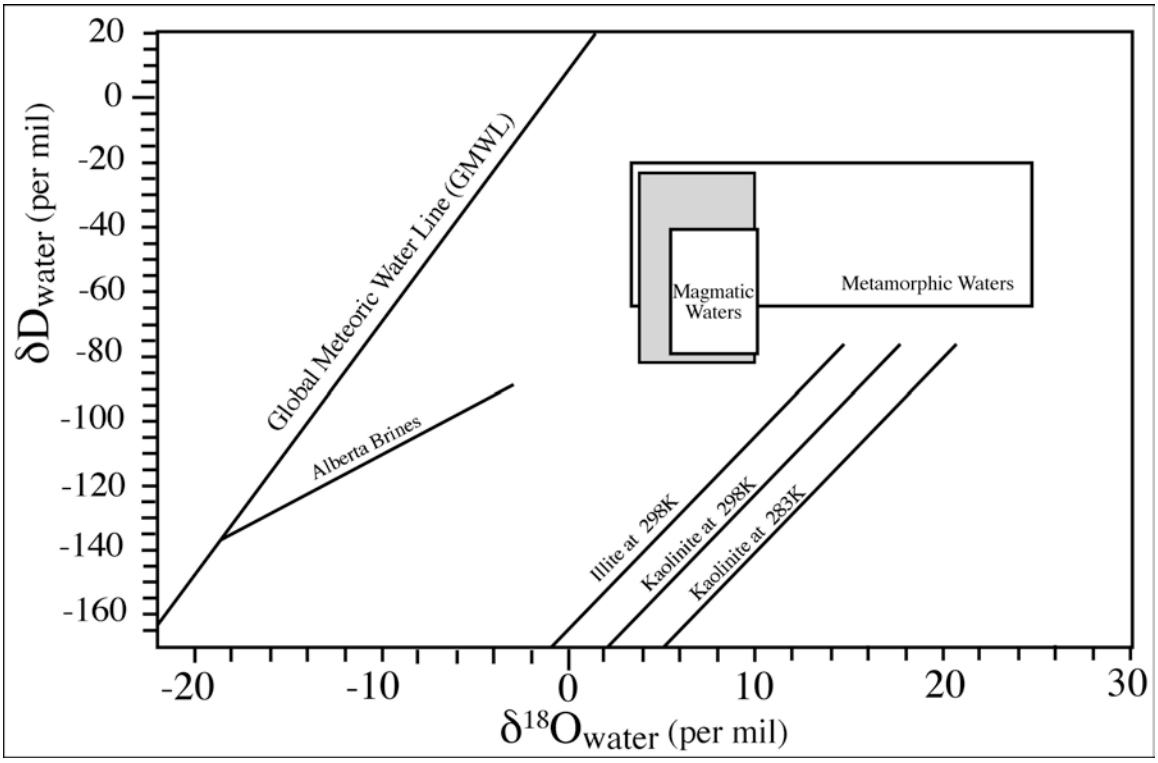

Figure 3.1: Graph of oxygen and hydrogen isotopes of fluids for different rock types and measured waters measured relative to VSMOW. After Taylor, 1974. Shaded field represents the field for orogenic gold fluids from Kerrich and Cassidy, 1994.

Because of its abundance and sensitivity to temperature changes, the primary isotopic signature of oxygen is very susceptible to overprinting by later fluids and events. Even the process of cooling, if slow enough, may permit isotopic re-equilibration at a lower temperature, destroying the original signature (Garlick and Epstein, 1967). Much effort has been made to establish the temperature at which point no more significant

fractionation will occur due to cooling of the rock for commonly studied silicate and oxide minerals (Sharp, 2007). As the Musselwhite gold deposit has undergone syn and post-emplacement metamorphism (indicated by gold trapped in garnet), and possibly experienced multiple phases of prograde metamorphism, there is considerable potential for resetting of the isotopic signature. However, if the fluid events have happened post-peak metamorphism, it may be possible to estimate the original oxygen isotopic signature of fluids that accompanied mineralisation of orogenic gold deposits.

Hydrogen isotopic data has been collected on hydrous minerals, such as chlorite, biotite, muscovite, amphiboles and whole rock samples in an effort to better constrain the isotopic signature of plutons and their interactions with surrounding rocks and fluids (e.g., Turi and Talylor, 1970; O'Neil and Chappell, 1977; O'Neil et al., 1977; Nabelek et al., 1983; Harford and Sparks, 2001) and also the interactions of meteoric and magmatic fluids in the creation of hypabyssal mineral deposits (Harris et al., 2005). Suzuoki and Epstein (1976) proposed that because of its sensitivity to temperature, yet comparatively low concentrations in rocks, hydrogen isotopes could potentially be used as a thermometer in the same way as oxygen had been. However, it was found that hydrogen fractionation is not solely a function of temperature and fluid compositions, but also is controlled in part by composition of the mineral, especially in mafic minerals where site substitution is common (Suzuoki and Epstein, 1976).

Recently, geochemists have attempted to use nitrogen to determine the source for fluids of orogenic gold deposits (Jia, 2001; Jia and Kerrich, 2001; Pitcairn et al., 2005). Historically, nitrogen has been ignored in rocks, largely because concentrations of

nitrogen in rocks are very low, and only recently have techniques been developed that allow for measurement of nitrogen isotopes in rocks. Nitrogen has an advantage over oxygen, as it is not as susceptible to overprinting or homogenization, due to its lesser abundance in rocks. In holocrystalline rocks, nitrogen is found replacing potassium as ammonium ions in potassium feldspar, biotite, muscovite, and interstitally in quartz (Honma and Itihara, 1981). Concentrations in these minerals ranges from a few ppb to more than 10000 ppm, depending on the mineral and conditions to which the mineral has been exposed, with sedimentary rocks having generally higher concentrations than metamorphic or igneous rocks (Handel et al., 1986; Jia and Kerrich, 2000; Pitcairn et al., 2005). Nitrogen can also be absorbed into clay minerals and found in organic material in sediments and soils (Sharp, 2007). As sediments undergo diagenesis and metamorphism, nitrogen is progressively lost from the crystal lattice with increasing temperature, the lighter isotope being lost preferentially (Haendel et al., 1986). Jia and Kerrich (2001) demonstrated that in metavolcanic rocks, nitrogen fractionates with increasing metamorphic grade, and gives isotopic signatures that are distinct from the signature of magmatic plutons.

3.2 Previous work

Previous isotope studies of the Musselwhite Mine (Otto, 2002) primarily focused on the stable isotope geochemistry of quartz-carbonate alteration and pyrrhotite mineralisation associated with gold mineralisation. Oxygen isotopic data from quartz veins yielded $\delta^{18}O$ values of 12.1 to 13.4 ‰ (Otto, 2002). Isotopic signatures of fluids derived from quartz fall on the edge of the metamorphic-magmatic overlap range for waters (Fig. 3.1; Otto, 2002). Carbon and oxygen isotopes of carbonate alteration related

to gold mineralisation showed ranges of -4.5 to -0.6 ‰ and +10.7 to +11.9 ‰, respectively (Otto, 2002). Sulphur isotopic data of pyrrhotite collected from all units of the Northern Iron Formation range between +1.9 and +22‰, with the majority falling below +5 ‰, and were determined to be magmatic in origin (Otto, 2002).

This study aims to compliment and add to the previous body of research in existence and to reveal further insights as to the nature of the fluids that have generated gold mineralisation at the Musselwhite mine.

3.3 Regional isotopic geochemistry

Locations of regional samples are shown in Fig. 3.2. Regional nitrogen signatures of biotite from the rocks yield values of – 6.9 to 5.1 ‰ (Table 3.1). When the nitrogen isotopic signature is plotted against nitrogen concentrations, all but one of the samples plot in the same approximate area as the granite domain defined by Jia and Kerrich (2000; Fig. 3.3). The majority of the granitoids are characterized by nitrogen concentrations that are lower than those of Jia and Kerrich (2000; Fig. 3.3). Hydrogen isotopic signatures for the regional samples give values between -59 and -80 ‰ and oxygen isotopic signatures range of biotite for the regional samples range from +2.0 to +5.1 ‰.

Table 3.1: N, O, and D compositions of biotite from regional samples. See Fig. 3.2 for location of samples. *Italicized samples are duplicates of samples.

Sample #	Unit	N concentration (ppm)	δ^{15}N (per mil)	δ^{18}O (per mil)	δD (per mil)
E438508	granitoid	12.691	+3.2	+2.7	-74
*E438508**	granitoid	35.364	+6.0	---	---
E438515	granitoid	553.565	+6.1	+2.0	-79
E438517	granitoid	17.219	+1.6	+3.1	-72
E438523	granitoid	34.039	-0.9	+2.0	-73
E438525	granitoid	11.391	-6.9	+3.6	-67
E438528	granitoid	8.445	+1.5	+4.0	-66
E438529	granitoid	7.188	+3.0	+3.2	-77
E438530	granitoid	31.366	+1.5	+2.7	-59
E438531	granitoid	12.815	+5.1	+3.0	-77
E438532	ELS	8.048	-1.9	+5.1	-74
E438536	granitoid	15.091	-6.3	+3.1	-72
E438537	granitoid	4.169	-0.2	+3.5	-80
*E438537**	granitoid	12.135	+1.7	---	---

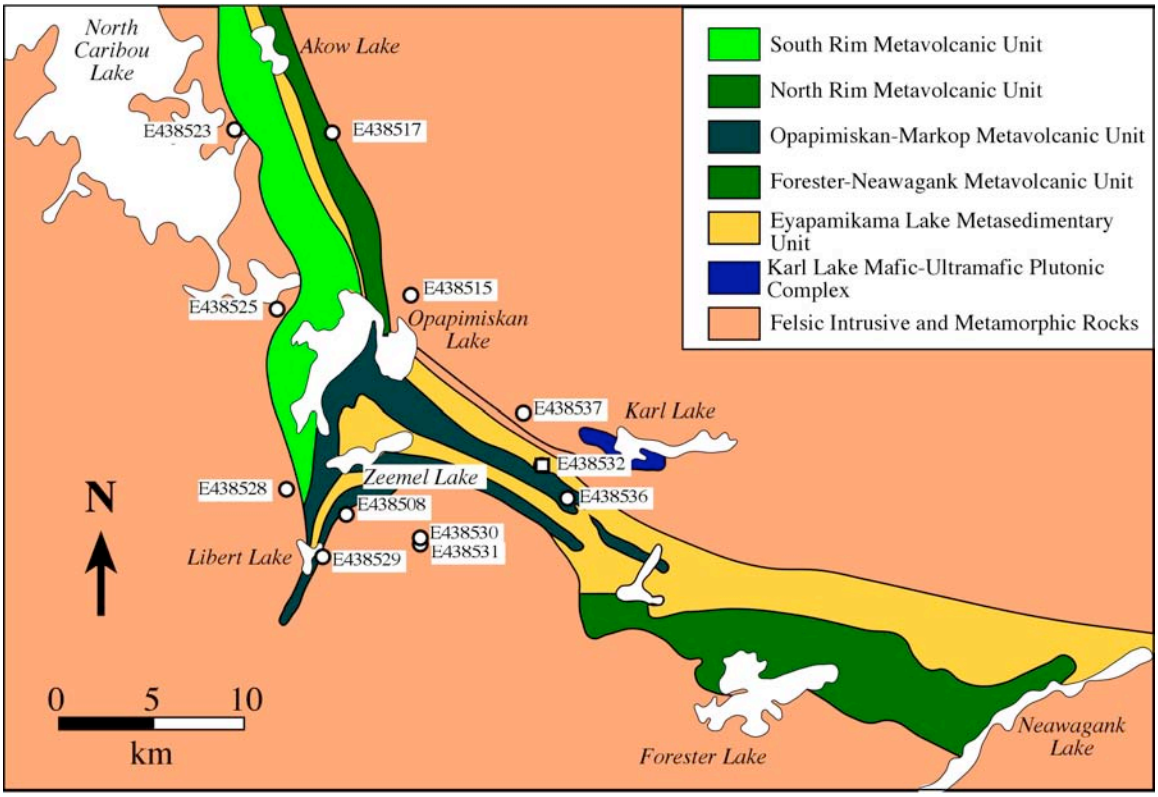

Figure 3.2: Locations of regional samples in the North Caribou Lake greenstone belt.

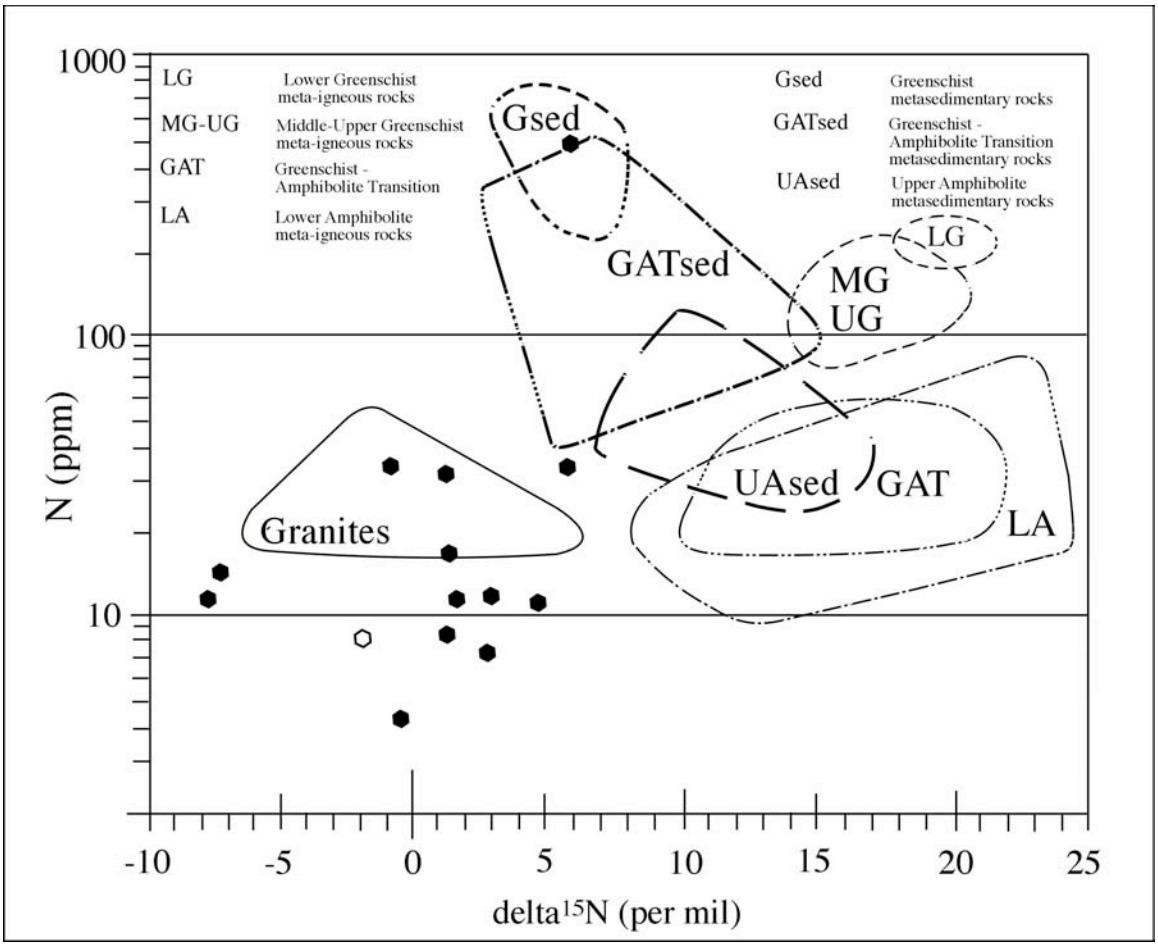

Figure 3.3: Nitrogen results of the regional biotite samples for the North Caribou Lake greenstone belt. Filled hexagons = graniotoid samples, blank hexagon = metasedimentary sample. Metasedimentary fields taken from Haendel et al (1986), metaigneous fields are from Jia and Kerrich (2000).

3.4 Mine results

Locations of samples can be found in Figure 3.4.The nitrogen signature of biotites from the 11700 N section of the Musselwhite Mine yield values from -1.3 to +11.1 ‰ and have nitrogen concentrations of 10 ppm to around 150 ppm (Table 3.2; Fig. 3.5). Hydrogen isotopic data for the mine biotites ranges from -55 to -100 per mil, with and average δD of -86 per mil (see Table 3.2). Oxygen isotopic values for biotite are between +7.1 and +8.9 per mil.

Table 3.2: Table of isotopic data of samples from the Musselwhite mine. Unit names are based on mine terminology: 4f - biotite-garnet schist, 4ea –silicate facies IF, 4b – oxide facies IF, 2 – mafic metavolcanic rocks, 2t – altered metavolcanic rock, 6 – metasedimentary rocks. *Italicized samples represent reruns and duplicates.

		Biotite				Quartz
Sample #	Unit	N concentration (ppm)	$\delta^{15}N$ (per mil)	$\delta^{18}O$ (per mil)	δD (per mil	$\delta^{18}O$ (per mil)
E354010	4b	6.753	-0.3	+8.8	-78	+12.8
E354013	4ea	8.441	+5.4	+8.3	-91	+12.9
E354016	4b	22.507	+5.1	+8.9	-84	+12.9
E354018	4b	27.162	+2.1	+8.9	-88	+14.1
E354020	4b	38.061	+3.3	+8.6	-99	+14.7
E354024	4ea	68.944	+7.5	+7.1	-80	+12.7
E354025	2t	21.365	+5.4	+7.2	-91	+12.5
E354026	4ea	26.274	+6.5	+7.9	-86	+13.0
E354029	4f	33.644	+8.0	+8.8	-97	+15.0
E354032	4f	61.022	+8.3	+8.4	-85	+13.2
E354039	4ea	36.173	+7.0	+8.5	-100	+13.3
*E354039**	4ea	34.983	+6.3	---	---	---
E354040	4b	22.041	+6.2	+8.0	-82	+12.6
E354041	2	149.627	+1.9	+7.5	-92	+13.0
*E354041**	2	176.438	+2.4	---	---	---
E354043	4f	26.196	+6.0	+8.4	-83	+14.2
*E354043**	4f	127.536	+5.3	---	---	---
E354045	6	115.832	+2.1	+7.7	-89	+14.5
E354050	4b	22.527	+11.5	+8.0	-96	+13.5
E358103	4ea	32.233	+8.9	+10.1	-80	+14.8
*E358103**	4ea	32.213	+6.3	---	---	---
E358105	4f	38.132	+8.7	+8.5	-83	+15.3
E358106	4f	91.932	+3.8	+8.1	-84	+17.2
*E358106**	4f	95.179	+4.1	---	---	---
E358108	2t	44.470	+6.0	+7.3	-91	+16.2
E358109	2t	20.646	+5.1	+8.1	-97	+12.4
E358110	2	8.441	-1.7	+9.1	-55	---

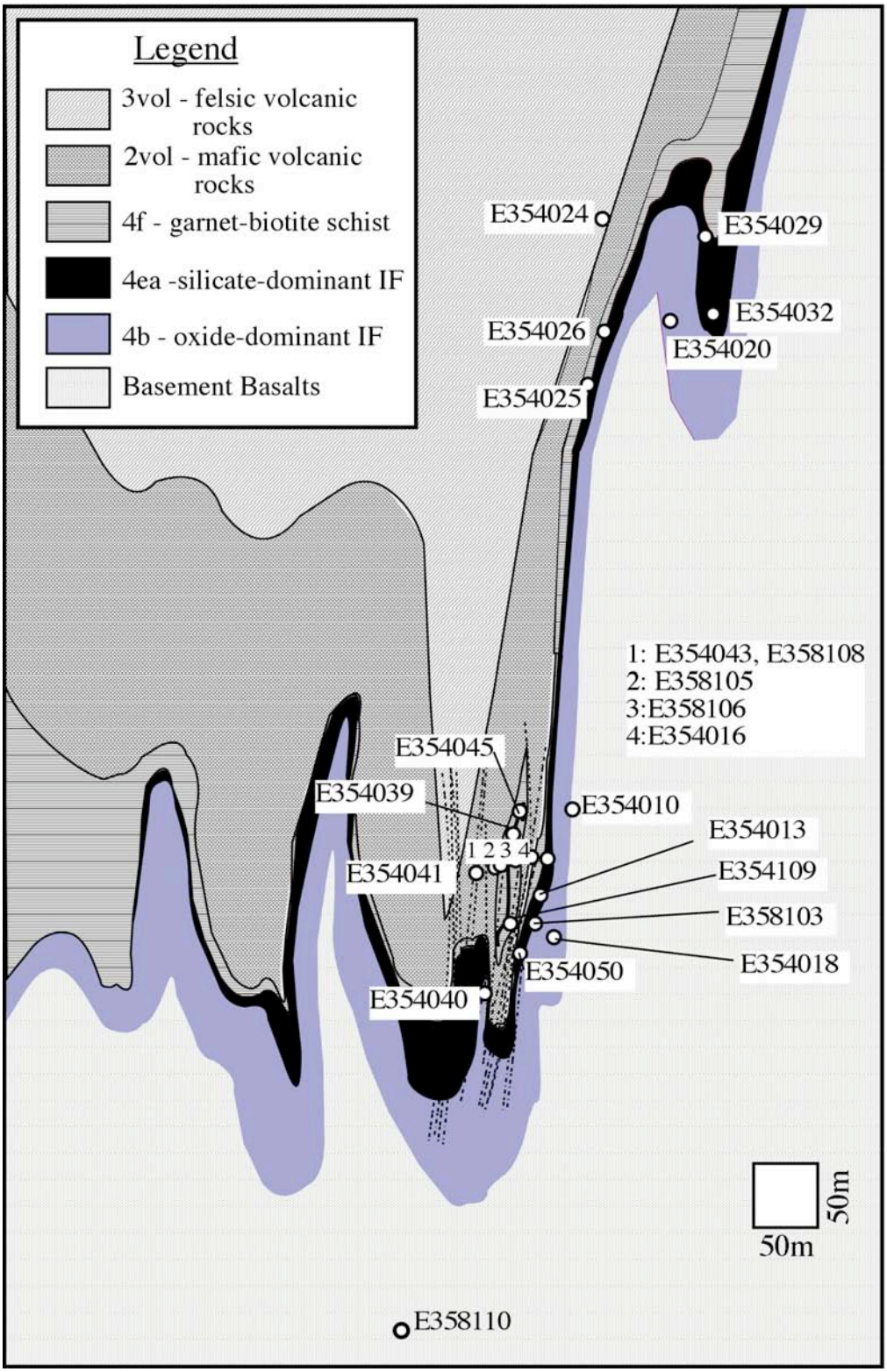

Figure 3.4: Locations of samples of the 11700N section of the Musselwhite Mine. Modified from files provided by Musselwhite Mine. Shear zones are marked with dashed lines.

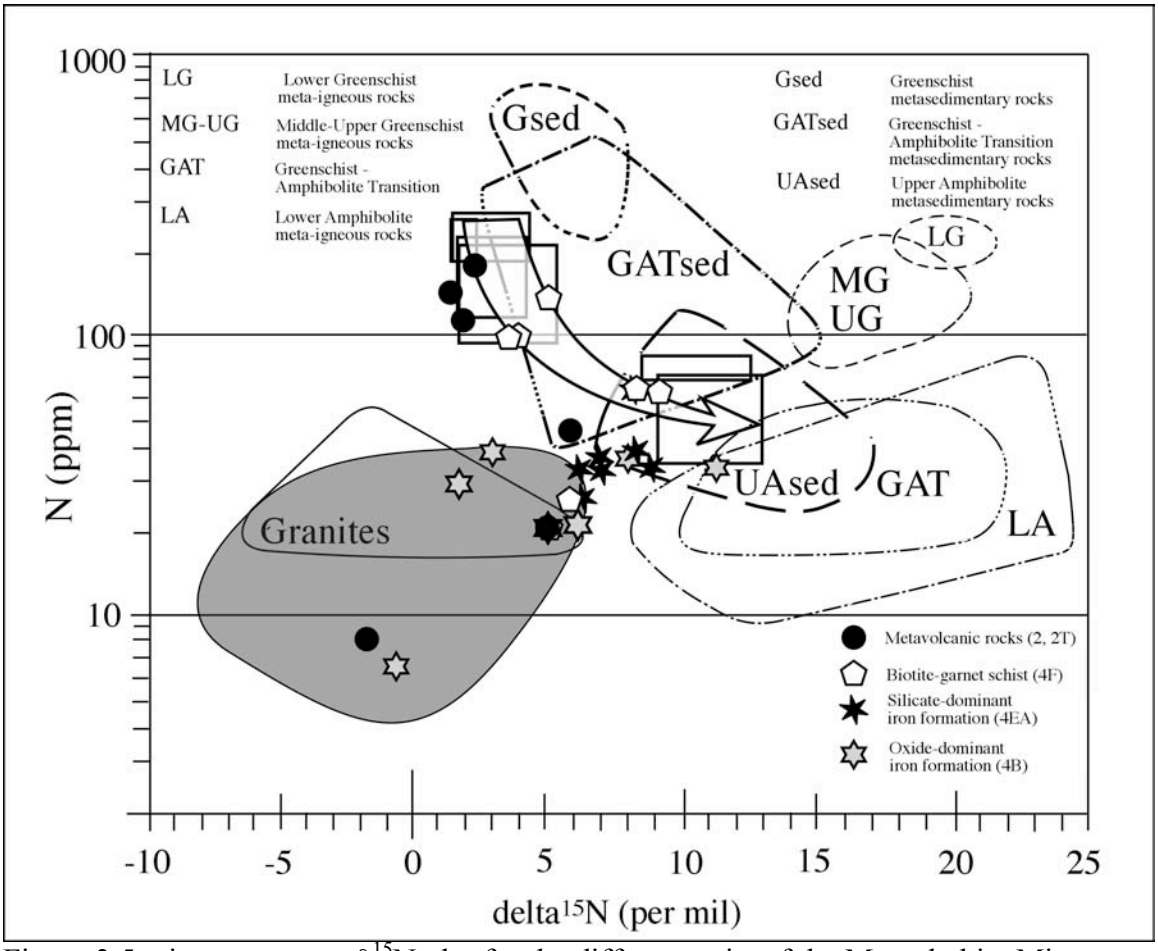

Figure 3.5: nitrogen versus $\delta^{15}N$ plot for the different units of the Musselwhite Mine. Shaded field represents regional granitoids. Metasedimentary fields after Haendel et al., 1986; metaigneous fields after Jia and Kerrich (2000).

Quartz samples collected from the mine give $\delta^{18}O$ values between +12.1 and +17.1 per mil (Table 3.2). When plotted spatially, lighter isotopic signatures coincide with shear zones, whereas slightly heavier quartz isotopes are associated with the oxide facies iron formation and biotite-garnet schist (Fig. 3.6).

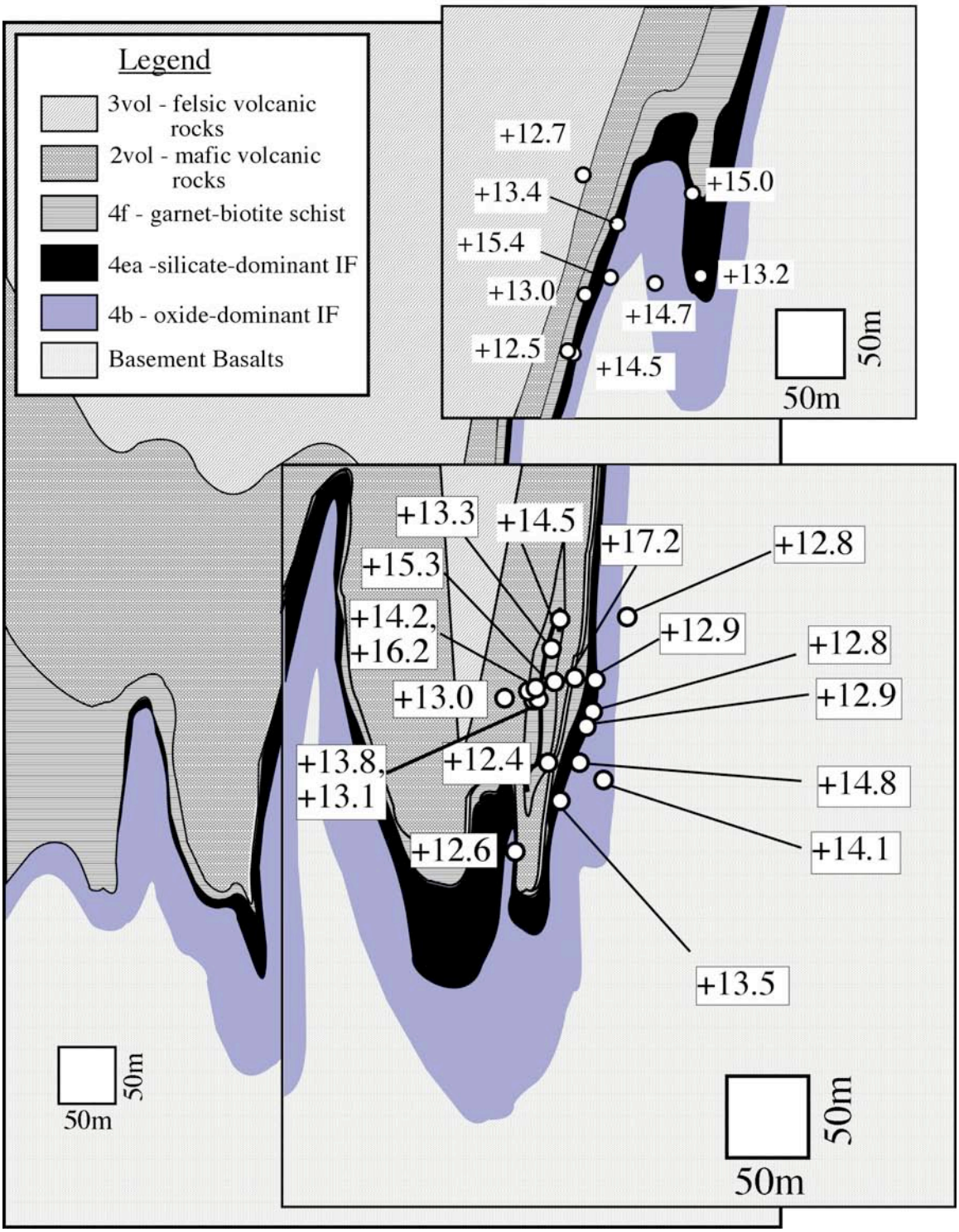

Figure 3.6: Oxygen isotopes of quartz of the Musselwhite Mine. Modified from files from the database of the Musselwhite Mine.

3.5 Discussion

3.5.1 Regional biotite

Oxygen and hydrogen isotopic values of the granitic plutons surrounding the North Caribou Lake greenstone belt are comparable to the isotopic values of Phanerozoic igneous plutonic rocks (e.g., Turi and Talylor, 1971; Taylor, 1974; O'Neil and Chappell, 1977; O'Neil et al., 1977). The nitrogen isotopic signatures for the plutonic rocks bounding the North Caribou Lake greenstone belt also fall within the isotopic range for felsic igneous plutonic rocks as defined by Jia and Kerrich, (2000). It should be noted that the nitrogen concentration in biotite of the felsic plutonic rocks of the North Caribou Lake greenstone belt are lower than those reported by Jia and Kerrich (2000). Considering that only a handful of studies have been conducted on the nitrogen concentrations of felsic plutonic rocks, and that the field defined by Jia and Kerriich (2000) has a flat base (indicative of the minimum detection limit), then the values for the felsic plutonic rocks surrounding the NCLGB are likely reasonable for granitic samples.

Sample E438515 has an extremely high nitrogen concentration compared to all samples, and especially for an igneous rock. This sample comes from the Dinnick Lake fault that marks the border between the North Caribou Terrane and the adjacent Island Lake Domain. Pitcairn et al (2005) reports samples with anomalously high N concentrations coming from a major shear zone (Hyde-Macraes Shear Zone) and attribute the high signature to N addition in the shear zone. Perhaps then the high N in sample E438515 can be explained by N addition to the rock during emplacement in the Dinnick Lake Shear Zone.

The metasedimentary sample E438532 is unusual geochemically for a metasedimentary rock, in that its O, H and N isotope compositions are identical to

igneous rocks rather than those of a metasedimentary rock. It does possess the highest O isotopic signature of all the regional rocks. A possible explanation for the signatures found in this sample is that the metasedimentary rock was altered by juvenile magmatic waters from a nearby pluton (such as E438536) or even underlying felsic pluton (e.g., Turi and Taylor, 1971).

3.5.2 Mine H_2O modeling

Temperatures of H_2O for the mine were initially estimated using the quartz-biotite thermometer of Bottinga & Javoy (1975) and the isotopic data for quartz and biotite at Musselwhite Mine. The estimated temperatures range from 343-622 °C. The temperatures calculated from these were used in all isotopic calculations of formation waters. Calculations were made using the online calculator of Beaudoin and Therrien (2008). Both sets of H_2O $\delta^{18}O$ calculations are presented in Table 3.3 for comparison. Temperatures can only be considered valid if equilibrium between quartz and biotite can be confirmed. Petrography seems to indicate that the quartz and biotite are in equilibrium in samples.

Table 3.3: Calculation of waters from quartz-biotite pairs of Musselwhite Mine.

Sample #	Biotite $\delta^{18}O$ (per mil)	Quartz $\delta^{18}O$ (per mil)	$\delta^{18}O$ (qtz-bt)	Temp. T(^{o}C)
E354010	+8.8	+12.8	4.0	622
E354013	+8.3	+12.9	4.6	569
E354016	+8.9	+12.9	4.0	622
E354018	+8.9	+14.1	5.2	542
E354020	+8.6	+14.7	6.0	474
E354024	+7.1	+12.7	5.6	498
E354025	+7.2	+12.5	5.3	517
E354026	+7.9	+13.0	5.1	531
E354029	+8.8	+15.0	6.2	463
E354032	+8.4	+13.2	4.8	553
E354039	+8.5	+13.3	4.8	553
E354040	+8.0	+12.6	4.6	569
E354041	+7.5	+13.0	5.5	504
E354043	+8.4	+14.2	5.8	486
E354045	+7.7	+14.5	6.8	432
E354050	+8.0	+13.5	5.5	504
E358103	+10.1	+14.8	4.3	561
E358105	+8.5	+15.3	6.8	432
E358106	+8.1	+17.2	9.1	343
E358108	+7.3	+16.2	8.9	349
E358109	+8.1	+12.4	4.3	594

3.5.3 Quartz-Magnetite thermometry

Confirmation of temperatures of regional metamorphic conditions independent of mineralized zones was attempted by use of quartz-magnetite thermometry of hydrothermally undisturbed iron formation. Oxygen isotope results for quartz and magnetite pairs are shown in Table 3.4.Temperatures were calculated using the equations of Bottinga and Javoy (1975) with the assumption that equilibrium was achieved and that the quartz magnetite pairs were not part of any alteration phase. The $\delta^{18}O$ values of quartz-magnetite pairs from undisturbed oxide iron formation gave an estimated temperature of 455-561 °C. These temperatures agree with the earlier estimates of peak

metamorphic temperatures made by Hall and Rigg (1986), Breaks et al. (2001), and Otto (2002).

Table 3.4: calculated temperatures of quartz-magnetite pairs of Musselwhite Mine.

Sample #	Magnetite $\delta^{18}O$ (per mil)	Quartz $\delta^{18}O$ (per mil)	Δ (qtz-mt)	Temp. **T(^{O}C)**
E354012	5.1	13.9	8.7	526
E354031	2.7	13.2	10.5	455
E358101	6.0	14.1	8.0	561

3.5.4 Isotopes of Musselwhite Mine

When plotting nitrogen isotope compositions versus nitrogen concentrations of biotite, the majority of samples from Musselwhite Mine fall between the field for granites and the upper amphibolite metasedimentary domain (Fig. 3.5). A distinct positive trend can be seen in the majority of samples. This positive trend is the opposite of what is expected in regional prograde metamorphic settings. Haendel et al. (1986) found that with increasing metamorphic grade, $\delta^{15}N$ is preferentially lost from sedimentary material into the fluid phase. A similar trend is seen in the work done by Jia (2006; Fig. 3.7). A positive trend in nitrogen concentration and $\delta^{15}N$ has been documented where magmatically derived fluids have interacted with metamorphic rocks (Bebout et al., 1999; Fig. 3.7).

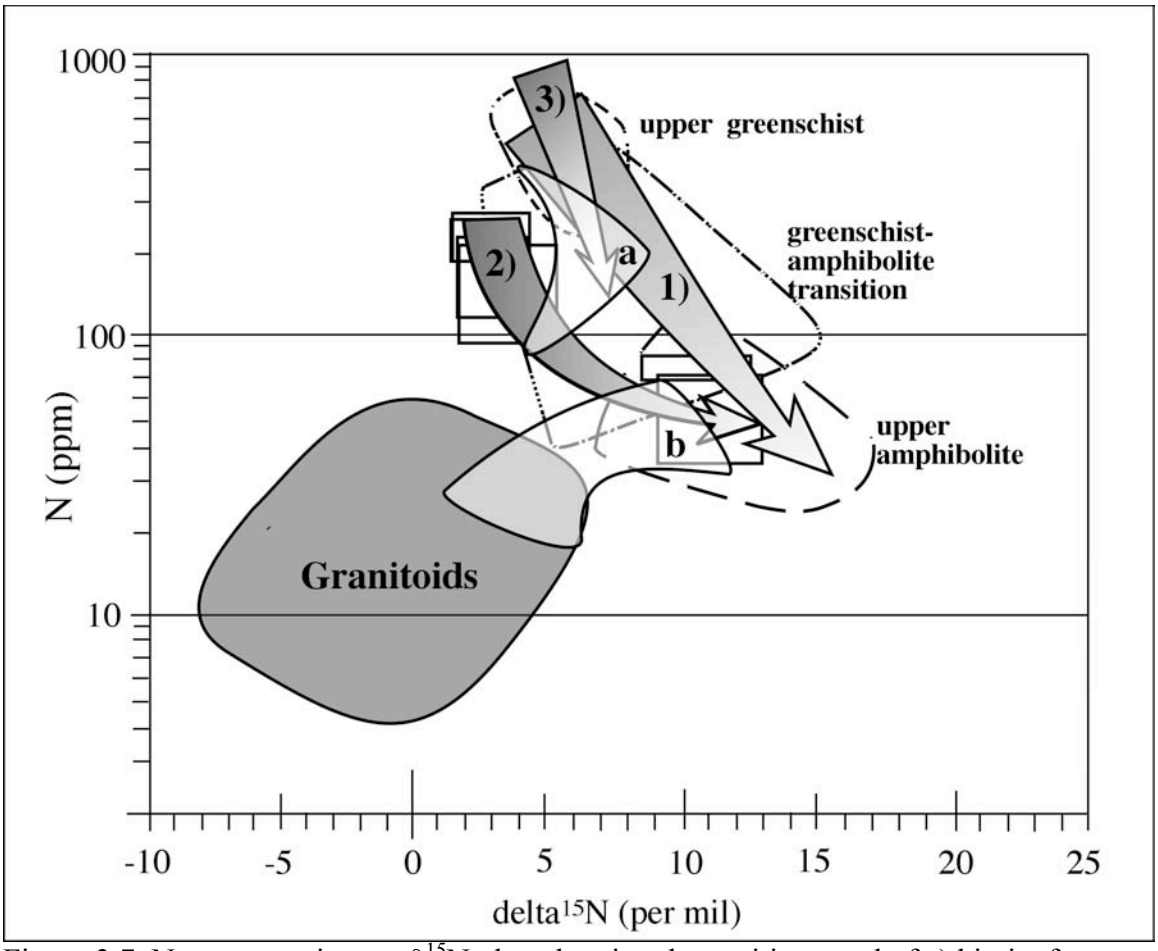

Figure 3.7: N concentration vs. $\delta^{15}N$ plot, showing the positive trend of a) biotite from the aureole of the Skiddaw intrusion from Bebout et al. (1999) b) biotites from Musselwhite. The negative trends are 1) Haendel et al. (1986; fields shown in dashed lines) 2) N signature shift during progressive metamorphism of the Cooma complex from Jia (2006) 3) N signature shift with increasing metamorphic grade of rocks distal to the Skiddaw intrusion from Bebout et al. (1999).

A small population of mine samples clusters away from the main trend between the fields for granites and greenschist facies metasedimentary rocks (see Fig. 3.5). These points correspond with the stratigraphic top of the deposit, and are garnet-biotite schists with a detrital component. Because of their position in mine stratigraphy and petrography, these data points are interpreted to be the least altered, original metasedimentary signature of the schist that caps the Northern Iron Formation. It is also of interest to see that not all the samples of biotite-garnet schist unit fall within this

population, indicating different sources for biotites within the unit. Moran (2008) also identified some biotite-garnet schist samples as having undergone significant metasomatism. It is then likely that the different isotopic populations represent these two different types of biotite.

The oxygen signatures of biotite from Musselwhite Mine are low when compared with typical metamorphosed pelitic rocks (e.g., Turi and Talylor, 1971; O'Neil and Chappell, 1977; O'Neil et al., 1977; Sharp, 2007). The isotopic signature of the quartz samples from the iron formation averages around 13.9‰ These values are comparable to those found in the ca. 3 Ga Fig Tree Formation by Perry (1967) where the anomalously low signatures are attributed to a lower isotopic signature of ocean waters. It is possible then that the low oxygen signatures of biotite samples at Musselwhite could be explained as a reflection of low oxygen isotopes of the Archean atmosphere and oceans.

It is interesting to note that the heaviest quartz oxygen isotopes correlate to the capping biotite-garnet schist and oxide-facies iron formation, whereas the light oxygen isotopic signature of the silicate-dominant iron formation is lower than either of these, and is in the same range as quartz from veins associated with gold (Otto, 2002). The lighter isotopic signatures of quartz in the silicate-dominant iron formation may then be an indication that the same fluids that created the quartz veins associated with gold also were responsible for the mineral assemblage of this unit.

The two samples (E354010 and E358110) that have the highest δD values and among the lowest $\delta^{15}N$ values are located below the iron formation (Table. 3.2, Fig. 3.8). These isotopic signatures are markedly different than the rest of the biotite. The signatures of these two samples are very close to those of igneous signatures. Thus it is likely that biotite found adjacent to the basement metavolcanic rocks reflect the isotopic

characteristics of the basement basalts. It is also interesting to note that this is not the case for the metasedimentary package found on top of the Northern Iron formation. This could mean that the biotite located at the base of the Northern Iron Formation has interacted or crystallized from magmatically derived hydrothermal fluids, rather than being metasedimentary in origin.

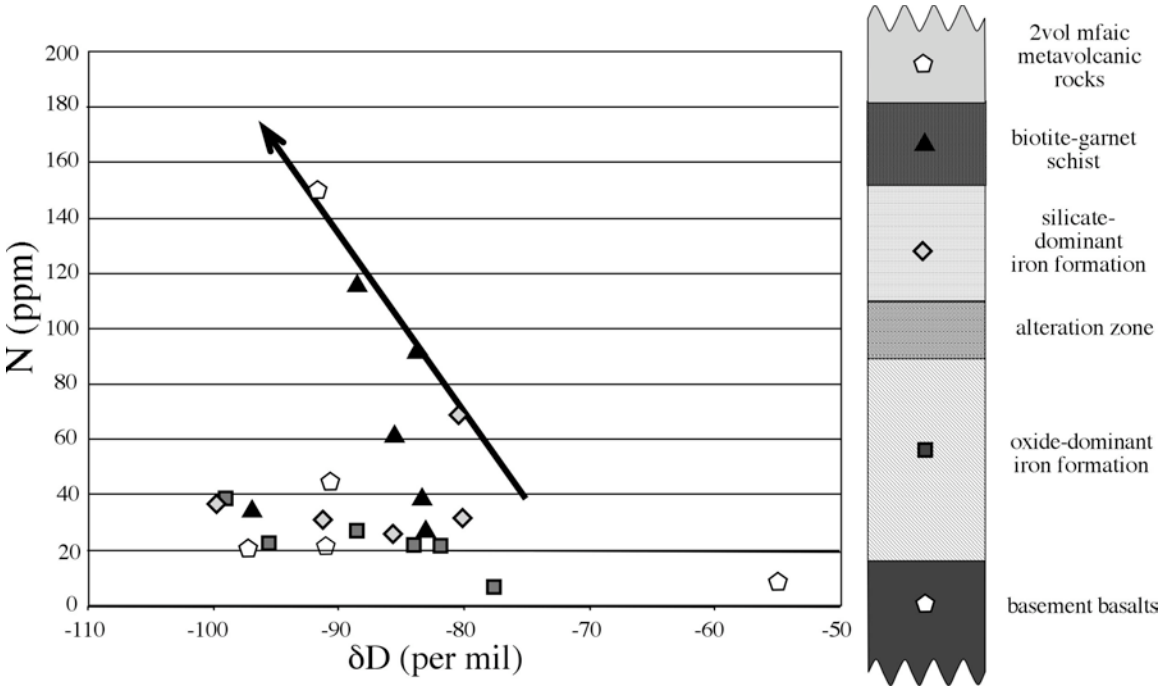

Fig 3.8: Plot of N concentration vs. δD of biotite samples and stratigraphy from Musselwhite. The two samples from the basement basalts are shown in white.

Hydrogen isotopic signatures display scatter between samples of the same unit, as seen in Table 3.2, indicating that the biotite forming fluids were not derived from a single, homogenized source as one would expect from metamorphic or meteoric fluids as the large fluid reservoirs of both would effectively homogenize all δD values (Taylor, 1974). The wide range of δD for the mine indicates that isotopic equilibration between biotite and fluids appears to have happened post-peak metamorphism, otherwise the δD signature would have most likely been homogenized. The δD values below -91 per mil for biotite for the mine fall outside the previously estimated values for biotite produced

by metamorphic fluids alone (Taylor, 1974). Biotite for metamorphic rocks with δD signatures below this value are interpreted to be the result of interaction of magmatic fluids and metamorphic rocks from adjacent plutons during contact metamorphism (Taylor, 1974). However, this is not the sole possible case to explain a light isotopic signature. The low hydrogen values of the deposit can be caused by other factors: 1) organic matter may have imparted a light isotopic signature, as organic processes favour lighter isotopes (Sharp, 2007), 2) high iron content in the biotite will favour isotopically light hydroxyl ions (Suzuoki and Epstein, 1976), 3) meteoric fluids (Taylor, 1974), 4) degassing of magmatic fluids at shallow levels will impart a light δD to minerals (Taylor et al., 1983; Harris et al., 2005). There is debate about when the onset of life occurred on earth and the role of bacteria in certain kinds of ore deposits, such as iron formations (Pinti et al., 1991; D'Hondt et al., 2004; Hoffman and Bolhar, 2007). Because of the uncertainty surrounding the onset of life in the Archean, it is possible that bacteria may have had influence on the rocks at Musselwhite mine, and that the light hydrogen isotope signature could have come from organic detritus. Stromatolites have been identified in the ca. 3 Ga Steep Rock platform in the Western Wabigoon domain (Kusky and Hudleston, 1999), establishing that bacteria have been around since at least 3.0 Ga. Given that the age of the North Caribou Lake greenstone belt is around 2.9 Ga, it is entirely possible that organic matter has played a role in the isotopic signatures of the rocks of the Musselwhite Mine. However, if the light hydrogen signature had come from organic matter, it would have imparted a corresponding light nitrogen signature upon the deposit, as light isotopes are favoured due to the kinetic nature of biologic processes (Sharp, 2007). However, this isotopic range overlaps with the isotopic range for igneous rocks (Sharp, 2007). The presence of organic matter would also increase the nitrogen

concentration of the rocks considerably, as the amount of nitrogen contained in organic matter is typically higher than that contained in igneous or sedimentary rocks free of organic matter (Junium and Arthur, 2007). Nitrogen concentrations in biotites within the deposit are quite low, when compared to the data of organic-bearing sedimentary rocks (e.g., Orberger et al., 2005). Moreover, higher nitrogen concentrations in biotite do not generally correlate with the light hydrogen isotopic signature (Fig. 3.8). It should be noted that there are a few points in the Musselwhite mine that show very good correlation between nitrogen concentration and hydrogen isotopic signature. It is possible that for these few samples organic matter did have influence on the isotopic signature. However, the lack of correlation between N concentration and δD for the majority of biotite samples rules out metamorphism of an organic-rich predecessor as the origin of the light δD signature for most biotite samples at Musselwhite Mine.

Meteoric waters will impart a negative hydrogen signature to hydrous minerals (Taylor 1974). However, they also have a corresponding light oxygen isotopic signature, due to fractionation effects on precipitated water (Craig, 1961; Sharp, 2007). The heavy oxygen signatures of biotite rules out meteoric waters, especially in the midst of an orogeny, where the altitude effect would impart a light isotopic signature to the meteoric waters (Sharp, 2007).

Fluids exsolved from a pluton which was isotopically light in H or from hypozonal degassing are possible sources of the lighter isotopic signatures (Taylor et al., 1983; Harris et al, 2005). The estimated depth at peak metamorphism was around 9 km depth (Hall and Rigg, 1986). Since isotopic signatures for the mine indicate Au emplacement occurred post-peak metamorphism, the 9 km depth represents a maximum depth, and Au emplacement likely occurred at a shallower depth. Moreover, there is no

current evidence in the regional data for an isotopically light δD felsic pluton .Thus, it seems far more likely that the lightest hydrogen isotopic signatures found at Musselwhite are a result of hypabyssal degassing of fluids of magmatic origin during uplift. However, another possible explanation for the light hydrogen signature is due to selection of isotopically light hydrogen because of the presence of high amounts of iron within the biotite structure (Suzuoki and Epstein, 1976). As the Au deposit formed within an iron formation, it is reasonable to assume that biotite formed in and around the Northern Iron Formation would have a much higher iron content than those of surrounding rocks, and that this in turn would cause fractionation of light hydrogen of the biotite at Musselwhite mine.

The nitrogen, oxygen and hydrogen isotopic signatures of Musselwhite Mine all indicate that there has been influence of magmatic fluids in the rocks. There even seems to be some broad correlation with lower isotopes correlating with shear zones. Investigation of the relationship, if any, between biotite mineral chemistry and isotopic signature is the subject of the next chapter.

4.1 Introduction

In an effort to better comprehend the geological setting around Musselwhite Mine, sampling was done in the surrounding region (Fig. 4.1). Whole rock geochemistry analyses were provided courtesy of Musselwhite Mine. In addition, fourteen samples (nine mine samples and five regional samples) were selected for SEM-EDS analysis. SEM-EDS data was collected on mine biotite samples that form a cross section of the PQ Deeps (Fig. 4.2).

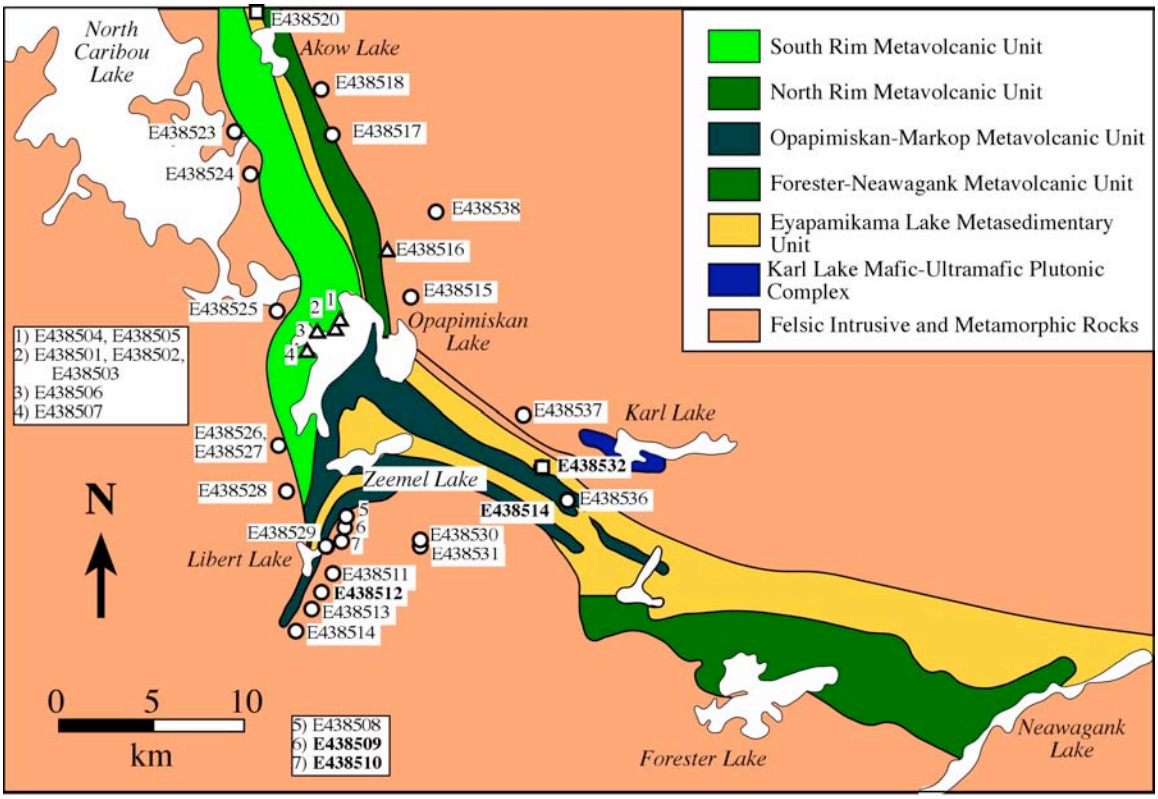

Figure 4.1: Map of the North Caribou Lake greenstone belt, showing locations of samples. Circles = felsic rocks, squares = metasedimentary rocks, triangles = mafic rocks. Samples in bold had biotite composition analysed on SEM. After Breaks et al. (1986).

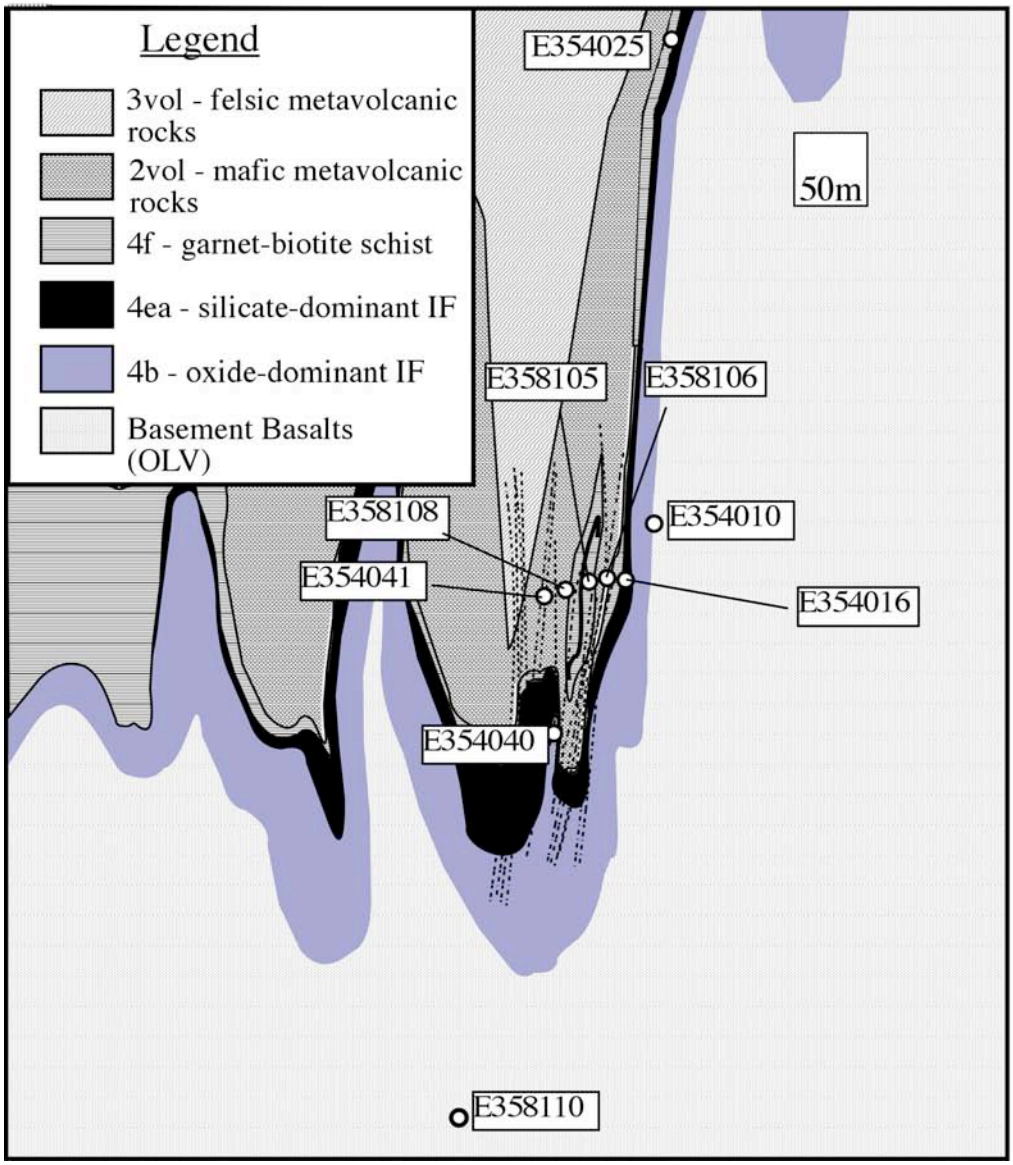

Figure 4.2: Cross section of the 11700N section of the Musselwhite Mine, showing samples on which mineral chemistry analyses were performed. Modified from files provided by Musselwhite Mine.

SEM-EDS data was collected in order to investigate the origin of the light hydrogen isotopic signature seen in the rocks at Musselwhite Mine and to help resolve some of the issues regarding the origins of the minerals themselves. The study undertaken here looks at the major element composition of biotite from the mine and from regional samples.

4.2 Previous studies

Previous workers have collected SEM and microprobe data on the minerals comprising the rocks of the Musselwhite deposit. Otto (2002) analyzed a variety of minerals including garnet, chlorite, hornblende, plagioclase and biotite in order to calculate temperatures of formation and to estimate the peak metamorphic temperatures. Moran (2008) expanded on this initial study and classified the various rock types according to whole rock and SEM data from thin sections and whole rock geochemistry.

4.3 Whole rock geochemistry

Whole rock geochemistry of the rocks of the North Caribou Lake greenstone belt and surrounding batholiths was analysed. Data for these analyses were provided courtesy of Musselwhite and can be found in Appendix B.

When plotted in terms of their total alkali vs. silica, the regional samples are essentially bimodal in population: they are either felsic or mafic, with the metasedimentary samples plotting with the felsic samples (Fig. 4.3).

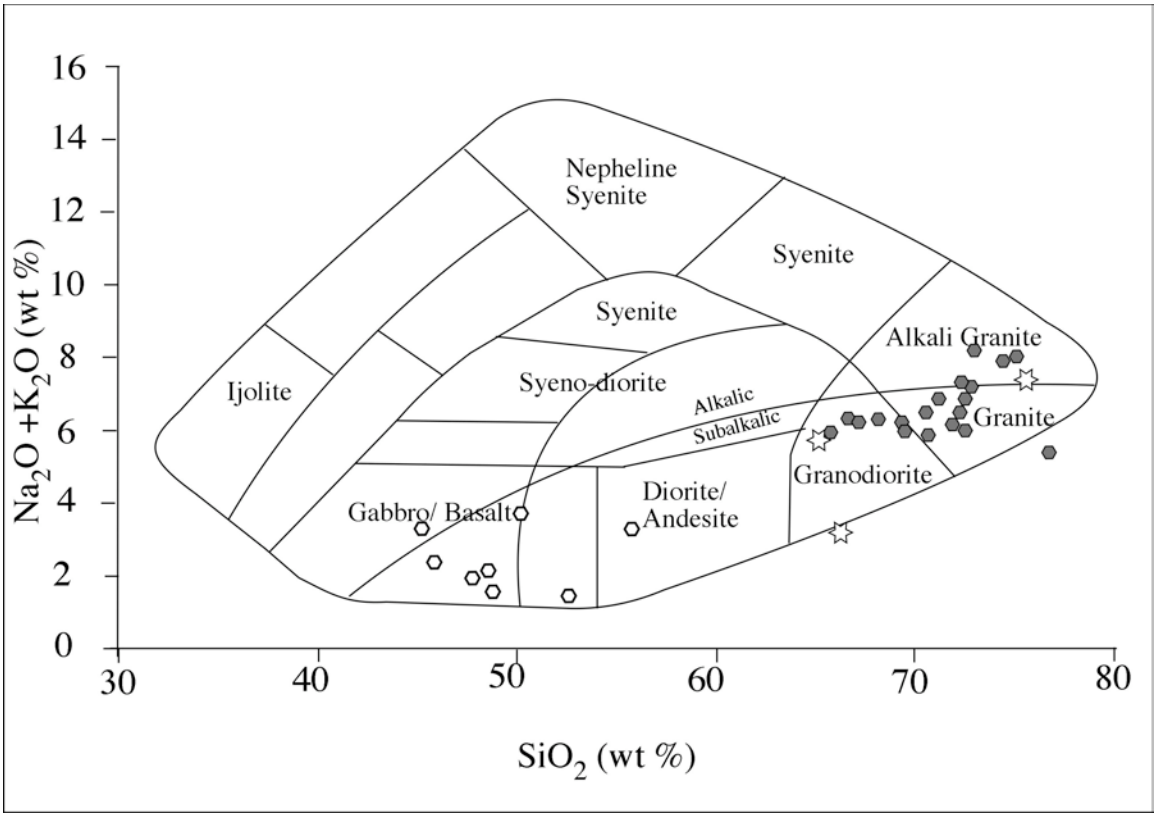

Figure 4.3: TAS diagram of the rocks of the North Caribou Lake greenstone belt and surrounding granitoids rocks. Open hexagons = mafic rocks, filled hexagons = felsic rocks, stars = metasedimentary rocks. After Wilson (1989).

The mafic rocks sampled in the North Caribou Lake greenstone belt plot almost exclusively in high-Mg tholeiite field (Fig. 4.4). The two points that plot as komatiitic basalts are E438504 and E438505.

When the granitic rocks found surrounding and within the North Caribou Lake greenstone belt are plotted in terms of their alkali components, the vast majority plot in the realm of trondhjemite-tonalite-granodiorite (TTG) field with only a few granites (Fig. 4.5).

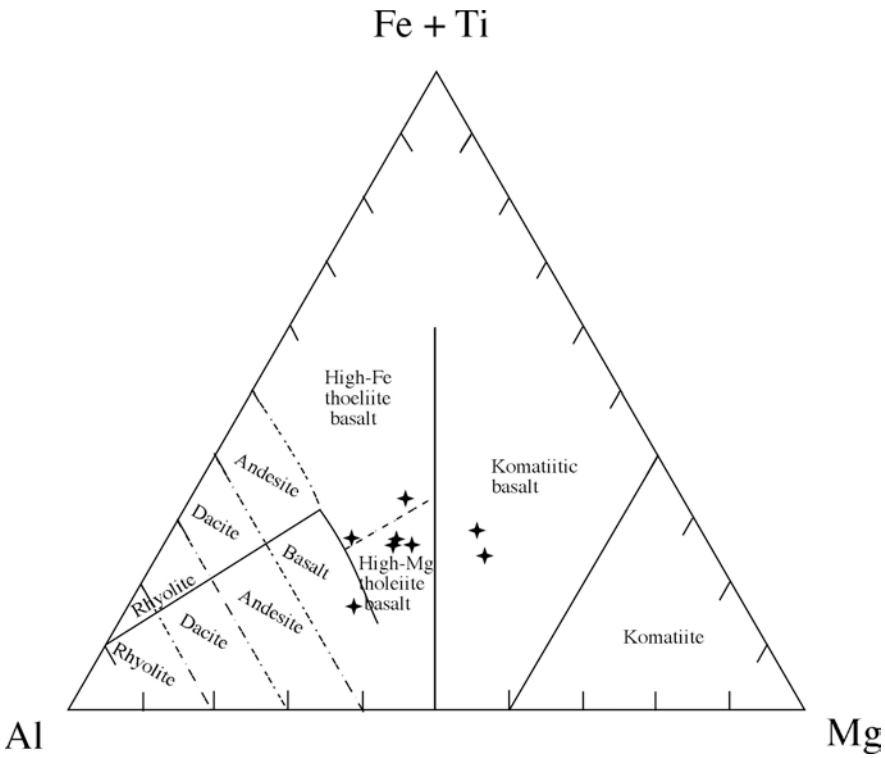

Figure 4.4: FTAM diagram of the mafic rocks of the North Caribou Lake greenstone belt. After Jensen (1976).

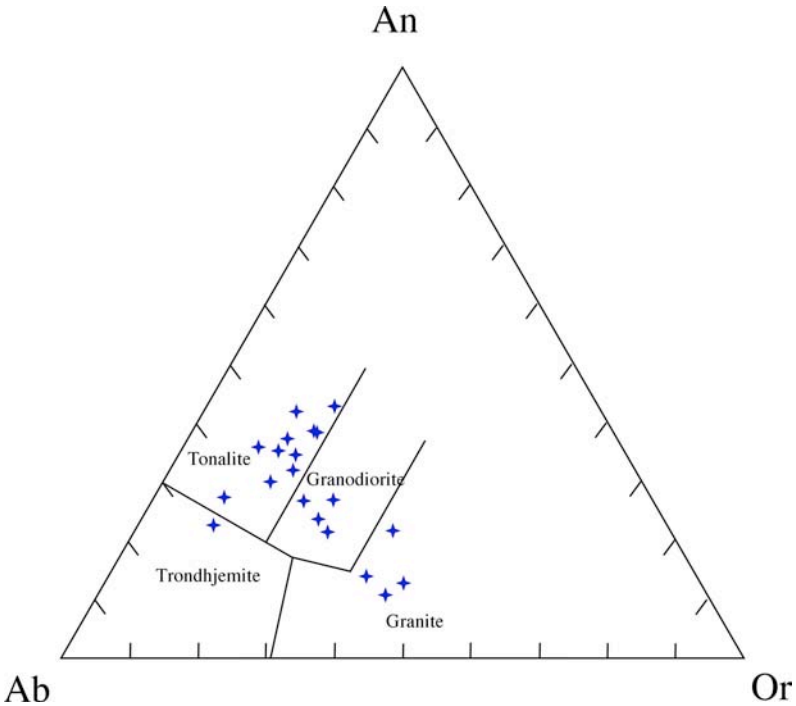

Figure 4.5: Alkali normalized plot of the granitic rocks found within and surrounding the North Caribou Lake greenstone belt. After Barker (1979).

4.4 SEM Data

4.4.2 Regional mineral chemistry

Five samples: four granitoids and one sedimentary sample were analysed by SEM-EDS. Analsyes can be found in appendix B. Biotites in these rocks are very uniform in composition and generally cluster (Fig. 4.6 a-d). The exception is sample E438509, which has a wider spread of silica and alumina content in biotite relative to the others (Fig. 4.6a). The metasedimentary sample E438532 has decidedly higher silica and MgO than the granitoids (Fig. 4.6c); however, it has the same alumina content as the granitoids (Fig 4.6a,b). Titanium contents of biotite are constant irrespective of other constituents (Fig. 4.6d).

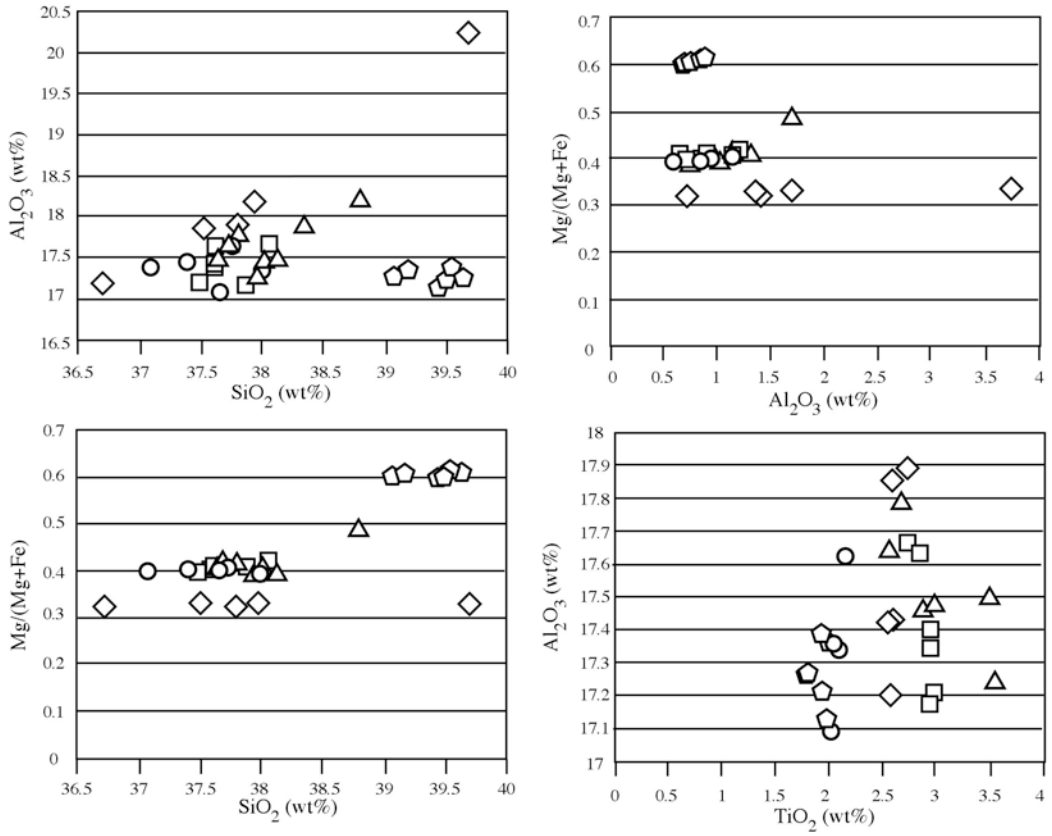

Figure 4.6: Oxide-oxide plots of biotites from plutonic rocks surrounding the NCLGB. Triangles, circles squares, diamonds = granitoids rocks, pentagons = metasedimentary rock.

4.4.2 Mine mineral chemistry

Results for the mine biotite compositions are reported in Appendix C. Data points for each sample are averages of biotite analyses at each spot taken. Additional biotite values for Musselwhite Mine were taken from the data of Moran (2008) and Otto (2002) for comparison. Error on measurement is approximately 1%.

When the data is plotted in terms of its Y site vs. total aluminum content, two distinct populations of biotite are seen to coexist; the majority of the samples cluster around and above the $(Mg, Fe)_5$ line whereas a small subset have higher Al_{tot} and consist of the mafic and felsic metavolcanic rocks (Fig. 4.7). Biotite compositions are mostly iron rich end members, but variance is seen (Fig 4.8).

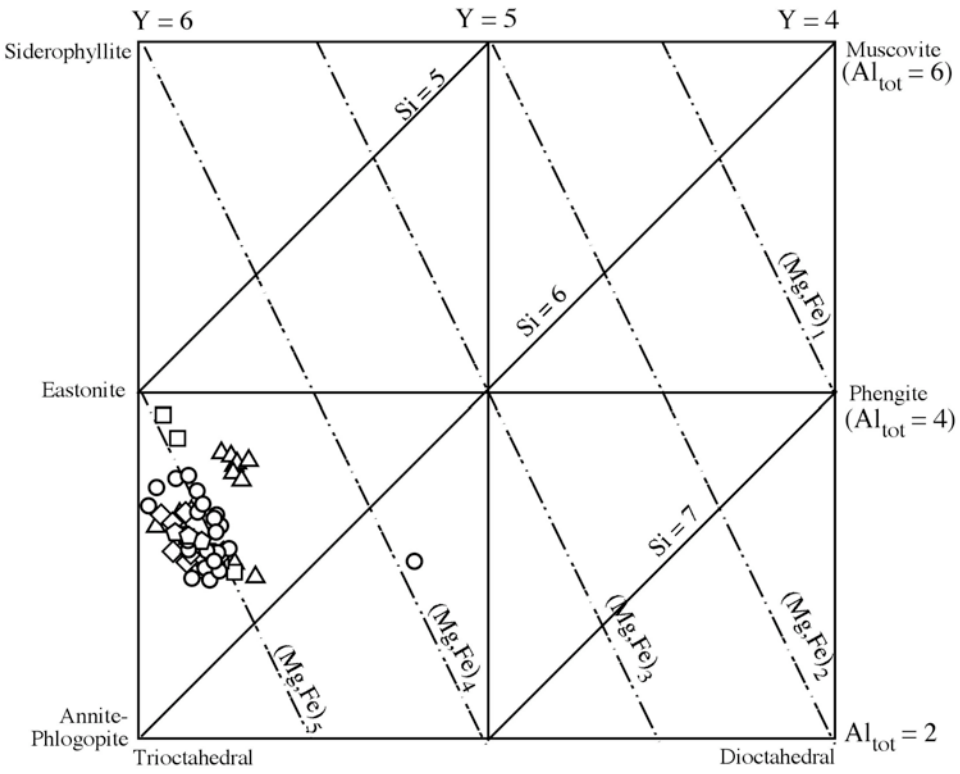

Figure 4.7: Plot showing Y site versus total aluminum content for the samples from Musselwhite. Triangles = felsic metavolcanic samples, circles = biotite-garnet schist, squares = mafic metavolcanic samples, diamonds = oxide-dominant iron formation, pentagons = silicate-dominant iron formation. After Deer et al. (1992).

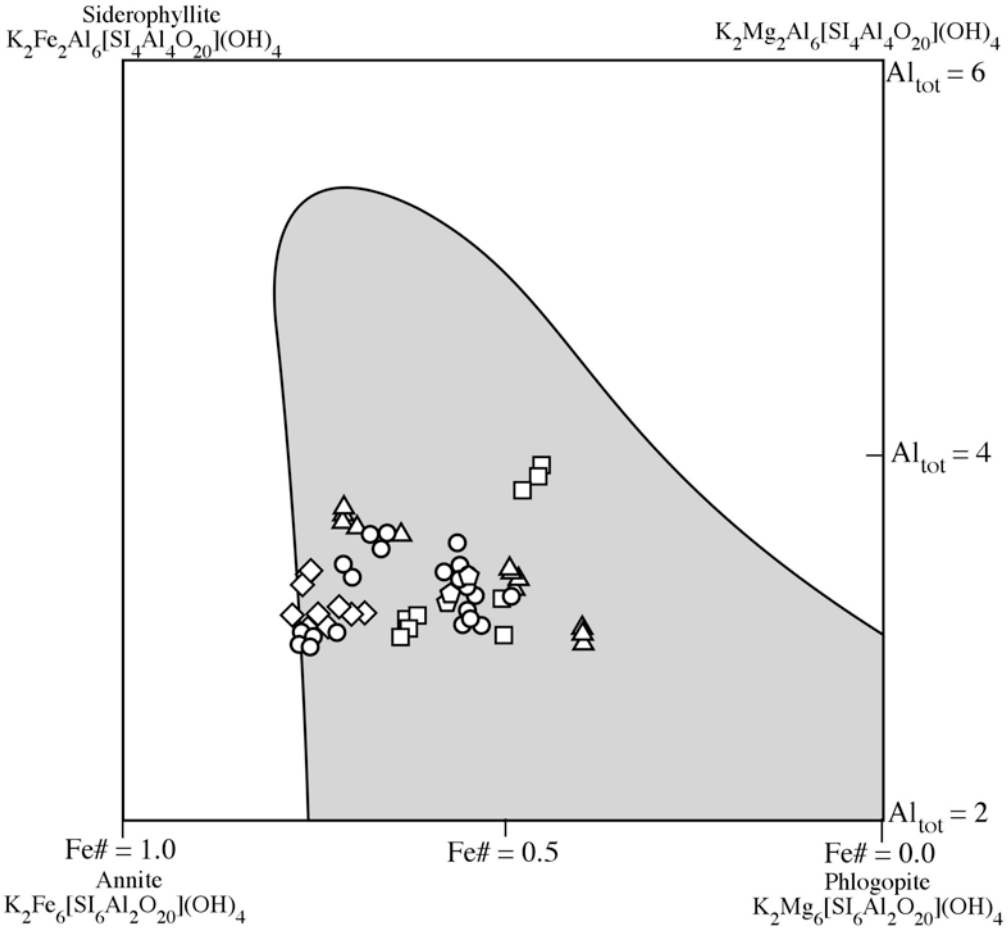

Figure 4.8: Plot showing biotite compositions of the samples from Musselwhite. Grey shaded area is the field for naturally occurring biotites in nature. Triangles = felsic metavolcanic samples, circles = biotite-garnet schist, squares = mafic metavolcanic samples, diamonds = oxide-dominant iron formation, pentagons = silicate-dominant iron formation. After Deer et al., 1992.

Silica has a weak positive correlation with Mg# of biotite (Figure 4.9b). No conclusive correlation exists between Mg# and silica content or alumina and silica content (Fig. 4.9a, c). Note how there is no division between any rock type from the others – all units overlap and are very similar in composition.

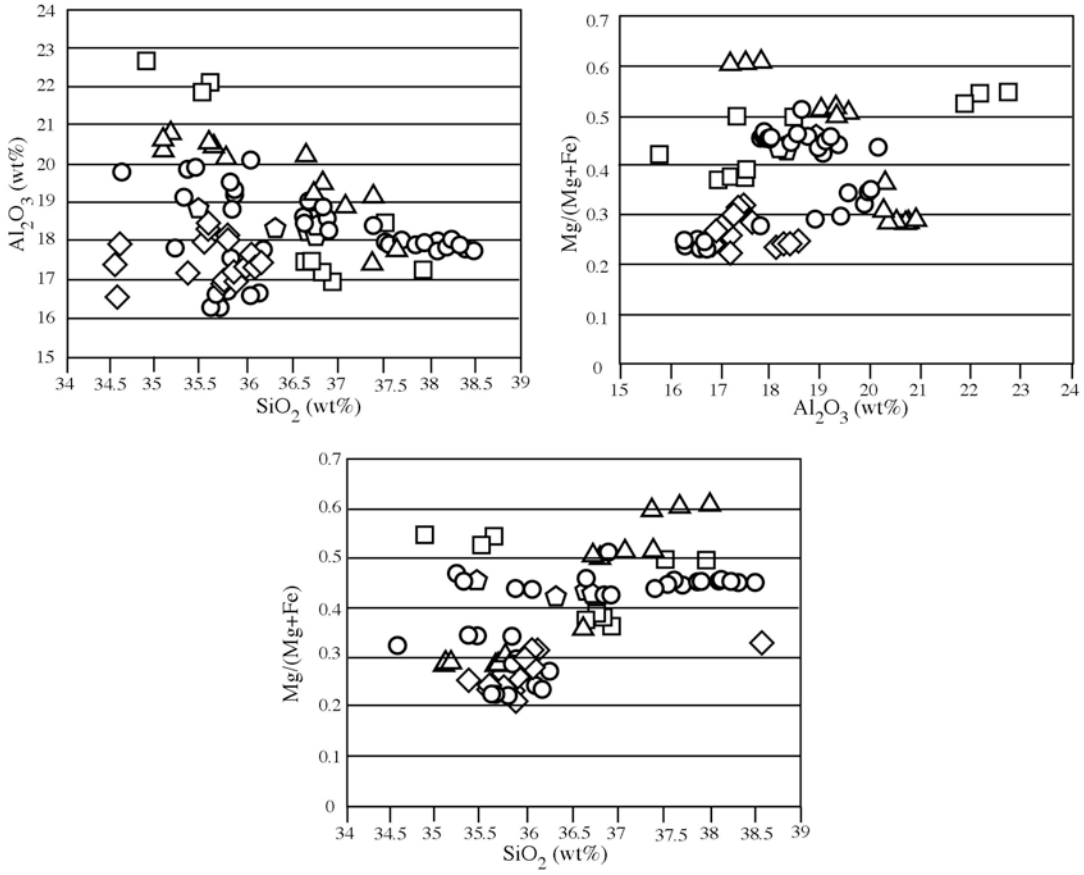

Figure 4.9: Oxide-oxide plots of biotites from the Musselwhite mine. Triangles = felsic metavolcanic samples, circles = biotite-garnet schist, squares = mafic metavolcanic samples, diamonds = oxide-dominant iron formation, pentagons = silicate-dominant iron formation.

When plotted against gold concentration, a weak correlation is seen between Si content of biotite and Au (Fig. 4.10a). When gold concentration is plotted against Mg# for the mine biotites, a weak positive correlation with scatter is seen (Fig. 4.10b). No correlation exists between gold and K_2O or alumina content (Fig. 4.10c,d).

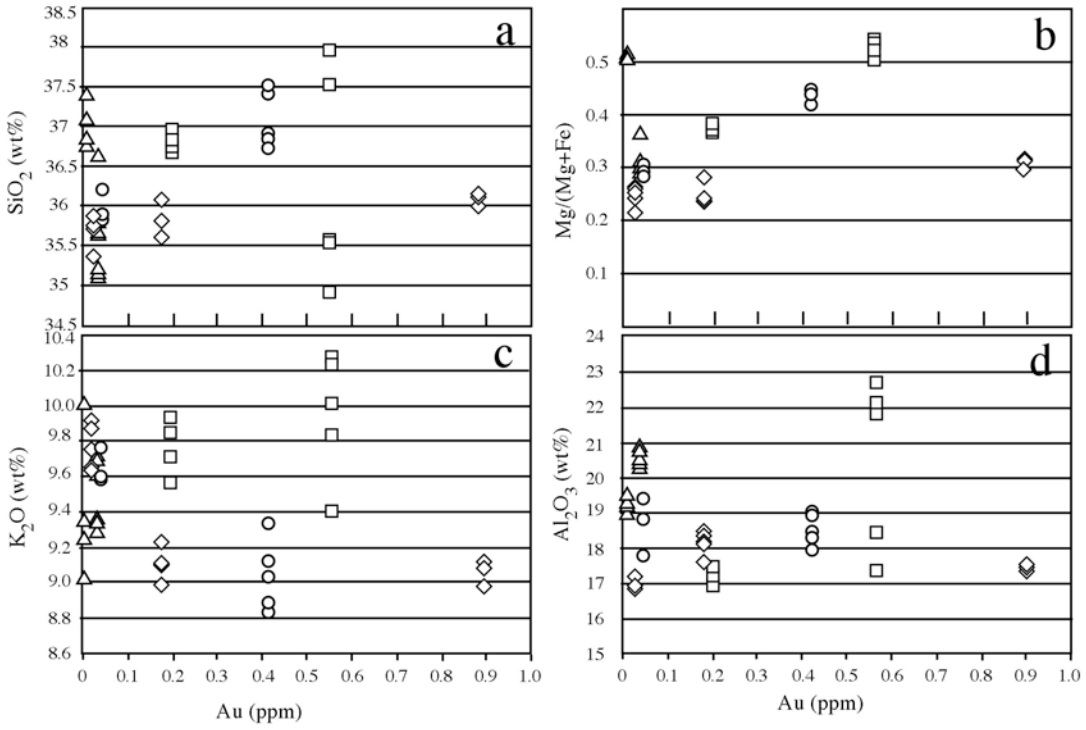

Figure 4.10: Oxide concentrations of biotite vs. whole rock gold concentrations at Musselwhite Mine. Triangles = felsic metavolcanic samples, circles = biotite-garnet schist, squares = mafic metavolcanic samples, diamonds = oxide-dominant iron formation.

When the SEM data of the thin sections is compared to isotope geochemistry of biotite mineral separates, a few trends are seen. Positive correlations between Mg# and light hydrogen isotopes and Mg# and heavier $\delta^{15}N$ exist (Fig. 4.11). No apparent trend is observed between Mg# and $\delta^{18}O$ (Fig. 4.11). No apparent trends are observed between stable isotopes and K_2O concentrations (Fig. 4.11). No apparent trends are observed between silica content of biotite and δD or $\delta^{18}O$ (Fig. 4.12).). However, a weak positive trends exists between SiO_2 content and increasing $\delta^{15}N$ (Fig 4.12). Alumina content also increases with increasing (i.e.: heavier) $\delta^{15}N$ but does not share any conclusive trends with δD or $\delta^{18}O$ (Fig. 4.12).

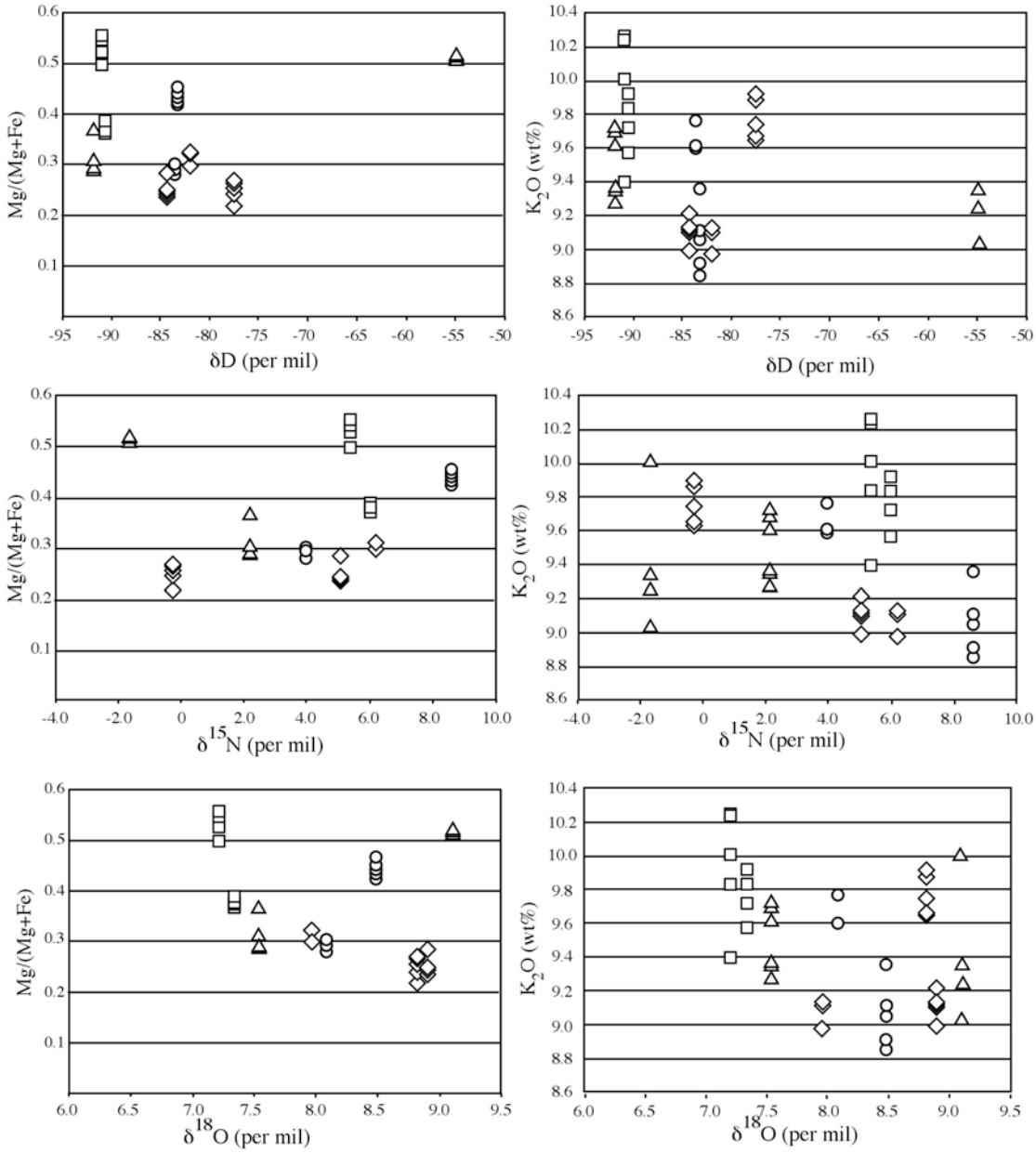

Figure 4.11: Mg# (left column) and K_2O (right column) vs. isotopic signatures of biotite samples at Musselwhite Mine. Triangles = felsic metavolcanic samples, circles = biotite-garnet schist, squares = mafic metavolcanic samples, diamonds = oxide-dominant iron formation.

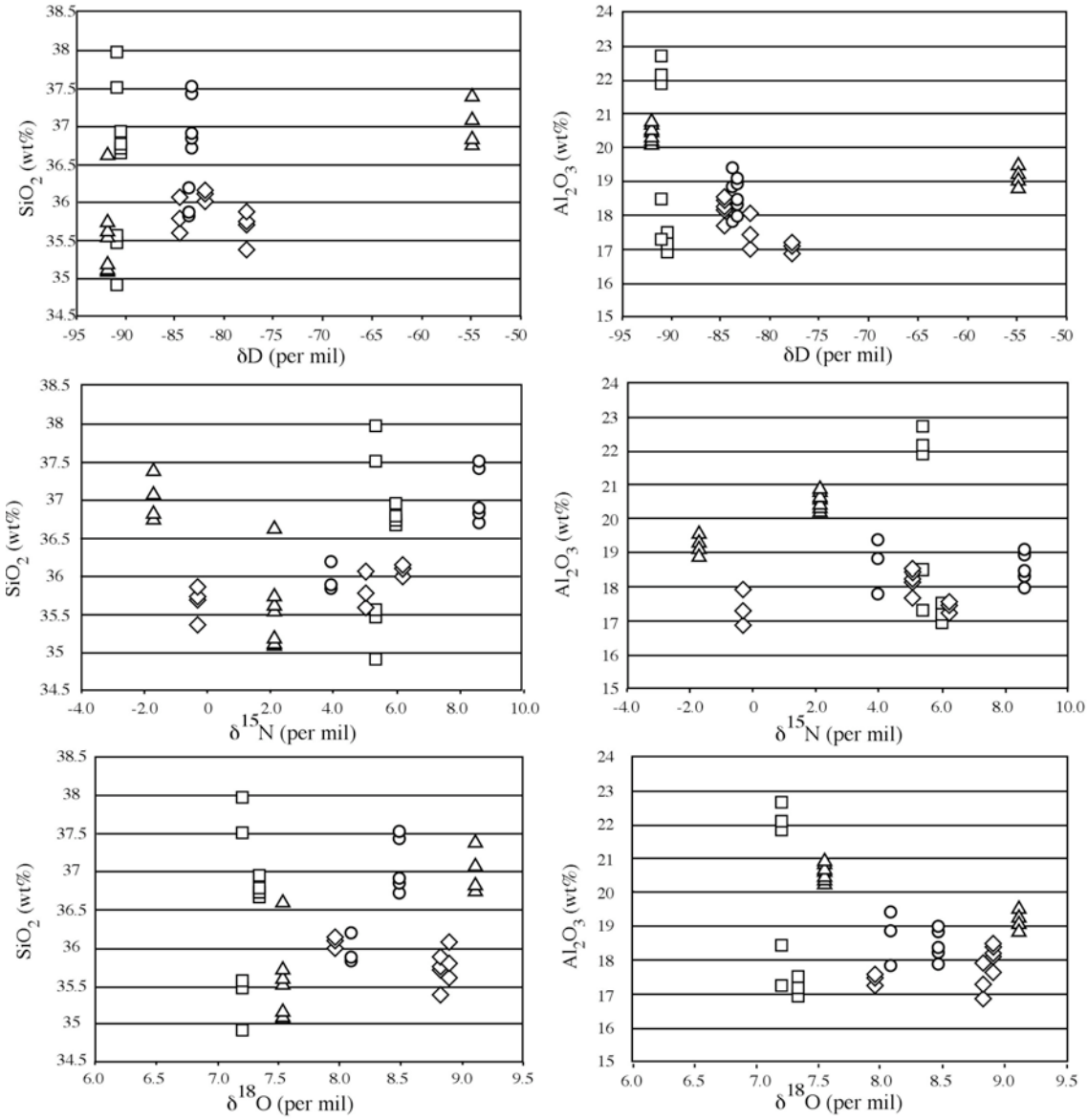

Figure 4.12: SiO_2 (left column) and alumina (right column) vs. isotopes of biotite samples at Musselwhite Mine. Triangles = felsic metavolcanic samples, circles = biotite-garnet schist, squares = mafic metavolcanic samples, diamonds = oxide-dominant iron formation.

4.5 Discussion

In Chapter 3, it was found that some hydrogen isotopic signatures of biotite were too light to be explained by metamorphic fluids and were not likely influenced by organic matter. However, there still are a few other possible explanations. Suzuoki and Epstein (1976) suggested that one cause of light hydrogen isotopes can be due to high iron content of biotite, as a result of the larger Fe cation causing a corresponding preference

for the smaller H ion in the hydroxyl space. The annite content of some of the biotites at the Musselwhite Mine are higher than those of the surrounding granitoids, as would be expected for biotite created within an iron formation. However, there is a negative correlation exists between phlogopite content and heavier hydrogen isotopes rather than a positive one as would be expected for iron-based hydrogen fractionation. This strongly suggests that hydrogen fractionation due to iron content is not the cause for the low negative isotopic signature of the biotite at Musselwhite. This leaves magmatic sources as a plausable source of light hydrogen isotopic signatures for the biotite samples at the Musselwhite Mine.

The silica and phlogopite content of biotite samples correlate positively. They also both correlate positively with the whole rock gold concentration. This suggests that biotites with higher silica and phlogopite content are more likely to be directly related to gold mineralization (and the quartz flooding associated with it). That low δD isotopes correlate positively with high Mg# and SiO_2-rich biotites further bolsters the suggestion that biotite and gold mineralisation are related to fluids of a magmatic nature.

The biotite compositions of the regional felsic rocks suggest that the metasedimentary sample E438532 is not derived directly from biotite of the granitoids surrounding the North Caribou Lake greenstone belt. However, the biotite is extremely high in silica and low in alumina (uncharacteristic of metasedimentary rocks) and also has the highest Mg# of all the regional biotites. It is possible then that the biotite in this rock could have been influenced by the same hydrothermal fluids as the rocks at Musselwhite.

Two different colours of biotite have been noted at Musselwhtie Mine: brown biotite that makes up the majority, and a much less common green variety. Not all samples in this study contain green biotite and even those that do generally still contain

brown biotite. In thin section, green biotite is closely associated with quartz veins and is found as inclusions in massive pyrrhotite. This suggests that green biotite is more directly associated with gold mineralisation than the brown variety is. Table 4.1 shows that the samples with significant green biotite are the ones with the lowest $\delta^{15}N$ (excluding the samples from the base of the Northern Iron Formation, E354010 and E358110).

Table 4.1: Table showing $\delta^{15}N$ and which species of biotite are present in samples from the Musselwhite Mine. X= significant presence, (*) = minor constituent.

Sample #	Unit	Biotite			
		N concentration (ppm)	$\delta^{15}N$ (per mil)	Brown	Green
E354010	4b	6.753	-0.3	X	
E354013	4ea	8.441	+5.4	X	X
E354016	4b	22.507	+5.1	X	X
E354018	4b	27.162	+2.1	X	X
E354020	4b	38.061	+3.3	(*)	X
E354024	4ea	68.944	+7.5	X	
E354025	2t	21.365	+5.4	X	(*)
E354026	4ea	26.274	+6.5	X	
E354029	4f	33.644	+8.0	X	
E354032	4f	61.022	+8.3	X	
E354039	4ea	36.173	+7.0	X	
E354039	4ea	34.983	+6.3	X	
E354040	4b	22.041	+6.2	X	
E354041	2	149.627	+1.9	X	
E354041	2	176.438	+2.4	X	(*)
E354043	4f	26.196	+6.0	X	(*)
E354043	4f	127.536	+5.3	X	X
E354045	6	115.832	+2.1	X	X
E354050	4b	22.527	+11.5	X	
E358103	4ea	32.233	+8.9	X	(*)
E358103	4ea	32.213	+6.3	X	(*)
E358105	4f	38.132	+8.7	X	(*)
E358106	4f	91.932	+3.8	X	(*)
E358106	4f	95.179	+4.1	X	X
E358108	2t	44.470	+6.0	X	X
E358109	2t	20.646	+5.1	X	
E358110	2	8.441	-1.7	X	

The presence of both green and brown biotite has been noted in greisen deposits (Glass et al., 1958; Dudoignon et al., 1988; Gottesmann and Forster, 2004) with brown biotite generally representing the primary phase and early fluid stages and green biotite being part of late stage hydrothermal alteration. Due to the common association of green biotite with quartz veins and pyrrhotite mineralisation, the green biotites of the Musselwhite mine may also represent late stage hydrothermal alteration. Although beyond the scope of this study, a study of the geochemical compositions of green and brown biotite may give further insight to mineralisation at Musselwhite Mine.

CHAPTER 5: DISCUSSION & CONCLUSIONS

5.1 Discussion

Nitrogen isotopes of biotite from Musselwhite Mine range between -1.5 and +9.0 per mil. The values overlap with those found for granites (Jia and Kerrich, 2000), basalt (Marty and Zimmerman, 1999; Nishizawa et al., 2007) and sedimentary and metasedimentary rocks (Jia, 2006; Haendel et al., 1986; Bebout et al., 1999). However, the nitrogen concentrations of the majority of biotite samples of the Musselwhite Mine are lower than any previously studied schist, which typically contain nitrogen concentrations in the hundreds of ppm, irrespective of age (Haendel et al., 1986; Boyd and Philippot, 1998; Pitcairn et al., 2005; Jia, 2006; Fig. 5.1). The cluster of points with high N concentration from Musselwhite lie within the field of data for the andalusite facies rocks (T= 500-600°C, P =3-4 kbar) of the Cooma complex, which is of the same metamorphic grade as Musselwhite (Jia, 2006). The Cooma complex is a packet of metasedimentary rocks that have undergone contact metamorphism with grade increasing toward the contact between the sedimentary rocks and the pluton (Jia, 2006). This strongly suggests that the interpretation of the high N samples from the Musselwhite mine as metasedimentary rocks that escaped influence of hydrothermal fluids is prudent. The majority of samples with lower N samples must then have formed from fluids different than those of the original metasedimentary rocks at Musselwhite.

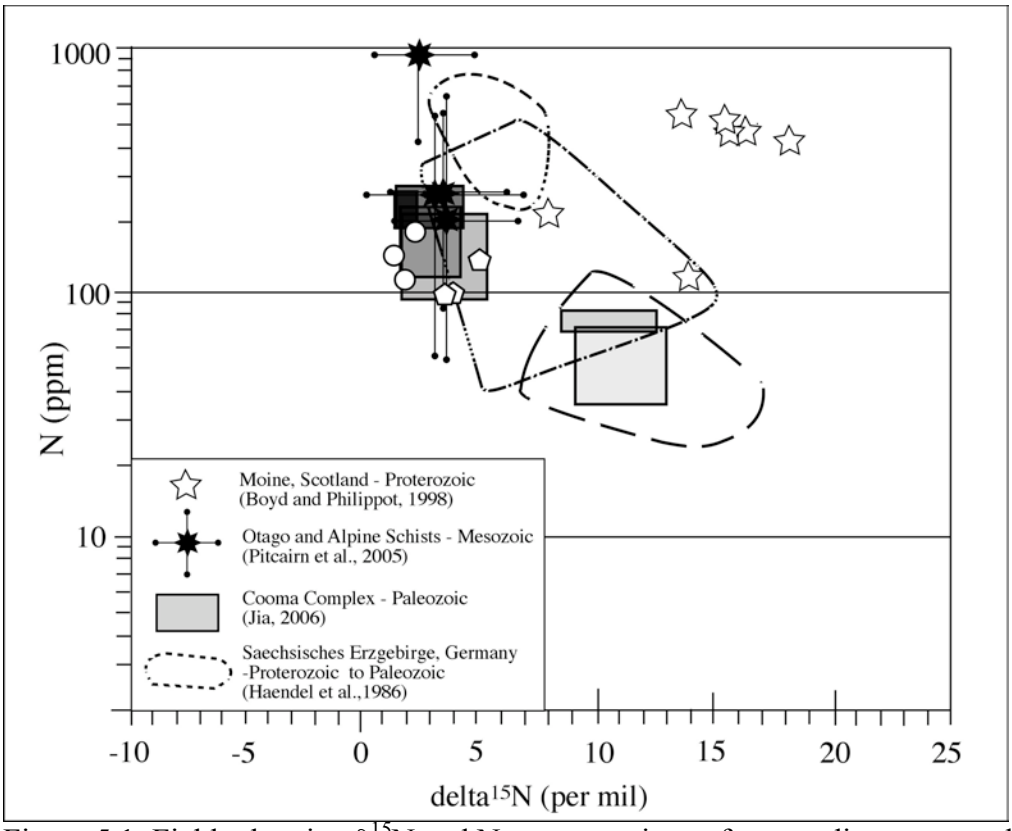

Figure 5.1: Fields showing $\delta^{15}N$ and N concentrations of metasedimentary rocks. White circles and pentagon are high N samples from this study.

The positive correlation of N concentration with increasing $\delta^{15}N$ of samples from Musselwhite makes it possible to speculate as to the origins of mineralisation at Musselwhite. There are a few ways a positive trend in nitrogen concentration vs. $\delta^{15}N$ could be created: 1) interaction of metamorphosed rocks with meteoric fluids 2) crystallization of biotite from metamorphic fluids of differing composition than those of the metamorphic rocks 3) interaction of metamorphic rocks and magmatically derived fluids. As previously discussed in Chapter 3, the hydrogen signatures of biotite as well as the estimated depth of formation rule out meteoric fluids as a possible source for the low nitrogen signature. It may be possible to create such nitrogen signatures from metamorphic fluids. Jia (2006) states temperatures below 600°C will result in a 1 to 2 per

mil shift in $\delta^{15}N$ due to N_2 being the dominant species lost to the fluid phase and shifts of 7-10‰ in $\delta^{15}N$ are possible at temperatures in excess of 600°C. However, the concentration of nitrogen in the fluid phase produced by the devolitilisation of hydroxyl-bearing minerals would be very low (Fig 5.2). The temperature range of quartz-biotite pairs from Musselwhite (343-622°C) indicate that the range of nitrogen isotopes could have been produced by fluids exsolved during metamorphism. Fractionation between biotite and N_2 or NH_3 in metamorphic fluids is highly dependent on initial compositions of the rock and the type of fractionation constrained, thus how far it can drive the data from the curve is difficult to assess. However, if fractionation is minimal, then it cannot account for the trend shown by the data for Musselwhite. Moreover, the temperatures of Musselwhite ranges from lower greenschist to middle-upper amphibolite facies – a very broad metamorphic range for such a small area.

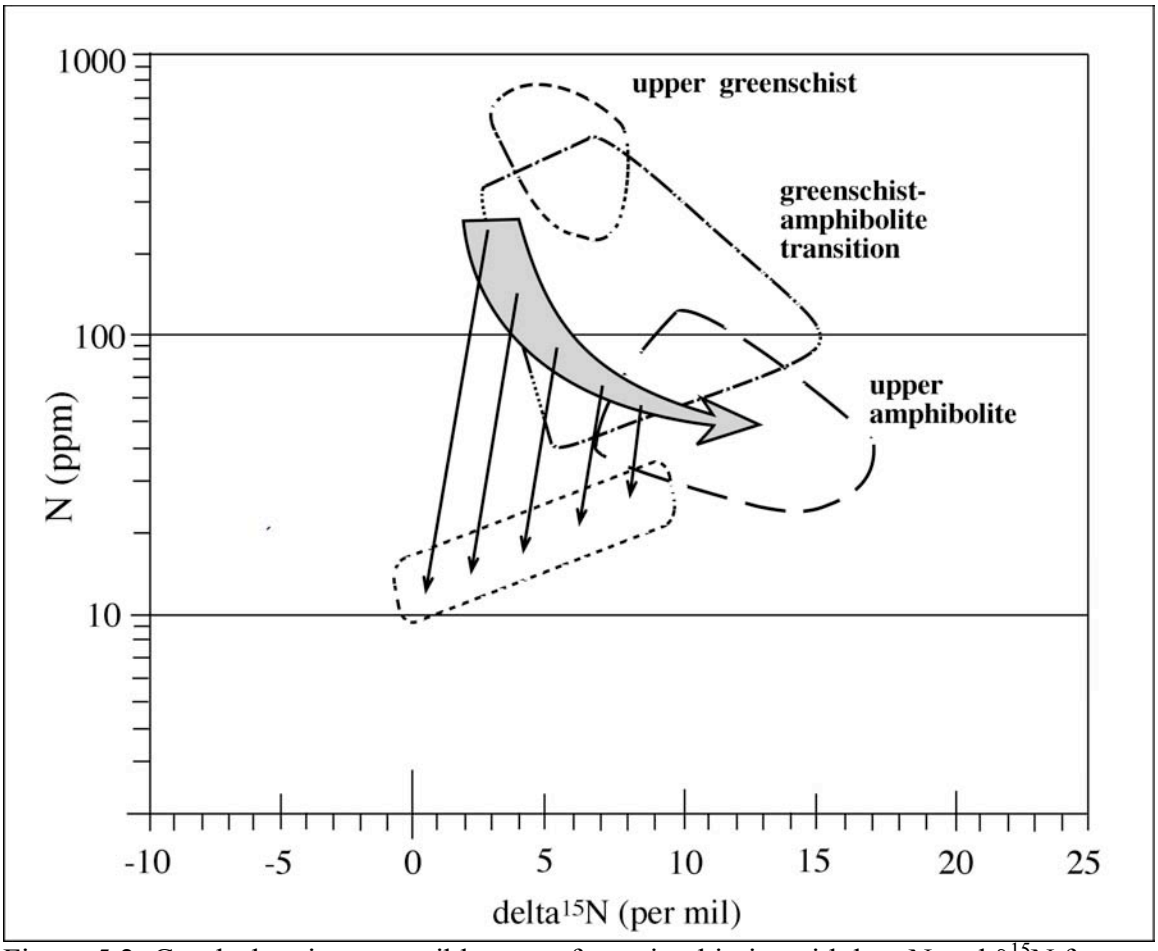

Figure 5.2: Graph showing a possible way of creating biotite with low N and $\delta^{15}N$ from metamorphic fluids. Grey arrow represents fractionation of samples from Jia (2006).

The positive correlation between N concentration and $\delta^{15}N$ and the broad range of $\delta^{15}N$ of the Musselwhite Mine (Fig. 3.5) could also be explained by the interaction of metamorphosed rocks with magmatic fluids. The work of Bebout et al. (1999) shows a positive correlation for samples adjacent to the Skiddaw pluton which were interpreted as a mix of metamorphic micas and micas affected by greisenization (i.e., magmatic fluids; Fig. 3.7). It is of interest to note that in the data of Jia and Kerrich (1999), if each mine's data are examined in isolation, most display positive correlations (Fig. 5.3). This positive correlation could also be an indicator of a magmatically-derived fluid influence in these deposits.

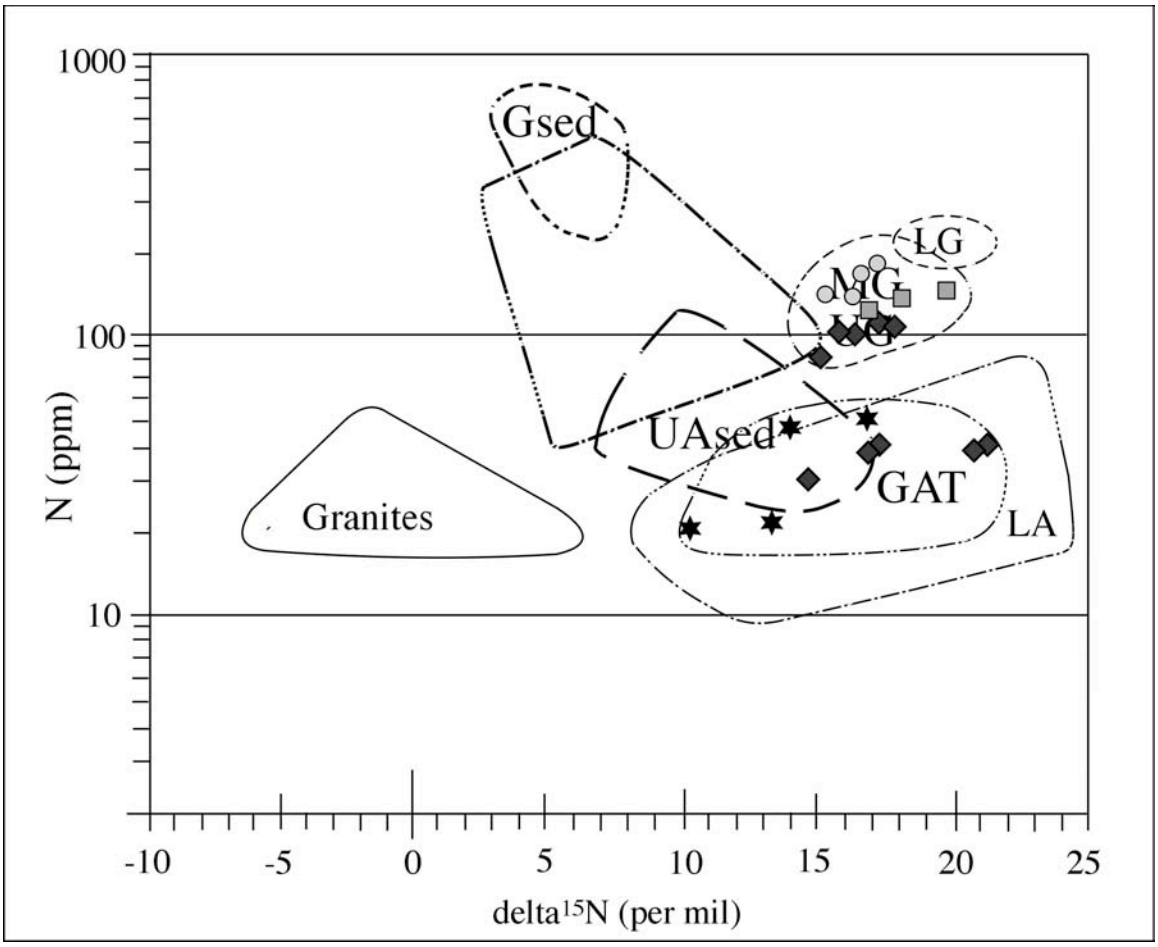

Figure 5.3: Positive correlations of nitrogen isotopic signatures of various gold deposits in the data set of Jia and Kerrich (1999). Circles = Dome, Squares = Goldhawk, Diamonds = Hollinger, and stars = Geraldton.

No correlation is observed between nitrogen signature of biotite and Au mineralisation in the samples from Musselwhite. This could be due to the presence of multiple fluid events that have recrystallised biotite, but did not all precipitate gold. However, the large sample size that was required to generate a detectable amount of nitrogen for analysis could also have masked any correlation. 300-2000 mg of biotite was collected for each sample, and although all care was taken to create pure samples, if a mix of more than one type of biotite was produced, the result would be an average between the two. This mix of biotites of different origins is a possible explanation as to

why there is no apparent correlation between Au mineralization and nitrogen isotopic signature, which might be expected if Au rich fluids were derived from a pluton, but would not be expected from metamorphic fluids being responsible for Au mineralisation.

The $\delta^{18}O$ signatures of biotite at Musselwhite Mine range between +7.1 and 10.1‰ and regional plutonic biotites surrounding the NCLGB have a $\delta^{18}O$ of +2.0 to +4.0‰. Turi and Taylor (1971) studied oxygen isotopes of the rocks of the French Valley Formation (quartz-biotite schist) and the Southern California batholith, which are comparable to the rock types in this study in that they represent metasedimentary rocks and plutons. Biotite $\delta^{18}O$ values of quartz-biotite schist of the French Valley Formation range between +11.6 and +20.0‰, with the majority of values falling above +16‰ (Turi and Taylor, 1971). Garlick and Epstein (1967) found the general $\delta^{18}O$ of schists to range between +13 and +18‰. Taylor and Epstein (1964) and Savin and Epstein (1970) found a similar general range for shales (+14 to +19‰). The biotites of the Southern California batholith range between +4 and +8 ‰ (Turi and Taylor, 1971) The $\delta^{18}O$ of biotites of the Musselwhite mine fall somewhere between the values of the biotites of the Southern California batholith and the values of biotite of the French Valley Formation. Turi and Taylor (1971) noted that biotite $\delta^{18}O$ values near the contact between the French Valley Fm. and the Southern California batholith indicated an exchange of fluids between the pluton and the surrounding schists. If that is true, and if the biotites of Musselwhite Mine were truly pelitic originally, then it is likely that the biotite values at Musselwhite Mine represent a fluid exchange between the schists and magmatic fluids.

Quartz $\delta^{18}O$ values for Musselwhite indicate exchange between magmatic fluids and metamorphic rocks. $\delta^{18}O$ of quartz samples range between 12.4 and 17.2 ‰, with the

lowest values associated with gold-bearing zones and the silicate dominant iron formation. The values of Otto (2002) for barren and gold-bearing quartz veins overlap with these values. The values for the mineralized zone at Musselwhite are similar to the values reported by Fyfe and Kerrich (1982) for the Yellowknife district (Campbell Shear: $\delta^{18}O$ = +11.49 to +12.53; Con shear: +11.50 to 12.25; Ptarmigan: +12.60 to +13.16; Surface: +13.51 to +13.56). However, there is a distinct increase in $\delta^{18}O$ of quartz both below and above the silicate dominant iron formation at Musselwhite. This contrasts with the findings in Fyfe and Kerrich (1982) that showed that the host rocks adjacent to the quartz veins have the same $\delta^{18}O$ as the gold veins. Quartz from the silicate dominant iron formation of Musselwhite yields values between 12-14 ‰ whereas the oxide dominant iron formation has a $\delta^{18}O$ 14 ‰ or higher and quartz from the biotite-garnet schist also has higher $\delta^{18}O$ than quartz sampled from the silicate dominant iron formation. The signature of the silicate facies iron formation and quartz veins of the Musselwhite mine possibly suggests either fluid-rock interaction of the heavier isotopic signature of the iron formation with an isotopically lighter fluid and/or that isotopically light fluids have overprinted the signature of the isotopically heavier fluids. The values of quartz taken from metasedimentary rocks of the Yellowknife district all fall in the same range as the quartz veins suggesting that the "host rocks" mentioned in Fyfe and Kerrich (1982) are in truth a part of the alteration halo surrounding gold mineralisation, as they are somewhat low compared to most sedimentary rocks (Sheppard, 1986).

H_2O calculations using oxygen isotopes from quartz and biotite pairs give fluids with compositions around +9.0 to +12.6‰. These values overlap with the values for

fluids from other Archean greenstone belts reported in Fyfe and Kerrich (1982). These values place the fluids in the area of overlap between magmatic and metamorphic fluids. However, the fact that the gold at Musselwhite occurs in a metasedimentary packet must be taken into consideration. The host rocks of the Musselwhite deposit have a distinctly higher $\delta^{18}O$ than do areas of mineralisation. This would suggest that magmatically derived fluids were responsible for mineralisation at Musselwhite Mine.

As stated in Chapter 1, currently there are two models postulated for the source of gold in orogenic gold deposits: the metamorphic model, where metamorphic fluids are responsible for the leaching, transport and deposition of gold, and the magmatic model where gold is transported in a magmatic body and exhaled with the fluid phase at time of crystallization. The N, O, and H isotopic values for the Musselwhite mine are more consistent with a magmatic-fluid model than a metamorphic fluid model. However, there are other points that must be addressed if the magmatic fluid model can be plausible. One of the major arguments against the magmatic theories for orogenic gold deposits is that Au mineralisation either pre or post-dates associated plutonic events (Kerrich and Cassidy, 1994). However, the methods used to date plutonic rocks and mineralisation in gold deposits are very different. Plutons are typically dated using U-Pb dating of zircons whereas orogenic gold deposits are dated by a variety of techniques, including Pb-Pb, K-Ar and Ar-Ar, Rb-Sr and Nd-Sm. Kerrich and Cassidy (1994) observe that the Pb-Pb technique used to date these deposits has an error of approximately 30 Ma, and that for other techniques such as Ar-Ar and Rb-Sr great care must be take to ensure that these

values have not been reset. Kerrich and Cassidy (1994) suggest that these errors are sufficient to make pluton emplacement and deposit genesis roughly coeval. Maas (unpublished data, 2006) reported four separate Nd-Sm ages, with the value of 2690 +/- 9 Ma as the preferred age of gold mineralisation at Musselwhite Mine. The batholith to the south of Musselwhite has yielded ages of 2729.4 +/- 7.1 and 2725.8 +/- 3.2Ma (Klipfel, 2002). The preferred Sm-Nd age is based on a two-point line between a pure garnet separate with less than 1% mineral inclusions and an averaged value of three whole rock samples (Maas, unpublished data, 2006). While this age is reported as being the most precise, the exclusion of data in order to achieve a precise result can be misleading and may ultimately be inaccurate. The age of 2695 +/- 25 Ma quoted in this study is the value obtained when all five samples (the four mentioned above and a garnet separate with around 20% inclusions) are plotted individually, as this represents all Nd-Sm data values obtained. In light of this Nd-Sm age, the zircon U-Pb ages reported by Klipfel (2002) of 2729.4 +/- 7.1 to 2725.8 +/- 3.2Ma are nearly within error of the age of mineralisation, and indicate that pluton emplacement occurred and gold mineralisation of the Northern Iron Formation may have been coeval. Maas (unpublished data, 2006) notes that the Sm-Nd age generated by the garnet separates (2664 +/- 19 Ma) is distinctly younger than those given by the whole rock –garnet combined values (2695+/-25Ma), and postulates LREE metasomatism post-garnet growth as a potential explanation. In addition, the multi-stage growth of garnets noted in the deposit in Chapter 2 may have affected the Sm-Nd date itself.

Another argument presented against magmatic theories of orogenic gold is the low concentrations of gold in igneous and metaigneous rocks. However, Connors et al. (1993) noted that volatile loss exhibits a strong, even overriding control on the Au content of an igneous body, as Au and metals will partition preferentially into the vapour phase. If gold is so partial to the vapour phase, then it is very likely that the initial gold concentration of a body of magma is very different to the final concentration of the resulting igneous pluton, and measurement of gold concentrations of rocks will yield very little information on the true initial concentration of gold in a given pluton. Mungall (2002) showed several possible scenarios that would allow for the creation of Au-rich magmas in a continental arc setting including: subduction of young, hot oceanic crust, stalling of a subduction slab, resulting in partial melting of the slab, subduction and secondary devolatilisation of a "warm" plate (intermediate between hot, young and old, cold oceanic crust), and flat subduction trapping asthenoshpere between plates. Thus it is possible to have emplacement of Au- rich magmas in an orogenic setting that upon devolatilisation would have no indication of having once been so.

The Musselwhite mine is classified as an orogenic gold deposit by Otto (2002) and as an iron-formation-hosted orogenic gold deposit by Blower and Kiernan (2003). However, as stated previously in Chapter 1, the term "orogenic gold" is used as a blanket term for most Archean greenstone deposits, regardless of genetic particulars and iron-formation-hosted merely describes the host rocks, not the mineralisation. When gold mineralisation is discovered in Archean terranes, there is a very strong tendency to automatically classify it as an orogenic gold deposit barring strong indicators to the

contrary. Part of this tendency is due the orogenic model's inclusion of metamorphosed terranes as one of their defining features.

Veins and stockworks of quartz and carbonate minerals, pyrite, albite, muscovite, pyrite and tourmaline are diagnostic gangue minerals of orogenic gold mineralisation (Kerrich, 1989). While quartz and carbonate are indeed associated with mineralisation of the Musselwhite mine, there are some features of the deposit that do not fit well with the orogenic-mesothermal gold model including: the presence of pyrrhotite rather than pyrite and its association with gold, the association of gold with "retrograde" chlorite-hornblende-calcite veins (Otto, 2002) and in garnets rather than quartz veins, the extreme scarcity of muscovite and sericite in the deposit, the presence of cobalt, lead and nickel tellurides associated with gold tellurides (Liefrovich, 2007), and the range of temperatures generated this study and chlorite temperatures from Otto (2002).

5.2 Conclusions

The nitrogen signature of biotites from the 11700 N section of Musselwhite Mine yield values from -1.3 to +11.1 ‰ and have nitrogen concentrations of 10 ppm to around 150 ppm. Hydrogen isotopic data for the mine biotites ranges from -55 to -100 per mil, with and average δD of -86 ‰. Oxygen isotopic values for biotite are between +7.1 and +8.9 ‰. The stable isotope geochemistry of biotite at Musselwhite Mine reveal two populations: one that represents the relatively unaltered biotite-garnet schist that caps the Northern Iron Formation and a second signature. The second population's signature could have been produced by crystallization of biotite from metamorphic fluids derived from

devolitilisation of metamorphic rocks, or by interaction of magmatic-derived fluids interacting with metamorphic rocks. When the range of temperatures of biotite at Musselwhite Mine is taken into consideration, it seems less likely that fluids produced by regional metamorphism are the cause of the isotopic signatures at Musselwhite Mine.

5.3 Recommendations

The current knowledge of nitrogen and its behaviour in rocks is very sparse. This is largely due to the low concentration of nitrogen in most rocks. Only recently has it become possible to measure the nitrogen isotopes of rocks and then only in certain minerals in large quantities. The result is an average isotopic signature for the mineral concentrate and a bias towards rocks containing a certain mineral. More studies, both experimental and empirical, are recommended to better constrain the isotopic signature of various rocks. A more extensive study of the compositions, both isotopic and mineralogical, of green and brown biotite and their abundances at Musselwhite would help to better understand the relationship of biotite with gold mineralisation and provide further insight into the nature of fluid-rock interactions at Musselwhite Mine.

REFERENCES

Actlabs, 2008. Lithogeochemistry for Exploration and Research. http://www.actlabs.com/gg_rock_litho_can.htm

Barker, F., 1979. Trondhjemites, Dacites and Related Rocks. Elsevier, New York.

Bebout, G.E., Cooper, D.C., Bradley, A.D., Sadofsky, S.J., 1999. Nitrogen-isotope record of fluid-rock interactions in the Skiddaw Aureole and granite, English Lake district. American Mineralogist, 84, p. 1495-1505.

Beaudoin, G., and Therrien, P., 2008. Stable isotope fractionation calculator (SIFC). www.ggl.ulaval.ca/cgi-bin/isotope/generisotope.cgi

Bierlein, F.P., Arne, D.C., Cartwright, I., 2004. Stable isotope (C, O, S) systematics in alteration haloes associated with orogenic gold mineralization in the Vicotrian gold province, SE Australia. Geochemistry: Exploration, Environment, Analysis, 4, p. 191-211.

Blower, S.J., and Kiernan, J., 2003. Technical Report: Musselwhite Mine. Internal report for Kinross Gold Corporation. 129 pp.

Bottinga, Y., and Javoy, M., 1973. Comments on oxygen isotope geothermometry. Earth and Planetary Science Letters, 20, p. 250-265.

Bottinga, Y., and Javoy, M., 1975. Oxygen isotope partitioning among the minerals in igneous and metamorphic rocks. Reviews of Geophysics and Space Physics, 13, p. 401-417.

Boyd, S.R., and Philippot, P., 1998. Precambrian ammonium biogeochemistry: a study of the Moine metasediments, Scotland. Chemical Geology, 144, p. 257-268.

Breaks, F.W. Bartlett, J.R., de Kemp, E.A., Finamore, P.F., Jones, G.R., Macdonald, A.J., Shields, H.N., and Wallace, H., 1984. Opapimiskan Lake Project: Precambrian Geology, Quaternary Geology, and Mineral Deposits of the North Caribou Lake Area, District of Kenora, Patricia Portion. Ontario Geological Survey, Miscellaneous Paper 119, S49, pp. 258-273.

Breaks, F.W., Osmani, I.A., Bartlett, J.R., Finamore, P.F. and Wallace, H., 1985. Opapimiskan Lake Project: Precambrian and Quaternary Geology of the North Caribou Lake Area, District of Kenora, Patricia Portion. Ontario Geological Survey, Miscellaneous Paper 126, S54, p. 268-276.

Breaks, F.W., Osmani, I.A., and de Kemp, E.A., 1986. Opapimiskan Lake Project: Precambrian Geology pf the Opapimiskan-Forrester Lakes Area, District of Kenora, Patricia Portion. Ontario Geological Survey, Miscellaneous Paper 132, p. 368-378.

Breaks, F.W., Osmani, I.A., and de Kemp, E.A., 2001. Geology of the North Caribou Lake Area, northwestern Ontario. Ontario Geological Survey, Open File Report 6023, 80 p.

Burrows, D.R., and Spooner, E.T.C., 1987. Generation of a magmatic H_2O-CO_2 fluid enriched in Mo, Au and W within an Archean sodic granodiorite stock, Mink Lake, northwestern Ontario. Economic Geology, 82, p.1931-1957.

Burrows, D.R., Wood, P.C., Spooner, E.T.C., 1986. Carbon isotope evidence for a magmatic origin for Archean gold-quartz vein ore deposits. Nature, 321, p. 851-854.

Card, K.D., 1990. A review of the Superior Province of the Canadian Shield, a product of Archean accretion. Precambrian Research, 48, p. 99-156.

Card, K.D., and Ciesielski, A. 1986. DNAG #1. Subdivisions of the Superior Province of the Canadian Shield. Geosciences Canada, Vol. 13(1), p. 5-13.

Colvine, A.C., 1989. An empirical model for the formation of Archean gold deposits: products of final cratonization of the Superior Province, Canada. In: *R.R. Keays, R.H. Ramsay & D. L. Groves;* Economic Geology Monograph 6 The Geology of Gold Deposits: The Perspective in 1988, p. 37-53.

Connors, K.A., Noble, D.C., Bussey, S.D., Weiss, S.I., 1993. Initial gold contents of silicic volcanic rocks: bearing on the behaviour of gold in magmatic systems. Geology, 21, p. 937-940.

Craig, H., 1961. Isotopic variations in meteoric waters. Science, 133, 1702-1703.

Davis, D.W. and Stott, G.M., 2001. Geochronology of several greenstone belts in the Sachigo Subprovince, northwestern Ontario, Ontario Geological survey, OFR6070.018

Deer, W.A., Howie, R.A., Zussman, J., 1992. Sheet silicates. In: An introduction to the Rock Forming Minerals, 2nd Edition. Prentice Hall, p. 279-387.

de Kemp, E.A., 1987. Stratigraphy, provenance and geochronology of Archean supracrustal rocks of western Eyapamikama Lake area, northwestern Ontario. Unpublished M.Sc. Thesis, Carleton University, 97 pp.

D'Hondt, S., Jøgensen, B.B., Miller, D.J., Batzke, A., Blake, R., Cragg, B.A., Cypionk, H., Dickens, G.R., Ferdelman, T., Hinrichs, K.U., Holm, N.G., Mitterer, R., Ford, K., Gettemy, G., Rutherford, S.D., Sass, h., Skilbeck, C.G., Aiello, I.W., Gulèrin, G., house, C.H., Iagaki, F., Meister, P., Naehr, T., Niitsuma, S., Parkes, R.J., Schippers, A., Smith,

D.C., Teske, A., Wiegel, J., Padilla, C.N., Acosta, J.L.S., 2004. Distributions of microbial activites in deep subseafloor sediments. Science, 306, p. 2216-2221.

Dudoignon, P., Beaufort, D., and Meunier, A., 1988. Hydrothermal and supergene alterations I the granitic cupola of Montebras, Creuse, France. Clays and Clay Minerals, 36, p. 505-520.

Fischer, T.P., Hilton, D.R., Zimmer, M.M., Shaw, A.M., Sharp, Z.D., Walker, J.A., 2002. Subduction and Recycling of Nitrogen along the Central American Margin. Science, 297, p 1154-1157.

Fyfe, W.S. and Kerrich, R.W., 1982. Gold: Natural Concentration Processes. In: *R.P. Foster* Gold '82: the Geology, Geochemistry and Genesis of Gold Deposits, p. 99-127.

Garlick, G.D., and Epstein, S., 1967. Oxygen isotopes in coexisting minerals of regionally metamorphosed rocks. Geochimica et Cosmochimica Acta, 31, p. 181-214.

Glass, J.J., Koschmannm A.H., and Vhay, J.S., 1958. Minerals of the cassiterite-bearing veins at Irish Creek, Virginia, and their paragenetic relations. Economic Geology, 53, p. 65-84.

Goldcorp, 2008. Operations – Musselwhite.
http://www.goldcorp.com/operations/musselwhite/

Golding, S.D., and Wilson, A.F., 1987. Oxygen and hydrogen isotope relationships in Archean gold depoits of the Eastern Goldfields province, Western Australia: constraints on the source of Archean gold-bearing fluids. Geology Department and University Extension, University of Western Australia, Publication no. 11, p. 203-213.

Gottesmann, B., and Förster, H.J., 2004. Sekaninite from the Satung granite (Erzgebirge, Germany): magmatic or xenolithic? European Journal of Mineralogy, 16, p. 483-491.

Groves, D.I., Goldfarb, R.J., Gebre-Mariam, M., Hagemann, S.G., Robert, F., 1998. Orogenic gold deposits: a proposed classification in the context of their crustal distribution and relationship to other gold deposit types. Ore Geology Reviews, 13, p. 7-27.

Haendel, D., Mühle, K., Nitzsche, H.M., Stiehl, G., and Wand, U., 1986. Isotopic variations of the fixed nitrogen in metamorphic rocks. Geochimica et Cosmochimica Acta, 50, p. 749-758.

Hall, R.S. and Rigg, D.M., 1986. Geology of the West Anticline Zone, Musselwhite Prospect, Opapimiskan Lake, Ontario, Canada. In: *Macdonald, A. J.* Gold '86: An International Symposium of the Geology of Gold Deposits, Proceedings. p. 124-136.

Harford, C.L., and Sparks, S.J., 2001. Recent remobilization of shallow-level intrusions on Mentserrat revealed by hydrogen isotope composition of amphiboles. Earth and Planetary Science Letters, 185, p. 285-297.

Harris, A.C., Golding, S.D., White, N.C., 2005. Bajo de la Alumbrera copper-gold deposit: stable isotope evidence for a porphyry-related hydrothermal system dominated by magmatic aqueous fluids. Economic Geology, 100, p. 863-886.

Hill, M.L., Cheatle, A.M., and Liefrovich, R., 2006. Musselwhite Mine: an orogenic gold deposit in the western Superior Province. Geological Association of Canada, Montreal 2006 Abstracts, 31, p. 67.

Hodgson, C.J., 1993. Uses (and Abuses) of Ore Deposit Models in Mineral Exploration. *Sheahan, P.A., Cherry, M.E.:* Ore Deposit Models Volume II, Geoscience Canada Reprint Series 6, Geological Association of Canada, p. 1-12.

Hoffman, A., and Bolhar, R., 2007. Carbonaceous cherts in the Barberton greenstone belt and their significance for the study of early life in the Archean record. Astrobiology, 7, p. 355-388.

Hollings, P., 1995. Report on the trace element geochemistry of samples from the Musselwhite property, Sachigo Subprovince. Internal Report for Placer Dome, 4 p.

Hollings, P., 1996. New analyses from the Musselwhite property, Sachigo subprovince. Internal report for Placer Dome, 9 p.

Hollings, P. and Kerrich, R., 1999. Trace element systematics of ultramafic and mafic volcanic rocks from the 3 Ga North Caribou Lake greenstone belt, northwestern Superior Province. Precambrian Research 93, 257-279.

Honma, H., and Itihara, Y., 1981. Distribution of ammonium in minerals of metamorphic and granitic rocks. Geochimica et Cosmochimica Acta, 45, p. 983-988.

Jensen, L.S., 1976. A new cation plot for classifying subalkalic volcanic rock. Ontario Geological Survey, Miscellaneous Paper 066, 18 p.

Jia, Y., 2001. Nitrogen isotope characteristics of orogenic lode gold deposits and terrestrial reservoirs. Unpublished PhD thesis, University of Saskatchewan, 225 p.

Jia, Y., 2006. Nitrogen isotope fractionations during progressive metamorphism: a case study from the Paleozoic Cooma metasedimentary complex, southeastern Australia. Geochimica et Cosmochimica Acta, 70, p. 5201-5214.

Jia, Y., and Kerrich, R., 2000. Giant quartz vein systems in accretionary orogenic belts: the evidence for a metamorphic fluid origin from $\delta^{15}N$ and $\delta^{13}C$ studies. Earth and Planetary Science Letters, 184, p. 211-224.

Jia, Y., Li, X., and Kerrich, R., 2001. Stable isotope (O, H, S, C and N) systematics of quartz vein systems in the turbidite-hosted Central and North Deborah gold deposits of the Bendigo gold field, Central Victoria, Australia: Constraints on the origin of ore-forming fluids. Economic Geology, 96, p. 705-721.

Junium, C.K., and Arthur, M.A., 2007. Nitrogen cycling during the Cretaceous, Cenomanian-Turonian Oceanic Aoxic Event II. Geochemistry, Geophysics, Geosystems. 8(3) Q03002, 18 pp.

Kerrich, R., 1989. Geodynamic setting and hydraulic regimes: shear zone hosted mesothermal gold deposits. In: *J.T. Burnsall.* Geological Association of Canada Short Course Notes, Vol. 6, 89-128.

Kerrich, R., and Cassidy, K.F., 1994. Temporal relationships of lode gold mineralization to accretion, magmatism, metamorphism and deformation – Archean to present: a review. Ore Geology Reviews, 9, p. 263-310.

King, R.W., and Kerrich, R., 1989. Strontium isotope compositions of tourmaline from lode gold deposits of the Archean Abitibi greenstone belt (Ontario-Quebec, Canada): implications for source reservoirs. Chemical Geology, 79, p. 225-240.

Klipfel, P., 2002. Musselwhite U-Pb zircon and Ar-Ar dates: synthesis and interpretation. Internal report prepared for Placer Dome. 23 pp. plus abstracts.

Kroos, B.M., Jurisch, A., Plessen, B., 2006. Investigation of the fate of nitrogen in Paleozoic shales of the Central European Basin. Journal of Geochemical Exploration, 89, p. 191-194.

Kusky, T.M., and Hudleston, P.J., 1999. Growth and demise of an Archea carbonate platform, Steep Rock Lake, Ontario, Canada. Canadian Journal of Earth Sciences, 36, p. 565-584.

Liefrovich, R., 2007. Detailed petrographic and mineralogical study of high-grade pyrrhotite-carbonate vein from the drill hole #03-PQU-062. Internal report for Musselwhite, 19 p.

Marty, B., and Zimmerman, L., 1999. Volatiles (He, C, N, Ar) in mid-ocean ridge basalts: Assessment of shallow-level fractionation and characterization of source composition. Geochimica et Cosmochimica Acta, 63, p. 3619-3633.

Meinert, L.D., Dipple, G.M., and Nicolescu, S., 2005. World skarn deposits. *J.W. Hedenquist, J.F.H. Thompson, R.J. Goldfarb and J.P. Richards*; Economic Geology 100th Anniversary Volume, Society of Economic Geologists, p. 299–336.

Miller, D.N. Jr., 1957. Authigenic Biotite in Spheroidal Reduction Spots, Pierce Canyon Redbeds, Texas and New Mexico. Journal of Sedimentary Research, 27, p. 177-180.

Moran, P., 2008. Lithogeochemistry of the sedimentary stratigraphy and metosomatic alteration in the Musselwhite gold deposit, North Caribou Lake metavolcanic-metasedimentary belt, Superior Province, Canada: implications for deposition and mineralization. Unpublished MSc thesis, Lakehead University 351 p.

Mueller, A.G., 1997. The Nevoria gold skarn deposit in Archean iron-formation, Southern Cross greenstone belt, Western Australia: I. Tectonic setting, petrography, and classification. Economic Geology, 92, p. 181-209.

Müller, P.J., and Mangini, A., 1980. Organic carbon decomposition rates in sediments of the Pacific manganese nodule belt dated by ^{230}Th and ^{231}Pa. Earth and Planetary Science Letters, 51, p. 94-114.

Mungall, J.E., 2002. Roasting the mantle: slab melting and the genesis of major Au and Au-rich Cu deposits. Geology, 30, p. 915-918.

Nabelek, P.I., O'Neil, J.R., Papike, J.J., 1983. Vapor phase exsolution as a controlling factor in hydrogen isotope variation in granitic rocks: the Notch Peak granitic stock, Utah. Earth and Planetary Science Letters, 66, p. 137-150.

Nishizawa, M., Sao, Y., Ueno, Y., Shigenori, M., 2007. Speciation and isotope ratios of nitrogen in fluid inclusions from seafloor hydrothermal deposits at ~3.5 Ga. Earth and Planetary Science Letters, 254, p. 332-344.

O'Neil, J.R., and Chappell, B.W., 1977. Oxygen and hydrogen isotope relations in the Berridale batholith. Journal of the Geological Scoiety of London, 133, p. 559-571.

O'Neil, J.R, Shaw, S.E., and Flood, R.H., 1977. Oxygen and hydrogen isotope compositions as indicators of granite genesis in the New England batholith, Australia. Contributions to Mineralogy and Petrology, 62, p. 313-328.

Orberger, B., Gallien, J.P., Pinti, D.L., Fialin, M., Daudin, L., Gröcke, D.R., Pasava, J., 2005. Nitrogen and carbon partitioning in diagenetic and hydrothermal mmierals from Paleozoic Black Shales, (Selwyn Basin, Yukon Territories, Canada). Chemical Geology, 218, p. 249-264.

Otto, A., 2002. Ore forming processes in the BIF-hosted gold deposit Musselwhite Mine, Ontario, Canada. M. Sc. Thesis, Freiberg Institute of Minig and Technology 86 pp. plus appendices.

Pan, Y., Fleet, M.E., and Stone, W.E., 1991. Skarn mineralization (Cr, Fe, Au) in an Archean greenstone belt, White River property, Hemlo area, Ontario. Economic Geology, 86, p. 1626-1645.

Perry, E.C., 1967. The oxygen isotope chemistry of ancient cherts. Earth and Planetary Science Letters, 3, p. 62-66.

Pickard, A.L., 2002. SHRIMP U–Pb zircon ages of tuffaceous mudrocks in the Brockman Iron Formation of the Hamersley Range,Western Australia. Australian Journal of Earth Sciences, 49, p. 491–507.

Pinti, D.L., Hashizume, K. and Matsuda, J., 2001. Nitrogen and argon signatures in 3.8 to 2.8 Ga metasedimentary rocks: Clues on the chemical state of the Archean ocean and the deep biosphere. Geochimica et Cosmochimica Acta, 65, p. 2301-2315.

Pitcairn, I.K., Teagle, D.A.H., Kerrich, R., Craw, D., Brewer, T.S., 2005. The behavior of nitrogen and nitrogen isotopes during metamorphism and mineralization: evidence from the Otago and Alpine Schists, New Zealand. Earth and Planetary Science Letters, 233, p. 229-246.

Piroshco, D.W., Breaks, F.W., Osmani, I.A., 1989. The geology of gold prospects in the North Caribou Lake greenstone belt, District of Kenora, northwestern Ontario. Ontario Geological Survey, OFR5689,

Pollard, S., Brown, P., Klipfel, P., 2002. Placer Dome Canada Ltd Musselwhite Mine Geological Information Package. Internal report for Placer Dome, 30 pp.

Poulsen, K.H., 1995. Lode Gold. *Eckstrand, O.R., Sinclair, W.D., and Thorpe, R.I.* Geology of Canada, no. 8: Geology of Canadian Mineral Deposit Types. Geological Survey of Canada, p. 323-350.

Rayner, N., and Stott, G.M., 2005. Discrimination of Archean Domains in the Sachigo Subprovince. (Poster).

Sano, Y., Takahata, N., Nishio, Y., Fischer, T.P., Williams, S.N., 2001. Volcanic flux of nitrogen from the Earth. Chemical Geology, 171, p. 263-271.

Savin, S.M., and Epstein, S., 1970. The oxygen and hydrogen isotope geochemistry of ocean sediments and shales. Geochimica et Cosmochimica Acta, 34, p. 43-63.

Sharp, Z., 2007. Principles of Stable Isotope Geochemistry. Prentice Hall, 344 p.

Stemler, J.U., Richards, J.P., Mulenbachs, K., 2006. A fluid inclusion and stable isotopic investigation of the Boston lode-gold deposit, Hope Bay volcanic belt, Nunavut. Exploration and Mining Geology, 15, p. 101-121.

Sheppard, 1986. Characterization and isotopic variation in natural waters. *Valley, J.W., Taylor, H.P. Jr., O'Neil, J.R.*: Stable Isotopes in High Temperature Geological Processes. Mineral Society of America, Vol. 16, p. 165-184.

Stott, G.M., Corkery, T., Leclair, A., Boily, M. and Percival, J. 2007. A revised terrane map for the Superior Province as interpreted from aeromagnetic data; Institute on Lake Superior Geology Proceedings, 53rdAnnual Meeting, Lutsen, MN, v.53, part 1, p. 74-75.

Suzuoki, T., and Epstein, S., 1976. Hydrogen isotope fractionation between OH-bearing minerals and water. Geochimica et Cosmochimica Acta, 40, p. 1229-1240.

Taylor, B.E., Eichelberger, J.C., Westrich, H.R., 1983. Hydrogen isotopic evidence of rhyolititc magma degassing during shallow intrusion and eruption. Nature, 306, p. 541-545.

Taylor, H.P. Jr., 1974. The application of oxygen and hydrogen isotope studies to problems of hydrothermal alteration and ore depositon. Economic Geology, 69, p. 843-883.

Thurston, P.C., Osmani, I.A., Stone, D., 1991. Northwestern Superior Provinc; Review and terrane analysis. Ontario Geological Survey Special Volume 4, p. 81-142.

Turi, B., and Taylor, H.P. Jr., 1971. An oxygen and hydrogen isotope study of a granodiorite pluton from the Southern California Batholith. Geochimica et Cosmochimica Acta, 35, p. 383-406.

Valaas, E.P., 2004. Oxygen isotope thermometry in contact metamorphosed Biwabiik iron-formation. M.Sc. Thesis, University of Wisconsin, 65 p.

Vallance, J., Cathelineau, M., Boiron, M.C., Fourcade, S., Shepherd, T.J., Naden, J., 2003. Fluid-rock interactions and the role of late Hercynian aplite intrusion in the genesis of the Castromil gold deposit, northern Portugal. Chemical Geology, 194, p. 201-224.

Valley, J.W., 1986. Stable isotope geochemistry of metamorphic rocks. In: Valley, J.W, Taylor, H.P Jr., O'Neil, J.R. Stable Isotopes in High Temperature Geological Processes. Mineralogical Society of America, p.445-486.

Wells, R.C., 1995. Petrographic and lithogeochemical report on samples from the Musselwhite project, East Bay synform including observations on the geological setting of gold mineralization. Internal report prepared for Placer Dome, 20 pp. plus abstracts.

Wilson, M., 1989. Igneous Petrogenesis. Unwin Hyman, London.

Wood, P.C., Burrows, D.R., Thomas, A.V., Spooner, E.T.C., 1986. The Hollinger-McIntyre Au-quartz vein system, Timmins, Ontario, Canada; geologic characteristics, fluid properties and light stable isotope geochemistry. In Macdonald, A.J. Gold '86: and international symposium on the geology of gold deposits, Proceedings, p. 56-80.

Zheng, Y., 1993. Calculation of oxygen isotope fractionation in hydroxyl-bearing silicates. Earth and Planetary Science Letters, 120, p. 247-263.

Appendix A

Whole rock geochemistry of the rocks of the North Caribou Lake greenstone belt

SAMPLE	SiO2	Al2O3	Fe2O3	CaO	MgO	Na2O	K2O	Cr2O3	TiO2	MnO	P2O5	SrO	BaO	LOI	Total
E438514	72.35	15.06	2.33	1.92	0.40	4.35	2.59	0.005	0.15	0.04	0.063	0.02	0.04	0.41	99.71
E438513	72.10	15.18	2.53	2.16	0.48	4.36	2.17	0.005	0.16	0.04	0.08	0.02	0.03	0.65	99.96
E438508	66.52	16.82	3.54	3.56	1.34	4.29	2.10	0.005	0.48	0.05	0.134	0.04	0.06	0.73	99.67
E438509	68.06	16.76	3.03	3.45	1.10	4.69	1.67	0.005	0.38	0.04	0.113	0.05	0.05	0.55	99.95
E438510	72.25	14.60	2.05	1.76	0.53	3.55	3.80	0.005	0.24	0.04	0.062	0.03	0.08	0.64	99.62
E438511	72.85	15.54	1.06	1.18	0.26	4.31	3.91	0.005	0.09	0.02	0.043	0.03	0.05	0.52	99.86
E438512	71.00	15.52	2.40	2.27	0.63	4.20	2.74	0.005	0.27	0.02	0.082	0.03	0.1	0.34	99.6
E438515	70.44	16.26	2.52	2.54	0.59	4.93	1.64	0.005	0.28	0.03	0.076	0.04	0.03	0.45	99.83
E438517	71.73	15.39	2.15	2.66	0.68	4.38	1.85	0.005	0.27	0.03	0.074	0.03	0.03	0.43	99.71
E438520	69.36	15.91	2.92	2.97	0.91	4.57	1.48	0.005	0.35	0.04	0.082	0.04	0.05	1.12	99.8
E438523	76.61	12.55	1.98	1.47	0.36	4.58	0.89	0.005	0.14	0.02	0.034	0.01	0.04	0.44	99.12
E438524	72.38	15.27	2.38	2.09	0.69	5.08	0.95	0.005	0.22	0.03	0.035	0.02	0.04	0.65	99.83
E438525	65.56	16.74	4.51	3.91	1.62	4.38	1.55	0.005	0.49	0.06	0.178	0.07	0.05	0.67	99.79
E438526	75.01	13.94	1.02	0.87	0.15	3.97	4.10	0.005	0.04	0.02	0.017	0.01	0.02	0.39	99.55
E438527	70.53	15.97	2.75	3.00	0.77	4.73	1.18	0.005	0.32	0.04	0.09	0.05	0.03	0.41	99.87
E438528	69.23	16.18	3.06	3.00	0.95	4.44	1.81	0.005	0.34	0.04	0.102	0.05	0.05	0.57	99.82
E438529	67.05	16.42	3.77	3.56	1.46	4.29	1.99	0.005	0.36	0.05	0.158	0.06	0.09	0.64	99.9
E438530	74.24	14.03	1.41	1.04	0.27	3.67	4.28	0.005	0.09	0.03	0.04	0.01	0.04	0.34	99.5
E438531	72.64	15.20	1.72	1.77	0.48	4.37	2.87	0.005	0.18	0.03	0.067	0.03	0.06	0.45	99.86
E438504	45.69	17.00	8.87	15.32	4.11	2.31	0.11	0.05	1.08	0.22	0.082	0.02	0.005	5.03	99.89
E438505	52.40	16.66	11.10	11.03	4.13	1.15	0.35	0.05	1.15	0.25	0.09	0.01	0.01	1.39	99.77
E438506	48.41	15.74	12.30	11.57	6.41	2.05	0.13	0.04	1.05	0.22	0.087	0.01	0.005	1.82	99.84
E438519	50.00	14.85	13.49	8.68	6.88	3.35	0.38	0.01	0.75	0.21	0.055	0.01	0.01	1.23	99.91
E438507	48.61	15.63	13.15	10.67	7.38	1.49	0.13	0.05	1.08	0.21	0.105	0.01	0.005	1.33	99.85
E438516	55.60	14.19	8.30	8.68	8.33	3.12	0.23	0.1	0.27	0.15	0.023	0.01	0.01	0.85	99.87
E438521	47.59	14.33	15.87	10.89	6.36	1.74	0.24	0.03	1.81	0.22	0.128	0.03	0.01	0.72	99.97
E438518	45.08	14.62	15.97	7.67	9.70	2.14	1.16	0.05	1.55	0.24	0.119	0.02	0.04	1.51	99.87
E438522	66.15	14.87	5.22	4.48	2.92	1.51	1.73	0.005	0.59	0.09	0.148	0.02	0.05	2.06	99.83
E438532	65.07	15.38	4.45	3.85	3.25	3.64	2.08	0.02	0.62	0.07	0.173	0.04	0.05	1.23	99.92
E438534	75.43	13.38	1.81	0.17	0.49	1.70	5.73	0.005	0.12	0.005	0.021	0.01	0.08	0.94	99.88

SAMPLE	As	Ba	Bi	Ce	Cr	Cu	Ga	La	Mo	Nb	Ni	Pb	Rb	Sb	Se
E438514	6	330	2	10	6	5	2	20	2	7	5	14	96	2	1
E438513	5	220	2	20	38	10	2	10	2	9	5	12	86	2	1
E438508	5	460	2	60	17	10	2	40	2	12	10	16	78	2	1
E438509	2.5	410	2	50	43	10	2	30	2	5	10	13	59	2	1
E438510	5	590	2	50	10	10	2	30	2	9	5	27	122	2	1
E438511	5	390	2	10	36	5	2	10	2	7	5	33	189	2	1
E438512	5	770	2	60	8	5	2	20	2	5	5	18	110	2	1
E438515	2.5	220	2	30	34	10	2	10	2	5	5	12	52	2	1
E438517	6	230	2	30	32	5	2	20	2	7	10	14	68	2	1
E438520	5	350	2	30	10	10	2	10	2	3	10	11	36	2	1
E438523	7	360	2	70	27	10	2	30	2	7	5	10	24	2	1
E438524	5	280	2	10	5	5	2	10	2	11	5	12	35	2	1
E438525	7	380	2	70	30	5	2	40	2	6	10	13	66	2	1
E438526	2.5	130	2	10	8	5	2	10	2	10	5	32	212	2	1
E438527	5	210	2	10	29	10	2	10	2	3	5	12	55	2	1
E438528	2.5	390	2	40	12	10	2	10	2	3	10	11	57	2	1
E438529	2.5	660	2	70	32	20	2	40	2	4	10	16	82	2	1
E438530	5	300	2	10	31	5	2	5	2	11	10	29	223	2	1
E438531	2.5	460	2	20	28	10	2	5	2	10	5	18	158	2	1
E438504	11	20	2	20	290	110	2	5	2	3	130	4	2	2	1
E438505	7	80	2	10	311	150	2	5	2	3	150	2	8	2	1
E438506	6	10	2	10	273	140	2	5	2	3	120	2	2	2	1
E438519	10	70	2	5	85	30	2	10	2	2	40	5	10	2	1
E438507	6	10	2	10	292	140	2	10	2	2	140	2	2	2	1
E438516	8	110	2	5	573	5	2	5	2	1	100	4	4	2	1
E438521	9	40	2	10	174	90	2	5	2	5	70	10	7	2	1
E438518	9	330	2	5	324	30	2	10	2	4	180	5	40	2	1
E438522	7	380	2	40	37	100	2	30	2	6	20	7	56	2	1
E438532	5	410	2	40	121	20	2	30	2	6	70	13	66	2	1
E438534	2.5	580	2	20	15	5	2	10	2	9	10	9	145	2	1

SAMPLE	Sn	Sr	Ta	Th	Ti	U	W	Y	Zr	Zn	V
E438514	6	132	5	11	908	2	5	6	104	40	10
E438513	6	138	5	10	1005	2	5	7	125	40	10
E438508	6	367	5	13	2820	4	5	14	175	60	40
E438509	5	410	5	8	2200	2	5	7	145	50	30
E438510	5	197	5	17	1385	4	5	12	129	40	20
E438511	7	228	5	8	600	4	5	6	67	30	10
E438512	7	247	5	17	1675	2	5	6	172	50	20
E438515	5	331	5	5	1655	2	5	5	125	50	20
E438517	6	258	5	9	1595	2	5	8	93	30	20
E438520	2.5	329	5	4	2020	4	5	7	107	30	30
E438523	6	85	5	21	858	2	5	35	212	20	5
E438524	5	146	5	9	1330	2	5	35	95	30	20
E438525	5	555	5	12	2890	2	5	11	147	60	60
E438526	7	50	5	18	341	12	5	17	51	20	5
E438527	2.5	393	5	5	1895	2	5	3	113	40	30
E438528	6	411	5	8	1990	2	5	4	122	50	30
E438529	2.5	525	5	11	2110	4	5	9	123	60	50
E438530	7	89	5	21	572	2	5	13	94	30	10
E438531	6	192	5	14	1100	4	5	12	126	40	10
E438504	2.5	149	5	2	6390	2	5	20	61	80	290
E438505	2.5	84	5	2	6780	2	5	23	66	100	320
E438506	2.5	110	5	2	6200	2	5	21	61	90	290
E438519	2.5	61	5	2	4390	2	5	15	36	80	280
E438507	2.5	119	5	2	6330	2	5	22	63	100	300
E438516	2.5	81	5	2	1595	2	5	8	15	50	190
E438521	2.5	278	5	2	18100	2	5	29	103	140	370
E438518	2.5	140	5	2	9150	2	5	24	82	140	330
E438522	5	122	5	7	3480	2	5	15	141	50	100
E438532	2.5	331	5	10	3650	4	5	11	156	60	70
E438534	7	68	5	14	782	4	5	17	159	10	5

Appendix B

SEM-EDS data for regional biotite samples

Averaged and normalized values used for plots

	SiO2	TiO2	Al2O3	FeO	MnO	MgO	CaO	Na2O	K2O	Cr2O3	Y total	Al total	Fe/Fe+	Mg#
E43850	37.949	3.554	17.246	22.63	0.373	8.135	BDT	0.223	9.914	0.008	5.555	2.995	0.609	0.391
	37.698	2.574	17.649	22.317	0.327	9.07	BDT	0.168	10.021	0.078	5.656	3.067	0.58	0.42
	37.64	2.914	17.464	22.609	0.254	8.617	BDT	0.249	10.015	5.694	5.615	3.041	0.595	0.405
	37.802	2.676	17.792	22.323	0.245	8.802	BDT	0.27	10.034	0.078	5.634	3.089	0.587	0.413
	38.03	2.974	17.477	22.781	0.263	8.62	BDT	0.204	9.678	-0.055	5.647	3.028	0.597	0.403
	38.132	3.523	17.5	22.718	0.183	8.325	BDT	0.231	9.537	0.04	5.614	3.025	0.605	0.395
	38.81	2.163	18.203	20.444	0.669	10.998	BDT	-0.259	9.329	-0.294	5.773	3.084	0.511	0.489
E43851	37.733	2.143	17.633	23.244	BDT	8.905	BDT	BDT	9.771	BDT	5.738	3.068	0.594	0.406
	37.08	2.052	17.359	24.084	BDT	8.993	BDT	BDT	9.768	BDT	5.812	3.041	0.6	0.4
	37.409	2.161	17.442	24.068	BDT	9.053	BDT	BDT	9.257	BDT	5.829	3.043	0.599	0.401
	38.008	2.109	17.343	23.216	BDT	8.627	BDT	BDT	9.87	BDT	5.698	3.02	0.602	0.398
	37.659	2.012	17.088	23.8	BDT	8.863	BDT	BDT	9.942	BDT	5.762	2.985	0.601	0.399
E43851	38.052	2.746	17.668	22.605	BDT	9.023	BDT	BDT	9.512	BDT	5.701	3.054	0.584	0.416
	37.603	2.953	17.349	23.333	BDT	8.774	BDT	BDT	9.528	BDT	5.71	3.017	0.599	0.401
	37.629	2.868	17.637	22.845	BDT	8.862	BDT	BDT	9.489	BDT	5.71	3.061	0.591	0.409
	37.491	2.98	17.207	23.568	BDT	8.746	BDT	BDT	9.605	BDT	5.726	2.997	0.602	0.398
	37.608	2.965	17.399	22.996	BDT	8.763	BDT	BDT	9.655	BDT	5.675	3.024	0.595	0.405
	37.871	2.944	17.17	22.981	BDT	8.928	BDT	BDT	9.583	BDT	5.669	2.977	0.591	0.409
E43853	36.694	2.567	17.204	26.909	0.835	6.154	BDT	BDT	9.594	BDT	5.566	3.082	0.674	0.326
	39.681	2.534	20.247	21.044	BDT	5.854	BDT	BDT	10.01	BDT	5.389	3.432	0.667	0.333
	37.965	2.562	18.206	23.724	0.895	6.696	BDT	BDT	10.046	BDT	5.569	3.167	0.665	0.335
	37.802	2.734	17.892	24.175	0.946	6.538	BDT	BDT	10.092	BDT	5.59	3.143	0.674	0.326
	37.524	2.588	17.859	24.382	0.846	6.831	BDT	BDT	10.13	BDT	5.253	3.521	0.668	0.332
E43845	39.644	1.79	17.267	16.507	BDT	14.358	BDT	0.291	9.981	0.12	5.77	2.903	0.392	0.608
	39.522	1.935	17.219	16.651	BDT	14.31	BDT	0.129	10.063	0.167	5.78	2.896	0.395	0.605
	39.538	1.94	17.385	16.324	BDT	14.512	BDT	0.186	9.898	0.214	5.787	2.919	0.387	0.613
	39.093	1.814	17.272	16.857	BDT	14.423	BDT	0.239	9.851	0.547	5.829	2.908	0.396	0.604
	39.199	1.968	17.361	16.829	BDT	14.703	BDT	0.236	9.567	0.149	5.855	2.919	0.391	0.609
	39.455	1.995	17.135	16.968	BDT	14.293	BDT	0.234	9.86	0.067	5.808	2.885	0.4	0.6

Raw Data

E4385

	point 1-	point 1-	point 1-	point 1-	point 1-	point 2-	point 2-	point 2-	point 2-	point 2-	point 3-	point 3-	point 3-	point 3-	point 3-
Na2O	BDL	BDL	BDL	BDL	BDL	BDL	BDL	BDL	BDL	BDL	BDL	0.51	0.39	BDL	BDL
MgO	7.73	7.22	7.93	7.81	7.49	8.94	8.45	8.24	8.39	8.9	8.14	8.12	8.41	7.91	7.98
Al2O3	15.89	16.15	16.9	16.38	15.64	16.65	16.55	17.08	16.78	16.99	16.37	16.76	16.41	16.09	16.57
SiO2	35.52	35.76	36.02	36.13	34.71	35.45	35.88	35.84	36.35	35.91	36.16	35.74	35.11	35.13	35.03
K2O	9.72	9.41	9.25	9.05	9.1	9.35	9.82	9.75	9.21	9.67	9.39	9.7	9.36	9.21	9.48
CaO	BDL	BDL	BDL	BDL	BDL	BDL	BDL	BDL	BDL	BDL	BDL	BDL	BDL	BDL	BDL
TiO2	3.15	3.52	3.15	3.34	3.53	2.61	2.73	2.24	2.41	2.62	3.32	2.8	2.45	2.88	2.78
V2O3	BDL	BDL	BDL	BDL	BDL	BDL	BDL	BDL	BDL	BDL	BDL	BDL	BDL	BDL	BDL
Cr2O3	BDL	BDL	BDL	BDL	BDL	BDL	BDL	BDL	BDL	BDL	BDL	BDL	BDL	BDL	BDL
MnO	0.49	BDL	BDL	BDL	BDL	BDL	BDL	BDL	0.44	BDL	BDL	BDL	BDL	BDL	0.46
FeO	20.65	23.04	20.25	21.75	20.58	20.69	20.8	22.26	21.14	21.59	21.54	21.06	21.38	21.68	20.75
total	93.15	95.1	93.5	94.46	91.05	93.69	94.23	190.13	190.4	95.68	189.61	281.1	279.46	185.95	93.05
cation	4.95	4.94	4.92	4.92	4.92	4.97	4.95	4.97	4.93	4.98	4.92	4.97	4.99	4.95	4.94

	point 4-	point 4-	point 4-	point 4-	point 4-	point 5-	point 5-	point 5-	point 5-	point 5-	point 6-	point 6-	point 6-	point 6-
Na2O	0.39	BDL	BDL	BDL	BDL	BDL	BDL	0.39	BDL	0.4	BDL	BDL	BDL	BDL
MgO	8.4	8.59	-0.18*	7.9	8.1	7.99	8.03	8.12	8.12	8.33	7.62	8.02	7.65	7.8
Al2O3	16.81	17.32	0.35*	16.16	16.4	16.54	16.54	16.68	16.33	16.2	15.96	16.46	16.33	16.6
SiO2	34.99	35.91	0.54*	35.98	34.81	35.88	35.46	35.85	35.94	35.94	35.97	35.69	34.78	35.96
K2O	9.84	9.25	0.36*	9.23	9.28	9.33	9.08	8.81	9.21	9.14	9.11	8.87	8.89	8.74
CaO	BDL	BDL	BDL	BDL	BDL	BDL	BDL	BDL	BDL	BDL	BDL	BDL	BDL	BDL
TiO2	2.08	2.43	46.24	2.84	2.68	2.22	2.77	3.22	3.14	2.66	3.18	3.15	3.15	3.68
V2O3	BDL	BDL	BDL	BDL	BDL	BDL	BDL	BDL	BDL	BDL	BDL	BDL	BDL	BDL
Cr2O3	BDL	BDL	BDL	BDL	BDL	BDL	BDL	BDL	BDL	BDL	BDL	BDL	BDL	BDL
MnO	BDL	BDL	6.06	BDL	BDL	BDL	BDL	BDL	0.38	BDL	BDL	BDL	BDL	BDL
FeO	20.2	21.26	42.99	20.92	21.29	21.21	21.74	21.37	21.88	21.07	20.86	20.85	21.71	21.41
total	92.71	94.76	95.29	93.03	92.56	93.17	93.62	189.44	188.74	93.74	92.7	93.04	186.7	94.19
cation	4.99	4.96	4.83	4.92	4.97	4.94	4.94	4.93	4.93	4.95	4.91	4.91	4.94	4.89

E438510

	point 1-	point 1-	point 1-	point 1-	point 1-	point 2-	point 2-	point 2-	point 2-	point 2-	point 3-	point 3-	point 3-	point 3-	point 3-
SiO2	37.32	34.86	36.25	35.78	36.77	35.74	36.23	36.05	36.3	35.28	37.01	37.3	37.45	34.17	35.31
TiO2	1.82	2.14	2.14	2.16	2.01	1.68	2.32	1.89	1.44	2.61	2.58	1.97	2	1.79	2.13
Al2O3	17.37	16.31	17	16.93	16.96	16.63	17.09	17.27	17.14	15.96	16.78	16.75	17.26	17.66	16.05
FeO	22.34	21.84	23.76	21.25	22.3	23.32	23.69	23.2	23.47	22.97	23.08	22.39	22.66	25.57	22.87
MnO	BDL	0.69	0.55	BDL	BDL	0.45	0.7	BDL	0.55	BDL	BDL	BDL	0.56	BDL	0.72
MgO	8.88	7.91	8.52	8.73	8.68	8.87	8.65	8.77	8.43	8.83	8.07	8.87	8.9	9.6	8.41
CaO	BDL	BDL	BDL	BDL	BDL	BDL	BDL	BDL	BDL	BDL	BDL	BDL	BDL	BDL	BDL
Na2O	BDL	BDL	BDL	BDL	BDL	BDL	BDL	BDL	BDL	BDL	BDL	BDL	BDL	BDL	BDL
K2O	9.55	9.13	9.39	9.32	9.47	9.02	9.86	8.92	9.71	9.81	9.85	9.03	9.45	7.22	9.3
Cr2O3	BDL	BDL	BDL	BDL	BDL	BDL	BDL	BDL	BDL	BDL	BDL	BDL	BDL	BDL	BDL
total	97.28	92.88	97.61	94.17	96.19	95.71	98.54	96.1	97.04	95.46	97.37	96.31	98.28	96.01	94.79
cation	4.97	4.99	4.98	4.96	4.96	4.98	5.01	4.98	4.99	5.02	4.96	4.96	4.95	5	5

	point 4-	point 4-	point 4-	point 4-	point 4-	point 5-	point 4-	point 4-	point 4-	point 4-
SiO2	36.53	37.09	37.88	36.14	36.55	36.44	35.43	35.75	36.49	36.33
TiO2	1.87	1.93	2.29	1.9	2.24	2.24	1.78	1.88	1.99	1.76
Al2O3	16.02	16.95	17.26	16.69	17.14	16.26	16.31	16.4	16.69	16.21
FeO	22.05	21.52	22.45	23.24	23.25	22.84	22.61	22.25	23.49	22.85
MnO	0.51	0.72	0.59	BDL	0.59	0.72	0.57	BDL	0.7	0.46
MgO	8.52	8.83	8.28	8.43	7.73	8.76	7.95	8.57	8.85	8.35
CaO	BDL	BDL	BDL	BDL	BDL	BDL	BDL	BDL	BDL	BDL
Na2O	BDL	BDL	BDL	BDL	BDL	BDL	BDL	BDL	BDL	BDL
K2O	9.52	9.27	9.61	9.54	9.89	9.78	9.14	9.89	9.26	9.56
Cr2O3	BDL	BDL	BDL	BDL	BDL	BDL	BDL	BDL	BDL	BDL
total	95.02	96.31	98.36	95.94	97.39	97.04	93.79	94.74	97.47	95.52
cation	4.97	4.95	4.93	5	4.98	5	4.96	4.99	4.98	4.99

E438512

	point 1-	point 1-	point 1-	point 1-	point 1-	point 2-	point 2-	point 2-	point 2-	point 2-	point 3-	point 3-	point 3-	point 3-	point 3-
SiO2	35.01	36.81	34.93	36.88	35.65	34.54	34.88	35.41	34.51	35.33	34.38	35.36	35.04	34.62	35.25
TiO2	2.87	2.53	2.59	2.56	2.38	2.74	2.98	2.79	2.45	2.76	2.68	2.56	2.58	2.83	2.66
Al2O3	16.14	16.97	16.78	16.94	16.4	15.7	16.3	15.95	16.27	16.37	15.82	16.54	16.79	16.59	16.13
FeO	21.15	21.68	20.96	21.24	21.45	22.56	22.04	20.82	21.58	21.38	20.83	20.72	21.65	21.82	21.02
MnO	BDL	BDL	0.38	BDL	0.34	BDL	BDL	BDL	BDL	0.33	BDL	BDL	0.32	0.47	0.44
MgO	8.57	8.46	8.36	8.57	8.54	7.86	8.05	8.14	8.19	8.52	8.23	8.58	7.8	8.18	8.34
CaO	BDL	BDL	BDL	BDL	BDL	BDL	BDL	BDL	BDL	BDL	BDL	BDL	BDL	BDL	BDL
Na2O	BDL	BDL	BDL	BDL	BDL	BDL	BDL	BDL	BDL	0.33	BDL	BDL	0.35	BDL	BDL
K2O	8.72	8.85	8.84	9.25	9.15	8.65	8.89	8.89	8.85	8.98	8.87	9	8.29	8.88	9
Cr2O3	BDL	BDL	BDL	BDL	BDL	BDL	BDL	BDL	BDL	BDL	BDL	BDL	BDL	BDL	BDL
total	92.46	95.3	92.84	95.44	93.91	92.05	93.14	92	91.85	94	90.81	92.76	92.82	93.39	92.84
Cation	2.82	2.81	2.83	2.82	2.83	2.83	2.83	2.81	2.84	2.83	2.83	2.82	2.82	2.84	2.83

	point 4-	point 4-	point 4-	point 4-	point 4-	point 5-	point 5-	point 5-	point 5-	point 5-	point 6-	point 6-	point 6-	point 6-	point 6-
SiO2	34.68	34.55	33.87	34.22	31.99	34.82	34.79	34.6	34.14	34.84	35.19	34.84	35.12	34.28	34.47
TiO2	2.9	2.84	2.72	2.63	2.38	2.5	2.93	2.52	2.76	2.95	2.7	2.62	2.87	2.63	2.7
Al2O3	15.79	16.18	15.55	15.74	14.46	15.86	16.28	16.09	15.63	16.27	15.77	15.5	16.1	15.6	15.87
FeO	21.39	20.66	22.1	21.28	20.95	21.33	20.6	20.52	21.83	21.63	21.06	21.21	21.58	20.85	20.83
MnO	BDL	0.29	BDL	BDL	0.41	0.33	BDL	BDL	BDL	0.3	BDL	BDL	BDL	BDL	0.41
MgO	8.08	7.99	8.52	7.62	7.3	8.16	7.94	7.81	8.16	8.29	8.15	8.7	8.16	8.33	7.66
CaO	BDL	BDL	BDL	BDL	BDL	BDL	BDL	BDL	BDL	BDL	BDL	BDL	BDL	BDL	BDL
Na2O	BDL	BDL	BDL	BDL	BDL	BDL	BDL	BDL	0.39	BDL	BDL	0.37	0.37	0.36	0.41
K2O	8.76	8.92	8.5	8.76	8.42	9.05	8.76	8.7	8.72	9.24	8.79	8.77	8.66	8.97	8.81
Cr2O3	BDL	BDL	BDL	BDL	BDL	BDL	BDL	BDL	BDL	BDL	BDL	BDL	BDL	BDL	BDL
total	91.6	91.43	91.26	90.25	85.91	92.05	91.3	90.24	91.63	93.52	91.93	92.35	92.45	91.36	91.09
Cation	2.82	2.83	2.84	2.82	2.84	2.84	2.83	2.82	2.84	2.84	2.82	2.84	2.82	2.84	2.83

E438530

	point 1-	point 1-	point 1-	point 1-	point 1-	point 1-	point 2-	point 2-	point 2-	point 2-	point 2-	point 2-	point 3-
SiO2	37.25	35.15	36.52	36.32	62.76	25.71	35.63	37.84	37.31	36.81	36.92	47.78	36.14
TiO2	2.93	2.22	2.68	2.52	BDL	1.65	2.49	2.67	2.81	2.76	3	0.9	2.7
Al2O3	17.35	15.92	17.42	17.02	18.12	12.33	16.8	16.8	17.17	17.45	17.93	32.08	17.47
FeO	23.37	22.84	24.32	22.52	BDL	34	22.46	22.99	24.02	22.42	24.49	5.53	23.74
MnO	0.93	0.9	0.65	0.78	BDL	0.64	0.79	0.73	1.01	0.78	0.8	BDL	BDL
MgO	6.63	6.1	5.98	6.61	BDL	3.46	5.98	6.24	6.54	6.46	6.72	1.57	6.73
CaO	BDL	BDL	BDL	BDL	BDL	BDL	BDL	BDL	BDL	BDL	BDL	BDL	BDL
Na2O	BDL	BDL	BDL	BDL	1.39	BDL	BDL	BDL	BDL	BDL	BDL	BDL	BDL
K2O	9.74	9.08	9.36	9.5	14.6	6.62	9.72	9.92	9.59	9.45	9.14	11.19	9.42
Cr2O3	BDL	BDL	BDL	BDL	BDL	BDL	BDL	BDL	BDL	BDL	BDL	BDL	BDL
Total	98.2	92.21	96.93	95.27	96.87	84.41	93.87	97.19	98.45	96.13	99	99.05	96.2
Cation	4.93	4.94	4.91	4.91	4.38	5.15	4.93	4.89	4.9	4.9	4.9	4.49	4.93

	point 3-	point 3-	point 3-	point 3-	point 4-	point 4-	point 4-	point 4-	point 4-	point 4-	point 5-	point 5-	point 5-	point 5-	point 5-	point 5-
SiO2	36.32	36.56	36.55	37.25	37.09	34.83	34.14	36.69	37.83	36.86	37.85	36.81	37.14	35.36	36.92	47.14
TiO2	2.56	2.06	2.55	2.82	2.41	2.46	2.66	2.5	2.76	2.94	2.45	2.75	2.55	2.31	2.48	0.73
Al2O3	17.18	17.31	17.8	17.75	18.09	16.31	16.31	17.35	18.5	17.84	16.97	18.24	18.23	16.58	16.57	29.92
FeO	23.53	22.76	22.78	22.03	23.74	21.89	23.01	23.3	23.98	23.52	23.77	23.77	23.92	22.36	24.99	4.79
MnO	0.75	1.25	0.91	0.77	0.65	0.84	0.86	0.63	1.17	1.01	0.96	0.67	0.68	1.35	0.57	BDL
MgO	6.56	7.04	6.19	6.57	6.05	6.17	5.33	6.32	6.58	6.19	7.19	6.79	6.7	6.42	6.71	1.34
CaO	BDL	BDL	BDL	BDL	BDL	BDL	BDL	BDL	BDL	BDL	BDL	BDL	BDL	BDL	BDL	BDL
Na2O	BDL	BDL	BDL	BDL	BDL	BDL	BDL	BDL	BDL	BDL	BDL	BDL	BDL	BDL	BDL	BDL
K2O	9.73	9.49	9.55	9.83	10.03	9.38	8.89	10.58	10.09	9.68	9.64	10.02	10.17	9.78	9.5	10.96
Cr2O3	BDL	BDL	BDL	BDL	BDL	BDL	BDL	BDL	BDL	BDL	BDL	BDL	BDL	BDL	BDL	BDL
Total	96.63	96.47	96.33	97.02	98.06	91.88	91.2	97.37	100.91	98.04	98.83	99.05	99.39	94.16	97.74	94.88
Cation	4.95	4.94	4.9	4.89	4.91	4.92	4.91	4.96	4.9	4.9	4.94	4.92	4.96	4.95	4.94	4.48

E438532

	point 1-	point 1-	point 1-	point 1-	point 1-	point 2-	point 2-	point 2-	point 2-	point 2-	point 2-	point 3-	point 3-	point 3-	point 3-	point 3-
Na2O	BDL	BDL	BDL	BDL	BDL	BDL	BDL	8.42	0.35	BDL	BDL	BDL	BDL	BDL	1.39	BDL
MgO	14.05	13.75	14.08	13.51	13.04	14.17	13.45	BDL	13.52	13.61	BDL	13.62	14.13	14.03	10.09	13.19
Al2O3	16.5	16.3	17.3	16.21	16.04	16.38	16.44	24.64	16.28	16.48	1.12	16.15	16.25	17.29	11.27	16.14
SiO2	37.26	37.7	38.68	37.62	37.71	37.4	37.52	61.73	37.18	37.05	30.36	37.22	37.53	37.43	43.79	36.8
K2O	9.37	9.52	9.75	9.76	9.8	9.44	9.43	BDL	8.99	9.48	BDL	9.47	9.23	9.47	0.23	9.37
CaO	BDL	BDL	BDL	BDL	BDL	BDL	BDL	6.14	BDL	BDL	28.07	BDL	BDL	BDL	11.79	BDL
TiO2	1.83	2.07	1.84	1.9	1.61	1.84	2.01	BDL	1.69	1.78	36.52	1.68	1.85	1.47	BDL	1.91
Cr2O3	0.37	BDL	BDL	BDL	BDL	0.35	BDL	BDL	BDL	BDL	BDL	0.65	0.56	BDL	0.55	0.74
FeO	16.37	15.36	15.8	15.7	16.38	15.48	15.52	BDL	15.66	14.92	0.34	15.87	16.19	16.12	15.9	16.06
Total	95.75	94.7	97.45	94.7	94.58	95.06	94.37	100.93	93.67	93.32	96.41	94.66	95.74	95.81	95.01	94.21
Cation	2.85	2.84	2.84	2.84	2.85	2.85	2.83	2.5	2.84	2.84	2.43	2.85	2.84	2.86	2.69	2.85

	point 4-	point 4-	point 4-	point 4-	point 5-	point 5-	point 5-	point 5-	point 5-
Na2O	BDL	BDL	BDL	0.35	BDL	BDL	BDL	BDL	BDL
MgO	13.21	14.78	14.09	13.42	13.2	13.57	13.78	13.61	13.64
Al2O3	16.84	16.6	16.48	15.62	16.1	15.86	16.44	16.57	16.3
SiO2	36.71	36.24	37.74	37.31	36.62	38.07	37.54	37.1	37.82
K2O	9	8.25	9.42	9.46	9.12	9.33	9.2	9.59	9.53
CaO	BDL	BDL	BDL	BDL	BDL	BDL	BDL	BDL	BDL
TiO2	1.84	1.63	2.2	1.77	1.69	2.12	1.93	1.94	1.79
Cr2O3	BDL	BDL	BDL	BDL	BDL	BDL	BDL	BDL	BDL
FeO	16.11	15.36	16.1	15.97	15.61	16.4	16.33	15.8	16.35
Total	93.71	92.86	96.03	93.9	92.34	95.35	95.22	94.61	95.43
Cation	2.84	2.84	2.84	2.85	2.84	2.84	2.84	2.85	2.85

Appendix C

SEM data for biotite samples of the Musselwhite Mine

NORMALIZED DATA USED FOR PLOTS

	SiO2	TiO2	Al2O3	FeO	MnO	MgO	CaO	Na2O	K2O	Cr2O3	Y site tot	Al Tot	Fe#	Mg#
E354010	35.758	2.121	16.993	29.568	BDL	6.123	BDL	BDL	9.661	BDL	5.861	3.04	0.73	0.27
	35.736	2.41	16.891	29.863	BDL	5.391	BDL	BDL	9.872	BDL	5.786	3.032	0.757	0.243
	35.882	2.509	16.953	29.33	BDL	5.94	BDL	BDL	9.648	BDL	5.819	3.029	0.735	0.265
	35.375	2.456	17.243	29.169	BDL	5.62	BDL	BDL	9.746	BDL	5.778	3.098	0.745	0.255
	35.878	2.276	17.213	30.142	BDL	4.759	BDL	BDL	9.918	BDL	5.765	3.097	0.781	0.219
E354016	35.807	1.145	18.124	30.382	BDL	5.216	-0.043	0.292	9.112	0.02	5.885	3.252	0.766	0.234
	35.814	1.015	18.193	30.346	BDL	5.329	-0.067	0.239	9.216	0.028	5.905	3.264	0.762	0.238
	35.604	0.711	18.366	30.339	BDL	5.377	0.112	0.304	8.992	BDL	5.932	3.308	0.76	0.24
	35.604	1.113	18.52	29.749	BDL	5.386	0.098	0.347	9.133	0.055	5.863	3.319	0.756	0.244
	36.076	2.142	17.665	28.541	BDL	6.312	-0.027	0.315	9.12	0.123	5.832	3.137	0.717	0.283
E354040	36.115	2.173	17.451	27.523	BDL	7.191	0.046	0.365	9.123	0.01	5.85	3.095	0.682	0.318
	36.149	1.9	17.503	27.798	BDL	7.221	-0.07	0.301	9.103	-0.009	5.88	3.105	0.684	0.316
	35.993	2.205	17.364	28.303	BDL	6.826	-0.022	0.077	8.977	0.122	5.898	3.093	0.699	0.301
E354025	34.912	1.077	22.73	18.178	BDL	12.438	BDL	BDL	10.258	BDL	5.927	3.876	0.451	0.549
	35.592	1.067	22.163	18.213	BDL	12.167	BDL	BDL	10.248	BDL	6.014	3.818	0.457	0.543
	37.95	1.507	17.338	20.939	BDL	11.816	BDL	BDL	9.399	BDL	5.826	2.985	0.499	0.501
	35.52	1.305	21.86	18.866	BDL	11.723	BDL	BDL	10.012	BDL	5.887	3.743	0.475	0.525
	37.516	1.299	18.464	20.782	BDL	11.582	BDL	BDL	9.838	BDL	5.858	3.178	0.502	0.498
E358108	36.825	2.518	17.219	24.656	BDL	8.279	BDL	BDL	9.725	BDL	5.763	3.031	0.626	0.374
	36.952	2.924	16.958	24.729	BDL	7.975	BDL	BDL	9.92	BDL	5.721	2.981	0.635	0.365
	36.669	2.949	17.517	24.752	BDL	8.234	BDL	BDL	9.574	BDL	5.773	3.071	0.628	0.372
	36.735	1.968	17.536	24.589	BDL	8.687	BDL	BDL	9.841	BDL	5.808	3.089	0.614	0.386
E354041	35.206	2.214	20.873	26.279	BDL	6.044	BDL	BDL	9.692	BDL	5.761	3.662	0.709	0.291
	35.664	2.289	20.512	25.879	BDL	5.912	BDL	BDL	9.616	BDL	5.713	3.603	0.711	0.289
	35.121	2.436	20.737	25.98	BDL	5.949	BDL	BDL	9.696	BDL	5.735	3.649	0.71	0.29
	35.102	2.598	20.393	26.058	BDL	5.9	BDL	BDL	9.722	BDL	5.725	3.599	0.713	0.287
	35.612	2.194	20.695	25.786	BDL	5.851	-0.02	0.457	9.362	0.101	5.684	3.631	0.712	0.288
	35.781	2.439	20.262	25.516	BDL	6.326	-0.061	0.229	9.277	0.142	5.73	3.554	0.693	0.307
	36.633	2.393	20.319	23.396	BDL	7.612	0.025	0.242	9.347	0.162	5.703	3.518	0.633	0.367

E35401

	point 1-1	point 1-2	point 1-3	point 1-4	point 1-5	point 2-1	point 2-2	point 2-3	point 2-4	point 2-5	point 3-1	point 3-2	point 3-3	point 3-4	point 3-5	point 3-6
SiO2	33.28	34.19	35.24	33.23	34.65	39.62	39.62	34.3	33.95	32.54	35.07	33.09	35.13	34.21	35.58	33.04
TiO2	2.28	1.66	2.15	2	2.02	0.48	0.48	2.03	2.13	2.2	2.56	2.46	2.76	2.69	2.46	1.94
Al2O3	15.62	17.07	16.22	15.57	16.59	13.1	13.1	16.57	16.42	15.39	16.33	15.17	16.11	15.85	16.14	16.34
FeO	27.38	28.95	29.35	27.45	27.94	25.72	25.72	30.19	28.31	27.88	28.29	26.56	28.42	27.9	28.02	27.63
MnO	0.48	BDL	BDL	BDL	BDL	BDL	BDL	BDL	BDL	BDL	BDL	BDL	BDL	BDL	BDL	BDL
MgO	5.51	5.89	6.03	5.44	6.36	4.07	4.07	5.2	5.36	4.76	5.78	4.43	5.32	5.65	5.64	5.87
CaO	BDL	BDL	BDL	BDL	BDL	11.09	11.09	BDL	BDL	BDL	BDL	BDL	BDL	BDL	BDL	BDL
Na2O	BDL	BDL	BDL	BDL	BDL	0.82	0.82	BDL	BDL	BDL	BDL	BDL	BDL	BDL	BDL	BDL
K2O	9.17	8.77	9.91	9.04	9.2	1.54	1.54	9.31	9.4	9.2	9.63	9.12	9.05	9.16	9.57	8.93
Cr2O3	BDL	BDL	BDL	BDL	BDL	BDL	BDL	BDL	BDL	BDL	BDL	BDL	BDL	BDL	BDL	BDL
Total	93.72	96.53	98.9	92.73	96.76	96.44	96.44	97.6	95.57	91.97	97.66	90.83	96.79	95.46	97.41	93.75
Cation	5.01	5.01	5.02	4.99	4.98	4.77	4.77	5.02	4.99	5.01	5	4.96	4.96	4.99	4.97	5

	point 4-1	point 4-2	point 4-3	point 4-4	point 5-1	point 5-2	point 5-3	point 5-4	point 5-5
SiO2	33.37	36.71	34.13	34.01	35	34.02	34.97	34.43	33.52
TiO2	2.14	BDL	1.91	2.21	2.73	2.68	2.27	2.13	2.13
Al2O3	16.47	20.4	16.99	16	17.36	16.52	16.29	16.62	16.46
FeO	28.03	30.67	27.63	27.7	29.58	28.21	28.4	28.94	29.11
MnO	BDL	3.47	BDL	BDL	BDL	BDL	BDL	BDL	BDL
MgO	5.86	1.34	5.76	6.33	4.66	5.01	4.98	4.78	3.9
CaO	BDL	5.94	BDL	BDL	BDL	BDL	BDL	BDL	BDL
Na2O	BDL	BDL	BDL	BDL	BDL	BDL	BDL	BDL	BDL
K2O	9.35	0.38	9.25	9.17	9.55	9.82	9.14	9.42	9.88
Cr2O3	BDL	BDL	BDL	BDL	BDL	BDL	BDL	BDL	BDL
Total	95.22	98.91	95.67	95.42	98.88	96.26	96.05	96.32	95
Cation	5	4.69	5.01	5.03	4.99	5	4.97	4.99	4.99

E35401

	point 1-1	point 1-2	point 1-3	point 1-4	point 1-5	point 2-1	point 2-2	point 2-3	point 2-4	point 2-5	point 3-1	point 3-2	point 3-3	point 3-4
Na2O	BDL	BDL	BDL	BDL	BDL	BDL	0.37	0.39	BDL	n.m	0.4	BDL	0.45	0.49
MgO	5.37	5.12	5.19	5.19	5.11	5.37	5.24	5.01	5.1	4.97	5.43	5.37	5.3	5.05
Al2O3	17.58	17.29	17.9	17.9	18.2	17.42	17.69	17.89	17.87	18.13	17.62	18.36	18.11	18.15
SiO2	35.53	34.76	34.96	34.96	34.46	35.27	34.88	35.33	35.64	35.25	34.9	35.37	35	34.77
K2O	8.97	8.89	9.05	9.05	9.04	8.84	8.99	8.92	9.02	9.11	8.83	8.77	9.11	8.66
CaO	BDL	BDL	BDL	BDL	BDL	BDL	BDL	BDL	BDL	BDL	BDL	BDL	BDL	0.4
TiO2	1.13	0.94	0.8	0.8	1.09	1.18	1.01	1.26	1.04	1.15	0.78	0.88	0.7	0.44
Cr2O3	BDL	BDL	BDL	BDL	BDL	BDL	BDL	BDL	BDL	BDL	BDL	BDL	BDL	BDL
FeO	29.81	29.13	29.49	29.49	29.5	29.94	29.99	30.26	29.69	29.77	29.5	29.97	29.91	29.95
Total	98.39	96.13	97.39	97.39	97.4	98.02	98.17	99.06	98.36	98.38	97.46	98.72	98.58	97.91
Cation	2.86	2.86	2.86	2.86	2.86	2.86	2.87	2.86	2.85	2.86	2.87	2.86	2.88	2.87

	point 3-5	point 3-6	point 4-1	point 4-2	point 4-3	point 4-4
Na2O	BDL	0.39	BDL	0.42	BDL	0.37
MgO	5.12	5.41	6.26	6.06	6.09	6.16
Al2O3	17.83	18.37	17.49	16.83	16.67	16.77
SiO2	33.89	35.72	35.4	35.2	34.95	34.87
K2O	8.83	9.02	9.03	8.96	8.63	8.88
CaO	BDL	BDL	BDL	BDL	BDL	BDL
TiO2	0.96	1.22	1.81	1.88	2.08	2.56
Cr2O3	BDL	BDL	BDL	BDL	BDL	BDL
FeO	28.63	29.52	28.52	27.85	27.87	26.86
Total	95.26	99.65	98.51	97.2	96.29	96.47
Cation	2.86	2.86	2.86	2.86	2.84	2.85

E35402

	point 1-1	point 1-2	point 1-3	point 1-4	point 1-5	point 2-1	point 2-2	point 2-3	point 2-4	point 2-5	point 3-1	point 3-2	point 3-3	point 3-4	point 3-5	point 3-6
SiO2	34.44	34.2	34.66	33.93	33.35	35.14	33.34	33.2	34.17	35	36.96	36.63	35.39	36.69	38.28	36.36
TiO2	1.47	0.9	0.88	0.9	1.11	1.18	0.82	0.76	1.33	1.05	1.09	1.4	1.1	1.44	2.55	1.21
Al2O3	22.24	21.56	22.97	22.11	22.19	22.27	21.73	20.69	21.26	20.45	17.24	17.63	16.01	16.71	15.68	17.35
FeO	17.95	17.29	18.09	18.03	17.47	18.58	17.09	16.53	17.58	17.69	19.57	20.31	19.99	19.49	22.34	19.88
MnO	BDL	BDL	BDL	BDL	BDL	BDL	BDL	BDL	BDL	BDL	BDL	BDL	BDL	BDL	BDL	BDL
MgO	11.97	11.89	12.6	12.59	11.74	12.01	11.57	11.6	12.04	11.18	12.14	11.47	11.34	11.97	9.43	12.16
CaO	BDL	BDL	BDL	BDL	BDL	BDL	BDL	BDL	BDL	BDL	BDL	BDL	BDL	BDL	3.67	BDL
Na2O	BDL	BDL	BDL	0.71	BDL	BDL	BDL	BDL	BDL	BDL	BDL	BDL	BDL	BDL	BDL	BDL
K2O	9.84	10.05	9.93	10.43	9.87	10.21	9.81	9.5	10.1	9.58	9.36	9.75	8.95	9.27	7.56	9.62
Cr2O3	BDL	BDL	BDL	BDL	BDL	BDL	BDL	BDL	BDL	BDL	BDL	BDL	BDL	BDL	BDL	BDL
Total	97.91	95.89	99.13	98.7	95.73	99.39	94.36	92.28	96.48	94.95	96.36	97.19	92.78	95.57	99.51	96.58
Cation	5.04	5.04	5.05	5.11	5.06	5.05	5.05	5.02	5.04	4.99	5.02	5.02	5.02	5	4.93	5.03

	point 4-1	point 4-2	point 4-3	point 4-4	point 4-5	point 4-6	point 5-1	point 5-2	point 5-3	point 5-4	point 5-5
SiO2	32.72	33.65	35.71	33.78	35.21	35	35.38	33.94	36.59	37.68	37.47
TiO2	1.18	1.24	1.27	1.31	1.54	1.02	1.16	1.16	1.29	1.03	1.63
Al2O3	21.44	20.33	21.7	20.87	20.08	22.4	17.97	16.06	18.27	19.14	17.72
FeO	17.92	17.73	18.36	18.51	18.01	18.9	19.5	19.6	20.2	20.85	20.08
MnO	0.51	BDL	BDL	BDL	BDL	BDL	BDL	BDL	BDL	BDL	BDL
MgO	10.93	10.88	11.91	10.8	11.71	11.8	10.81	10.29	11.51	11.68	11.63
CaO	BDL	BDL	BDL	BDL	BDL	BDL	BDL	BDL	BDL	BDL	0.51
Na2O	BDL	BDL	0.53	BDL	BDL	BDL	BDL	BDL	BDL	BDL	BDL
K2O	9.62	9.53	10.01	9.41	9.78	9.72	9.34	8.99	10.08	9.96	9.1
Cr2O3	BDL	BDL	BDL	BDL	BDL	BDL	BDL	BDL	BDL	BDL	BDL
Total	94.32	93.36	99.49	94.68	96.33	98.84	94.16	90.04	97.94	100.34	98.14
Cation	5.05	5.03	5.04	5.03	5.02	5.03	5.01	5.01	5.03	5.01	4.99

E35404

	point 1-1	point 1-2	point 1-3	point 1-4	point 2-1	point 2-2	point 2-3	point 2-4
Na2O	BDL	0.55	0.36	BDL	BDL	BDL	0.54	0.38
MgO	6.83	6.93	7.1	6.86	6.57	6.98	7.38	7.21
Al2O3	16.99	16.35	16.73	17.23	16.47	17.04	17.32	17.17
SiO2	35.29	34.19	34.8	34.98	34.26	35.77	35.67	34.65
K2O	8.81	8.52	8.86	8.99	8.19	9.13	8.81	9.04
CaO	BDL	BDL	BDL	BDL	BDL	BDL	BDL	BDL
TiO2	2.44	1.85	1.91	2.19	2.22	2.2	1.48	1.84
Cr2O3	BDL	BDL	BDL	BDL	BDL	BDL	BDL	BDL
FeO	26.73	25.86	26.33	27.22	26.3	27.11	27.57	26.73
Total	97.09	94.25	96.09	97.47	94.01	98.23	98.77	97.02
Cation	2.85	2.86	2.86	2.85	2.83	2.85	2.87	2.87

	point 2-5	point 3-1	point 3-2	point 3-3	point 3-4	point 3-5
Na2O	BDL	BDL	BDL	BDL	BDL	BDL
MgO	6.99	6.89	6.83	1.52	1.61	6.25
Al2O3	17.13	16.85	17.26	21.85	21.89	16.65
SiO2	35.47	35.51	36.04	38.27	38.38	33.71
K2O	9.12	9.14	9.06	BDL	BDL	8.07
CaO	BDL	BDL	BDL	3.84	3.88	BDL
TiO2	1.48	2.23	2	BDL	BDL	2.21
Cr2O3	BDL	BDL	BDL	BDL	BDL	BDL
FeO	27.49	27.35	27.89	35.06	35.35	27.48
CuO	BDL	BDL	BDL	BDL	BDL	BDL
Ag2O	BDL	BDL	BDL	BDL	BDL	BDL
Au2O3	BDL	BDL	BDL	BDL	BDL	BDL
Total	90.69	91.08	92.25	99.02	99.5	88.12
Cation	2.86	2.85	2.85	2.64	2.64	2.84

E35404

	point 1-1	point 1-2	point 1-3	point 1-4	point 1-5	point 1-6	point 1-7	point 1-8	point 2-1	point 2-2	point 2-3	point 2-4	point 2-5	point 2-6
SiO2	33.75	33.87	33.92	34.39	34.19	46.65	57.02	57.55	35.09	35.47	35.53	34.1	34.48	36.22
TiO2	1.83	2.14	2.62	2.05	2.07	BDL	0.47	BDL	2.5	1.91	2.71	1.85	2.24	BDL
Al2O3	20.18	20.26	20.46	20.15	19.82	36.92	29.35	28.88	20.16	20.95	20.13	20.11	19.14	64.36
FeO	24.71	25.13	26.5	25.35	25.32	1.27	BDL	BDL	25.08	26.95	25.75	24.89	24.14	BDL
MnO	BDL	BDL	BDL	BDL	BDL	BDL	BDL	BDL	BDL	BDL	BDL	BDL	BDL	BDL
MgO	5.96	5.77	6.03	5.97	5.48	BDL	BDL	BDL	5.79	5.54	6.19	6.24	5.2	BDL
CaO	BDL	BDL	BDL	BDL	BDL	BDL	9.62	9.96	BDL	BDL	BDL	BDL	BDL	BDL
Na2O	BDL	BDL	BDL	BDL	BDL	BDL	6.41	5.63	BDL	BDL	BDL	BDL	BDL	BDL
K2O	9.36	9.43	9.2	9.34	9.5	10.55	BDL	BDL	9.48	9.75	9.42	9.24	9.21	BDL
Cr2O3	BDL	BDL	BDL	BDL	BDL	BDL	BDL	BDL	BDL	BDL	BDL	BDL	BDL	BDL
Total	95.79	96.6	98.73	97.25	96.38	95.39	102.87	102.02	98.1	100.57	99.73	96.43	94.41	100.58
Cation	4.95	4.98	4.96	4.96	4.93	4.43	4.4	4.35	4.93	4.96	4.95	4.97	4.92	4.21

	point 3-1	point 3-2	point 3-3	point 3-4	point 3-5	point 3-6	point 3-7	point 3-8	point 4-1	point 4-2	point 4-3	point 4-4	point 4-5	point 4-6	point 5-1	point 5-2
SiO2	33.83	31.44	34.2	34.57	35.36	35.71	46.47	46.16	34.23	34.7	33.47	34.55	34.33	2.34	24.19	17.77
TiO2	2.28	2.53	2.39	2.18	1.91	BDL	BDL	BDL	2.8	2.78	1.98	2.9	2.48	48.34	BDL	BDL
Al2O3	19.62	18.89	20.2	21.03	21.01	65.1	35.62	35.73	19.49	19.28	21.16	19.49	19.7	2.03	60.27	40.57
FeO	25.1	25.06	25.53	25.56	24.61	0.56	BDL	BDL	24.66	25.61	25.26	25.3	25.57	47.56	14.52	35.68
MnO	BDL	BDL	BDL	BDL	BDL	BDL	BDL	BDL	BDL	BDL	BDL	BDL	BDL	BDL	BDL	3.77
MgO	5.47	5.6	5.55	6.05	6.23	BDL	BDL	BDL	5.59	5.66	6.16	5.63	5.59	BDL	1.32	1.46
CaO	BDL	BDL	BDL	BDL	BDL	BDL	17.55	18.32	BDL	BDL	BDL	BDL	BDL	1.32	BDL	1.48
Na2O	BDL	BDL	BDL	BDL	BDL	BDL	1.4	1.43	BDL	BDL	BDL	BDL	BDL	BDL	0.46	1.33
K2O	9.44	9.31	9.44	9.16	9.54	BDL	BDL	BDL	9.29	9.43	9.54	9.77	9.22	BDL	BDL	BDL
Cr2O3	BDL	BDL	BDL	BDL	BDL	BDL	BDL	BDL	BDL	BDL	BDL	BDL	BDL	BDL	BDL	BDL
Total	95.74	92.83	97.31	98.55	98.66	101.37	101.04	101.64	96.06	97.46	97.57	97.64	96.89	101.59	100.76	102.06
Cation	4.98	5.02	4.95	4.95	4.94	4.24	4.38	4.4	4.92	4.95	5	4.95	4.96	4.72	4.56	5.06

E35810

	point 1-1	point 1-2	point 1-3	point 1-4	point 1-5		point 2-1	point 2-2	point 2-3	point 2-4	point 2-5	point 3-1	point 3-2	point 3-3	point 3-4	point 3-5
Na2O	BDL	BDL	BDL	BDL	BDL	Na2O	0.41	BDL	BDL	0.36	BDL	BDL	BDL	BDL	BDL	0.45
MgO	9.34	8.91	9.1	8.62	8.7	MgO	9.3	9.55	8.98	9.69	9.22	9.55	9.55	9.19	9.3	9.28
Al2O3	19	18.68	17.82	17.51	17.89	Al2O3	18.1	18.26	17.13	17.8	17.91	17.75	18.11	18.38	17.57	17.8
SiO2	36.66	35.19	35.84	33.8	33.5	SiO2	34.58	35.63	33.65	33.56	35.69	35.96	35.46	35.88	35.62	36.25
K2O	9.26	8.94	9.39	8.77	8.24	K2O	8.65	8.49	8.41	7.75	8.55	9	8.78	8.88	8.53	8.97
CaO	BDL	BDL	BDL	BDL	BDL	CaO	BDL	BDL	BDL	BDL	BDL	BDL	BDL	BDL	BDL	BDL
TiO2	1.87	1.89	1.7	1.74	1.56	TiO2	1.27	1.27	2.12	1.15	1.49	2.2	1.98	2.08	1.97	2.67
Cr2O3	BDL	BDL	BDL	BDL	BDL	Cr2O3	BDL	BDL	BDL	BDL	BDL	BDL	BDL	BDL	BDL	0.32
MnO	BDL	BDL	BDL	BDL	BDL	MnO	BDL	BDL	BDL	BDL	BDL	BDL	BDL	BDL	BDL	BDL
FeO	22.41	21.47	22.13	21.46	21.82	FeO	22.2	22.29	21.82	22.03	22.34	23.02	23.11	22.46	22.57	22.77
CuO	BDL	BDL	BDL	BDL	BDL											
Ag2O	BDL	BDL	BDL	BDL	BDL											
Au2O3	BDL	BDL	BDL	BDL	BDL											
Total	98.54	95.08	95.98	91.9	91.71	]	94.51	95.49	92.11	92.34	95.2	97.48	96.99	96.87	95.56	98.51
Cation	2.84	2.84	2.86	2.85	2.85		2.86	2.84	2.84	2.86	2.83	2.85	2.85	2.83	2.83	2.84

	point 4-1	point 4-2	point 4-3	point 4-4	point 4-5	point 5-1	point 5-2	point 5-3	point 5-4	point 5-5
Na2O	0.49	0.47	0.37	0.4	0.5	BDL	BDL	0.37	0.49	BDL
MgO	10	10	10.95	9.97	10.25	9.93	9.74	9.84	10.01	9.83
Al2O3	16.67	17.58	17.51	17.57	17.61	17.69	17.71	17.11	18.18	18.56
SiO2	35.81	36.01	37.39	36.33	35.85	36.35	36.01	35.3	36.91	36.28
K2O	8.71	8.37	9.07	8.83	8.75	8.66	8.18	8.54	8.77	8.63
CaO	BDL	BDL	BDL	BDL	BDL	BDL	BDL	BDL	BDL	BDL
TiO2	1.58	1.52	1.78	1.92	1.23	1.85	1.53	1.54	1.48	1.45
Cr2O3	BDL	BDL	BDL	BDL	BDL	BDL	BDL	BDL	BDL	BDL
MnO	BDL	BDL	BDL	BDL	BDL	BDL	BDL	BDL	BDL	BDL
FeO	22.13	22.08	21.78	22.22	21.73	22.64	22.61	21.98	21.92	22.27
Total	95.39	96.03	98.85	97.24	95.92	97.12	95.78	94.68	97.76	97.02
Cation	2.86	2.84	2.85	2.84	2.86	2.83	2.83	2.85	2.84	2.84

E35810

	point 1-1	point 1-2	point 1-3	point 1-4	point 1-5	point 1-6	point 1-7	point 1-8	point 2-1	point 2-2	point 2-3	point 2-4	point 2-5
Na2O	BDL	BDL	BDL	BDL	BDL	BDL	BDL	BDL	BDL	BDL	BDL	BDL	BDL
MgO	6.18	5.97	6.28	5.71	6.03	1.64	1.4	1.49	6.14	6.25	6.72	6.26	5.92
Al2O3	18.72	17.9	18.12	17.54	18.27	21.4	21.13	20.26	19.22	18.43	18.24	18.57	18.52
SiO2	34.87	34.61	35.22	33.12	34.15	38.28	37.93	36.25	33.78	34.58	34.96	33.91	34.53
K2O	9.18	9.47	9.3	9.11	8.96	BDL	BDL	BDL	9.69	9.31	9.5	9.01	9.26
CaO	BDL	BDL	BDL	BDL	BDL	4.06	3.24	3.21	BDL	BDL	BDL	BDL	BDL
TiO2	1.61	1.65	1.61	1.46	1.36	0.20*	0.06*	BDL	1.73	1.84	1.46	1.61	1.73
Cr2O3	BDL	BDL	BDL	BDL	BDL	BDL	BDL	BDL	BDL	BDL	BDL	BDL	BDL
FeO	25.46	27.15	26.7	26.52	25.94	35.66	34.93	33.4	25.08	25.3	24.78	23.55	25.5
CuO	BDL	BDL	BDL	BDL	BDL	BDL	BDL	BDL	BDL	BDL	BDL	BDL	BDL
Ag2O	BDL	BDL	BDL	BDL	BDL	BDL	BDL	BDL	0.46	BDL	0.46	BDL	BDL
Au2O3	BDL	BDL	BDL	BDL	BDL	BDL	BDL	BDL	BDL	BDL	BDL	BDL	BDL
Total	96.02	96.75	97.23	93.46	94.71	101.04	98.63	94.61	96.1	95.71	96.12	92.91	95.46
Cation	2.84	2.86	2.85	2.87	2.85	2.65	2.63	2.64	2.86	2.85	2.85	2.83	2.84

	point 3-1	point 3-2	point 3-3	point 3-4	point 3-5	point 4-1	point 4-2	point 4-3	point 4-4	point 4-5	point 5-1	point 5-2	point 5-3	point 5-4
Na2O	BDL	BDL	BDL	BDL	BDL	BDL	BDL	BDL	BDL	BDL	BDL	BDL	BDL	BDL
MgO	6.1	6.02	6.48	6.23	6.24	5.65	5.69	5.62	5.8	6.03	6.25	6.02	6.25	1.49
Al2O3	17.54	16.5	17.71	16.93	16.53	15.72	15.09	15.66	15.81	16.5	16.52	16.48	17	20.77
SiO2	34.91	35.33	34.62	34.2	34.13	35.1	33.44	35.19	35.19	34.76	34.4	34.75	35.13	37.68
K2O	9.2	9.24	9.37	9.05	9.1	8.83	9.06	9.11	9.43	8.78	8.91	9.04	9.1	BDL
CaO	BDL	BDL	BDL	BDL	BDL	BDL	BDL	BDL	BDL	BDL	BDL	BDL	BDL	2.5
TiO2	1.54	2.61	1.24	1.77	1.91	2.3	2.46	2.67	2.82	1.65	1.22	1.44	1.23	BDL
Cr2O3	BDL	BDL	BDL	BDL	BDL	BDL	BDL	BDL	BDL	BDL	BDL	BDL	BDL	BDL
FeO	26.13	26.93	26.28	26.67	26.96	28.01	27.16	27	27.61	27.87	27.74	26.94	26.96	36.34
CuO	BDL	BDL	BDL	BDL	BDL	BDL	BDL	BDL	BDL	BDL	BDL	BDL	BDL	BDL
Ag2O	BDL	BDL	BDL	BDL	BDL	BDL	BDL	BDL	BDL	0.45	BDL	BDL	BDL	BDL
Au2O3	BDL	BDL	BDL	BDL	BDL	BDL	BDL	BDL	BDL	BDL	BDL	BDL	BDL	BDL
Total	95.42	96.63	95.7	94.85	94.87	95.61	92.9	95.25	96.66	96.04	95.04	94.67	95.67	98.78
Cation	2.84	2.82	2.85	2.86	2.86	2.84	2.86	2.84	2.84	2.86	2.86	2.86	2.84	2.64

E35810

	point 5-5	point 5-6	point 5-7
Na2O	BDL	BDL	BDL
MgO	0.94	5.94	5.99
Al2O3	19.39	15.53	16
SiO2	35.29	33.89	34.27
K2O	BDL	8.94	8.81
CaO	2.98	BDL	BDL
TiO2	BDL	1.78	1.71
Cr2O3	BDL	BDL	BDL
MnO	2.17	BDL	BDL
FeO	33.01	26.76	27.33
CuO	BDL	BDL	BDL
Ag2O	BDL	BDL	BDL
Au2O3	BDL	BDL	BDL
Total	93.78	92.84	94.11
Cation	2.65	2.85	2.86

E35810

	point 1-1	point 1-2	point 2-1	point 2-2	point 2-3	point 2-4	point 2-5	point 3-1	point 3-2	point 3-3	point 3-4	point 3-5
SiO2	45.21	44.06	36.35	35.74	36.3	35.86	37.12	37.07	36.76	35.22	35.47	36.37
TiO2	0.75	1.1	2.51	2.23	2.82	2.21	2.65	2.67	3.06	3.3	2.52	2.75
Al2O3	13.19	12.91	17.29	16.57	16.7	17.28	16.95	17	16.87	16.27	16.21	16.66
FeO	21.35	21.72	24.63	23.44	24.51	23.62	25.27	24.23	24.59	22.97	24.38	24.9
MnO	0.55	BDL	0.48	BDL	0.58	BDL	BDL	BDL	BDL	0.7	0.39*	0.48
MgO	6.47	6.78	8.14	8.23	8.35	8.01	8.04	7.56	7.73	7.5	7.98	8.27
CaO	11.62	11.59	BDL	BDL	BDL	0.41	BDL	BDL	BDL	BDL	BDL	BDL
Na2O	0.63	0.82	BDL	BDL	BDL	BDL	BDL	BDL	BDL	BDL	BDL	BDL
K2O	1.37	1.15	9.84	9.56	9.82	8.96	9.73	9.72	9.83	9.37	9.77	9.87
Cr2O3	BDL	0.41	BDL	BDL	BDL	BDL	BDL	0.55	BDL	BDL	BDL	BDL
Total	101.14	100.54	99.24	95.77	99.08	96.35	99.76	98.8	98.84	95.33	96.33	99.3
Cation	4.68	4.7	5.01	4.98	5.01	4.94	4.98	4.94	4.94	4.94	5.02	4.99

	point 4-1	point 4-2	point 4-3	point 4-4	point 4-5	point 5-1	point 5-2	point 5-3	point 5-4	point 5-5
SiO2	36.67	36.65	36.08	36.41	34.67	35.38	36.78	36.47	36.03	45.94
TiO2	3	2.88	2.77	3.53	2.35	1.71	2.03	2.55	1.46	0.79
Al2O3	17	17.35	17.21	16.91	17.72	17.26	16.96	17.23	17.6	10.48
FeO	22.89	24.52	23.66	26.19	24.59	24.71	24.64	23.12	24.36	19.6
MnO	BDL	0.55	BDL	BDL	BDL	BDL	BDL	BDL	BDL	0.8
MgO	7.84	8.09	8.57	7.63	8.38	8.6	8.76	8.37	8.48	8.36
CaO	BDL	BDL	BDL	BDL	BDL	BDL	BDL	BDL	BDL	12.12
Na2O	BDL	BDL	BDL	BDL	BDL	BDL	BDL	BDL	BDL	BDL
K2O	9.57	9.82	9.84	9.85	8.07	9.39	9.63	9.91	9.82	0.74
Cr2O3	BDL	BDL	BDL	BDL	BDL	BDL	BDL	BDL	BDL	BDL
Total	96.97	99.86	98.13	100.52	95.78	97.05	98.8	97.65	97.75	98.83
Cation	4.93	4.97	4.98	4.96	4.96	5.02	4.99	4.96	5.02	4.65

E358110

	point 1-1	point 1-2	point 1-3	point 1-4	point 1-5	point 1-6	point 1-7	point 2-1	point 2-2	point 2-3
Na2O	BDL	0.43	BDL	0.62	0.41	BDL	BDL	0.56	0.38	0.49
MgO	11.47	11.44	11.59	11.92	11.25	16.28	11.5	11.29	11.56	12.13
Al2O3	18.32	17.66	17.97	18.24	18.78	17.13	18.48	18.79	18.29	18.82
SiO2	36.14	34.9	34.99	35.16	35.77	28.53	35.27	36.44	35.76	36.57
K2O	9.18	8.38	8.93	8.74	9.64	0.22	9.71	9.03	8.62	9.57
CaO	BDL	BDL	BDL	BDL	BDL	BDL	BDL	BDL	BDL	BDL
TiO2	1.18	1.22	1.02	1.31	1.11	BDL	1.01	1.18	0.9	1.31
Cr2O3	BDL	BDL	BDL	BDL	BDL	BDL	BDL	BDL	BDL	BDL
MnO	BDL	BDL	0.36	BDL	BDL	BDL	BDL	BDL	0.44	BDL
FeO	19.67	19.12	20.75	18.82	19.51	25.53	19.95	19.2	19.69	19.52
Total	95.96	93.15	95.61	94.81	96.47	87.69	95.92	96.49	95.64	98.41
Cation	2.14	2.14	2.16	2.15	2.16	2.14	2.16	2.14	2.14	2.16

	point 3-1	point 3-2	point 3-3	point 3-4	point 3-5	point 3-6	point 3-7
Na2O	0.46	BDL	BDL	BDL	BDL	BDL	BDL
MgO	11.18	0.31	16.99	11.06	11.76	10.26	BDL
Al2O3	19.52	37.52	23.21	18.02	19.47	17.45	BDL
SiO2	35.8	46.18	27.84	34.8	33.78	36.15	0.93
K2O	9.47	10.77	0.96	8.85	7.59	8.54	BDL
CaO	BDL	BDL	BDL	BDL	BDL	1.75	BDL
TiO2	1.39	0.29	0.45	1.37	1	3.02	BDL
Cr2O3	BDL	BDL	BDL	BDL	BDL	BDL	BDL
MnO	BDL	BDL	0.37	BDL	0.5	0.37	BDL
FeO	19.45	BDL	22.81	18.77	20.15	18.29	78.92
Total	97.27	95.07	92.63	92.87	94.25	95.83	79.85
Cation	2.15	1.9	2.14	2.14	2.14	2.12	2.96

	point 4-1
Na2O	BDL
MgO	14.55
Al2O3	17.87
SiO2	30.22
K2O	4.57
CaO	BDL
TiO2	1.01
Cr2O3	BDL
MnO	0.39
FeO	21.89
Rb2O	BDL
SrO	BDL
Total	93.09